Renewable and Sustainable Energy Reviews 39 (2014) 765–805

Contents lists available at ScienceDirect

Renewable and Sustainable Energy Reviews

journal homepage: www.elsevier.com/locate/rser

Photocatalytic CO_2 transformation into fuel: A review on advances in photocatalyst and photoreactor

Sreejon Das [a,b,*], W.M.A. Wan Daud [a]

[a] Department of Chemical Engineering, University of Malaya, 50603 Kuala Lumpur, Malaysia
[b] Department of Chemical Engineering & Polymer Science, Shahjalal University of Science & Technology, Sylhet 3114, Bangladesh

ARTICLE INFO

Article history:
Received 21 February 2014
Received in revised form
22 May 2014
Accepted 6 July 2014
Available online 7 August 2014

Keywords:
Photocatalyst
CO_2 transformation
Photoreactor
Hydrocarbon fuels

ABSTRACT

Over the past years, a serious contemplation has revealed the need to resolve two major complications: global warming due to rising levels of atmospheric carbon dioxide (CO_2) and the alarming consumption of energy resources. Solar fuel production from green CO_2 gas would be a convenient solution to resolve both problems simultaneously. Various conventional technologies and their limitations over CO_2 transformation into fuels are reviewed in this paper. In the main stream, the review categorizes different types of photocatalysts used in previous photocatalytic conversion of CO_2 processes (with detailed information regarding operating conditions, catalysts' preparation techniques, physical properties of catalysts, radiation sources, and selectivity) based on metal oxides, sulfides, phosphides, p-type and non-metal oxide semiconductors. Also, the catalysts modified by doping co-metals, noble metals, transition metals and non-metals for visible light response have been highlighted. Moreover, the recent prospect and advancement of novel sensitized catalysts by dye elements, phthalocyanines and quantum dots (QDs) for harnessing solar fuels are prominent in this outline. Reviews of this topic have also focused on the progression of photocatalytic reactors especially for CO_2 photoreduction. Recently, advanced optical fibers and monolith photochemical reactors have become prominent because of their vast photon-harvesting ability. However, this technology needs more implementation with efficient catalyst selection and the development of giant solar reactors for industrial establishment. The current scenario shows that immense prospects and opportunities still exist in this area, but require further investigation and establishment.

Contents

* Corresponding author at: Department of Chemical Engineering, University of Malaya, 50603 Kuala Lumpur, Malaysia. Tel.: +60 1136541029.
E-mail address: dsreejon@yahoo.com (S. Das).

http://dx.doi.org/10.1016/j.rser.2014.07.046
1364-0321/

1. Introduction

Energy consumption from fossil fuels have great importance because they can be burnt (oxidized to carbon dioxide and water), producing significant amounts of energy per unit weight. Fossil fuels are non-renewable assets because they take millions of years to form, and reserves are being exhausted much more rapidly than new ones are being made. The production and use of fossil fuels raise environmental concerns. According to the British Petroleum Statistical Review of World Energy 2013 [1], the consumption rates of energy have shown upward trends during the period from 1961 to 2010. A global movement towards the generation of renewable energy is therefore under way to meet the increased energy needs. The main renewable sources, such as sunlight, wind, tides, waves, geothermal heat, biomass and nuclear energy, all offer electricity with zero carbon dioxide emissions [2]. Waste to energy is one of the sustainable sources to utilize the biomass for producing 7–10 TW of energy [3,4]. Other renewable sources like wind, hydroelectric and tide/ocean current provide almost 2.1 TW, 1.5 TW and <2 TW of energy respectively [5]. On the other hand, energy generated from these renewable sources is quite a small portion of that required to meet the global energy crisis.

Solar energy is one of the renewable technologies used to harness the sun's energy and make it useable by solar heating [6,7], solar photovoltaics [8,9], solar thermal electricity [10,11], solar architecture [12,13] and artificial photosynthesis [14,15]. Every hour, the sun beams onto the earth's surface, providing more than enough energy to satisfy global energy needs for an entire year. Solar fuel is formed by utilizing the light to convert chemical energy [16] by artificial photosynthesis, or thermochemical reactions. The improvement of inexpensive, unlimited and clean solar energy technologies must have vast prolonged benefits. It will increase countries' energy sanctuary through reliance on an indigenous, inexhaustible and mostly import-independent resource, increase sustainability, reduce pollution, lower the costs of mitigating climate change, and keep fossil fuel prices lower than previously.

Beyond the energy demand, the physical proof shows that carbon dioxide from burning fossil fuels is the sole most significant climate-related greenhouse gas in the Earth's atmosphere [17–20]. According to the International Energy Agency (2012) [21], the aim of controlling climate warming to 2 °C is becoming more problematic and expensive with each year that passes. If proper steps are not taken before 2017, all of the tolerable carbon dioxide emissions would be locked-in by the energy infrastructure existing in 2017. Already, global carbon dioxide growth in the atmosphere rose by an average of around 1.5 ppm (8 billion tons) per year during the period from 1975 to 2002. Actually, the amount of carbon dioxide grew much more quickly [22], by 2.25 ppm (12 billion tons) per year in the atmosphere. Lately, global carbon dioxide growth has increased by more than 10 billion tons every year [23], but according to the US Department of Energy [24] estimations, natural processes can only absorb about half of that amount.

The abundance of CO_2 can be a blessing if it is properly utilized in solar fuel conversion [25], which is a recycling process of CO_2 to control global warming, as well as the fuel crisis [26,27]. Moreover, there are other conversion processes to turn CO_2 into fuels, which have been discussed in Section 2, but the disadvantages of those processes are the high temperature and high electrical voltage requirements to break the CO_2 molecules, limitations of raw materials, high cost operation, and unsustainability. In comparison, the photocatalytic conversion of solar fuel is more sustainable because of the zero addition of extra energy and the deteriorating environmental. Initially, this photocatalytic process was carried out by artificial lamp. Nowadays, it has received growing consideration due to the ability to harness solar energy by efficient photocatalytic development. The stability of catalysts and mild operating conditions are the main reason to choose this technology. However, more amplifications and developments are needed regarding the selection of solar-sensitive novel catalysts and an efficient architecture of solar-driven photoreactors to make this technology industrially feasible. Also, there are some unanswered issues regarding this technology, including selectivity of the photocatalytic reactions and the limited efficiency.

This review paper illustrates advancements in the photochemical transformation of CO_2 into carbonaceous fuels in terms of the promotion of different types of photocatalysts, which have been described in previous research. Rather than other technologies, the probability and prospect of photochemical CO_2 recycling under UV and visible light irradiation have been highlighted critically in the second section. Moreover, the recent developments in photocatalytic reactor systems for CO_2 conversion are also described in depth decoratively in the last part of this review. Also, the challenges faced in the selection of solar-sensitive photocatalysts and well equipped photoreactors are provided with number of recommendations.

2. Current trends to turn CO_2 into fuels

The application of carbon dioxide as a raw material in the production of chemicals and liquid energy compromises one way to diminish the increasing carbon dioxide accumulation. It is well known that carbon dioxide is very thermodynamically and kinetically stable, but that it is infrequently used to its full potential [28]. There are six vital carbon dioxide conversions (Fig. 1): chemical conversions, electrochemical reductions, biological conversions, reforming, inorganic conversions and photochemical reductions [29].

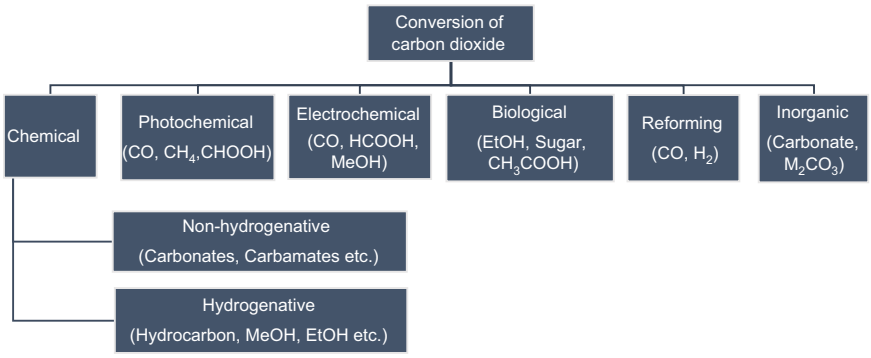

Fig. 1. Typical carbon dioxide conversion routes with prospective products [29].

The advantages and disadvantages of different modes of CO_2 conversion processes are given in Table 1.

CO_2 is categorized as anhydrous carbonic acid because of its strong attraction to nucleophiles and electron-donation reagents, which swiftly react with basic compounds. Chemical transformation is mainly based on industrial processes to produce salicylic acid, organic carbonates, urea and methanol [28]. The chemical reduction of CO_2 is achieved by the thermal conversion of CO_2 with carbon or coal itself according to reverse the Boudouard reaction. The reaction is endothermic and requires temperatures above 800 °C to run [36].

The electrochemical reduction of carbon dioxide (ERC) is used to turn carbon dioxide into more reduced chemical species using electrical energy [37]. It provides possible methods of producing chemicals or fuels, using CO_2 as a raw material [38]. The important issue is that it needs huge over-voltages for the direct electrochemical reduction of CO_2 on most electrode surfaces which subsequently reduces the conversion efficiency [39]. Sources of electrons are different between electrochemical and photoelectrocatalytic reduction. Electrons are provided by the applied current in electrochemical reduction, whereas in the photoelectrochemical reduction, electrons come from the interaction between the supplied semiconductor and exposed light radiation [40].

Biological transformation of CO_2 is a controlled natural photosynthesis process by which greenhouse gas problems can be solved in an ecological way [41]. A fixed environment is necessary to encourage photosynthetic processes such as the uniform distribution of light flux with the correct wavelength and heat to turn CO_2 into valuable yields like carbohydrates, hydrogen and oxygen [42]. Microalgae show 10 times better productivity for the sequestration of CO_2 by using sunlight than global plants [43,44]. The development of effective closed system bioreactors and a suitable climate to maintain the reaction environment are the main limitations of this biological process [45].

The reaction between CO_2 and methane in the absence of steam to form the synthesis gas is called dry reforming. The formation of synthesis gas through the dry reforming of methane could be an effective route to convert huge amounts of CO_2 through industrial applications [28,46]. On the other hand, the reaction is highly endothermic and needs a catalyst based on nickel such as Ni/MgO, Ni/$MgAl_2O_4$, etc., with huge temperatures of 800–1000 °C [36]. Using plasma to reform CO_2 by methane represents a new technology that provides highly efficient fuel compared to thermocatalytic methods, but the reaction in the presence of plasma is very complicated commercially due to the higher energy input [47].

Inorganic transformation of CO_2 is carried out by simple absorbents like calcium hydroxide or potassium hydroxide to react with CO_2 to produce calcium carbonate and potassium carbonate, which exhibits exothermic reactions [48]. This process can only be used in the formation of non-fuel products.

Recently, artificial photosynthesis or the photochemical reduction of CO_2 to fuel has become an attractive route due to its economically and environmentally friendly behavior. Basically, the fuel is derived from ample, low-cost raw materials such as water and CO_2 by employing semiconductor, transition–metal complexes. Transition–metal complexes and photosensitized catalysts exhibit high absorption ability to an important part of the solar energy spectrum and show longer-lasting excited states to activate CO_2 in the presence of water. The production of fuel is reliant on irradiation wavelength, light intensity, irradiation time and catalyst concentration [15,49]. Water is used as a reductant with the catalyst to split it into hydrogen and oxygen [50,51]. The reaction scheme of transformation of CO_2 into different types of hydrocarbon fuels in presence of H_2O is illustrated in Fig. 2.

The stability of a catalyst and its activity at normal operating conditions represent its acceptability to researchers. From an economical point of view, recycling of CO_2 to carbonaceous fuels under solar irradiation mimics natural photosynthesis without using extra energy and environmental effects. Conversely, this technology has some difficulties and barriers due to the non-effective catalysts, low yield and selectivity, as stated in the research [50,52,53]. To derive the solar fuel using sunlight, this technology needs highly efficient and selective photocatalysts. Not only that, the efficient design of a photoreactor is one of the most important challenges faced in the production of hydrocarbon on a commercial basis. Large illumination areas and equal distributions of certain wavelengths on the catalyst's surfaces are the main reasons for designing solar-driven photoreactors.

3. An overview of different sorts of catalysts used in CO_2 photoreduction

The photocatalytic recycling of CO_2 via by solar light irradiation is an effective route because it does not require any extra energy and there is no destructive effect on the environment. For visible light response, this technology urgently needs the development of effective photocatalysts which are usually used in the recycling of CO_2. Many researchers have already introduced different types of photocatalysts in this technology [54]. Some of the catalysts have shown high conversion rates and selectivities under visible light irradiation, while other catalysts were not feasible for visible light responses and presented low yield rates. To date, researchers are trying to improve the catalytic properties in terms of solar fuel conversion. In this review, a brief summary of photocatalysts is shown in Fig. 3, which is based on the recent advancements of photocatalytic CO_2 recycling.

Table 1
Current methods to turn CO_2 into fuel.

Authors (year)/Ref.	Conversion process	Reactants	Products	Overall advantages	Overall disadvantages
Obert and Dave (1999)/ [30]	Biological conversion	Gaseous CO_2, enzyme stock solution (10 mg/mL) and NADH (100 μmol) acts as a terminal electron donor	Methanol (21 μmol)	• All biological methods harvest cell mass containing high protein. • Light reaction and dark reaction are both carried out by photosynthetic microorganisms have the competency to coupling together. • Fixation of CO_2 does not severely depend on light. • It has biological capability to synthesize liquid fuels with high specificity and productivity. • The use of enzymes delivers a superficial low temperature route to generate fuel.	• The major challenge is regenerating ammonium by deamination of hydrolyzed proteins in a large scale biological process. • Biological photosystems can only utilize radiation within a restricted spectrum. • The saturation effect restricts the efficiency of solar energy capture. • It requires large two-dimensional (2D) light exposing surface areas.
Abe et al. (2009)/ [31]	Catalytic conversion	CO_2 and hydrogen in presence of Ru–TiO_2(G) catalyst	Methane (3.8×10^4 μmol h^{-1} g^{-1} catalyst)	•The methanation reaction is affected by mixture of a transition metal on oxide material at lower temperatures.	• The conversion of CO_2 to CH_4 is exothermic and it requires high temperature. • The activation of CO_2 and H_2O is the most energy demanding part and controls the process costs.
Yui el al. (2011)/ [32]	Photocatalytic conversion	CO_2 and H_2O in presence of 2 wt% Pd–TiO_2	Methane (0.56 μmol h^{-1} g^{-1} catalyst)	• Heterogeneous photocatalytic reduction of CO_2 over semiconductors is a probable mean to store alternating solar energy. • CO_2 is directly reduced photocatalytically by using molecular catalysts. • Sensitizing agent is sometimes used to enhance the absorption of light.	• The disadvantage of this approach is that it relies mainly on rare and expensive metals such as ruthenium or rhenium. • It is still a long way from efficient and commercially viable devices.
Angamuthu et al. (2010)/ [33]	Electrocatalytic conversion	CO_2 and H_2O (by using di-nuclear copper (I) complex electrode)	Lithium oxalate (six turnovers)	• Selective binding of CO_2 to the copper (I) ions propose a low-energy pathway. • Metallic Cu expresses exceptional selectivity and activity than others.	• Efficient electron transfer is hampered by the precipitation formed during the reaction onto the electrode surface. • This process requires high over-potential. • Fouling and deactivation of the electrodes can occur by impurities. • Mixture of products implying a costly separation step.
Ichikawa and Doi (1996)/ [34]	Photoelectrocatalytic conversion	CO_2 and H_2O (thin film titania–TiO_2 as photocatalyst and ZnO–Cu as electrocatalyst)	Hydrogen, methane and ethylene	• Semiconductors are truly stable under solar lighting. • This leads to significant over-potential for CO_2 reduction on semiconductor surfaces. • Direct conversion of solar energy to chemical energy is common in this process.	• Fouling and precipitation on the electrode surface can hamper efficient electron transfer. • Catalytic reduction process needs an external electrical potential bias to proceed. • Reactor design are still obligatory to permit the development of commercial processes.
Chueh et al. (2010)/ [35]	Thermochemical conversion	CO_2 and H_2O (by using Cerium oxide redox reactions)	CO and H_2 (efficiencies of 0.7–0.8%)	• Solar-driven thermochemical production of fuels. • Thermochemical conversion rates are higher. • Solar cavity-receiver reactor allows high-temperature heat transfer to the reaction sites.	•High initial investment costs is required for focusing lenses to sunlight and high-temperature reactors.

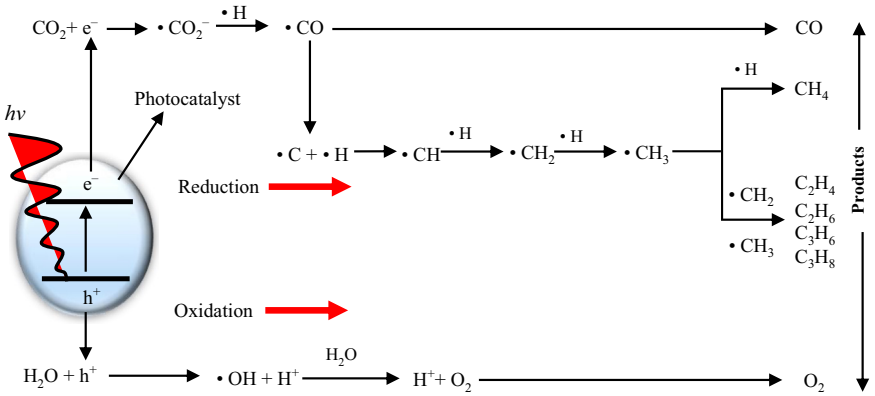

Fig. 2. General view of possible reaction paths for the photocatalytic reduction of CO_2 in the presence of H_2O.

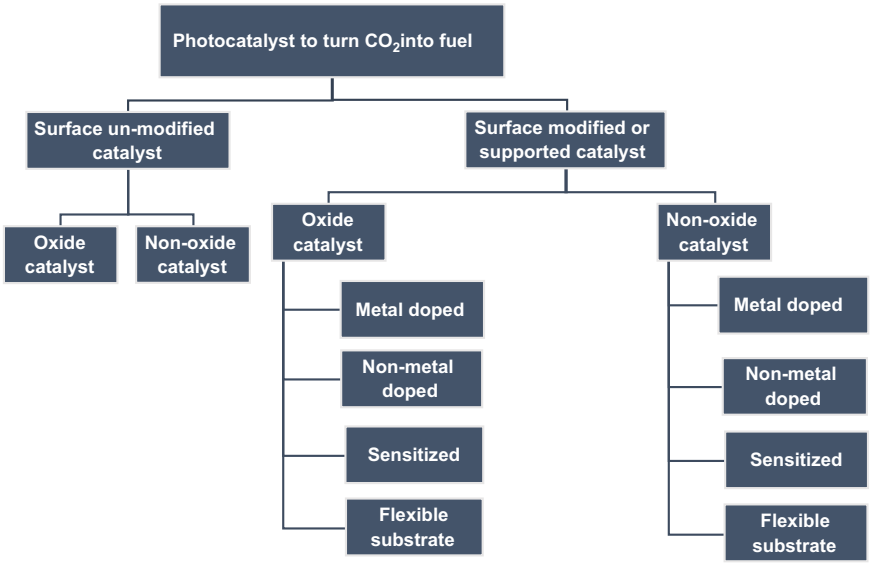

Fig. 3. Advancements of different sorts of photocatalysts on CO_2 recycling.

3.1. *Metal oxide photocatalysts for CO_2 recycling*

Metal oxide photocatalysis has been introduced to the practice of metal oxides as light-activated catalysts in several processes, such as breaking of organic and inorganic materials into valuable products [16,55,56], water treatment [57,58] and self-cleaning processes [59,60]. The first approach of CO_2 conversion to carbonaceous fuel by using metal oxide catalysts was established by Inoue et al. [61]. Modification of metal oxide photocatalysts has been already attempted by incorporating foreign elements/compounds with different supportive substrates [62–65] to decrease its particles' size, control crystal growth, and increase the surface area and pore volume. Different types of metal oxide photocatalysts which are commonly studied in various investigations are represented in this section, with detailed information and their effects on photocatalytic CO_2 transformation technology.

3.1.1. *Unmodified metal oxide photocatalysts*

Among the different types of metal oxides, TiO_2 is mostly used in the photocatalytic conversion of CO_2 to fuel because it is an inert, corrosion-resistant and inexpensive semiconductor. TiO_2 is found in nature as the recognized minerals rutile, anatase and brookite. For photocatalytic activity, the rutile and anatase forms show better performance on light irradiation. Both anatase and rutile forms exhibit a certain amount of band gap energy at around 3.2 eV and 3.0 eV, respectively. Due to the comparatively low band gap energy, the rutile phase is able to absorb some sort of visible light, while the anatase phase only shows responses to the ultraviolet (UV) region of spectra. However, rutile does not act as an efficient photocatalyst. The best photoactivity can be achieved by combining anatase with a small amount of rutile [66]. Detailed information for the metal oxide semiconductors used in the investigations of various photocatalytic CO_2 transformations is given in Table 2. A high surface area is necessary to increase the light absorption by titanium dioxide semiconductors. The surface area of TiO_2 is indirectly proportional to the size of the particle. Conversely, the size of the particle is directly proportional to the band gap energy. After a certain decrease of the particle size, semiconductor photocatalysts show high band gap energies as a result of shifting of the valence band energy to lower energies, whereas the conduction band energy is intensely shifted to higher energies [67]. On the other hand, significantly narrower band gap energy leads to an inadequate redox potential to achieve oxidizing and reducing reactions. For this reason, it is necessary to determine a structure which exhibits a settlement between the particle size and band gap energy range [68]. For example, a combination of 80% anatase and 20% rutile phases was used as a photoactive

Table 2
Recent studies on surface-unmodified metal oxide catalysts for CO_2 photoreduction; preparation methods and major findings.

Researcher (year)/Ref.	Catalyst/band gap energy	Catalyst treatment technique	Reactants (amount)/ radiation source/light intensity	Operating variables (T/P/pH/t/ QE), physical properties (W/SA/ PS/SC/MP)	Major product/ yield ($\mu mol\ h^{-1}\ g^{-1}$ catalyst)/ efficiency (%)	Comments
Xi et al. (2012)/ [76]	$W_{18}O_{49}$/2.7 eV	One-pot solution-phase method	CO_2 (saturated), water vapor (–)/visible light (> 420 nm)/–	(343/–/–/6/–), (–/–/nanowires with 1 nm/ –/supported)	Methane/666[a]/–	• Ultrathin nanowires appear strong light absorption from the visible to the NIR region. • All oxygen vacancies in the ultrathin nanowires are used up by carbon dioxide molecules, and no methane molecules are produced.
Li et al. (2012)/ [85]	HNb_3O_8/3.66 eV	Hydrothermal synthesis	CO_2 (saturated), water vapor (7 kPa)/350 W Xe lamp/–	(318/–/–/4/–), (0.1/ 39.4/1.12 nm particle/ –/supported)	Methane/3.58/–	• KNb_3O_8 and HNb_3O_8 nanobelts show greater activities for CO_2 photoreduction to methane than commercial TiO_2, and the KNb_3O_8 and HNb_3O_8 particles synthesized by conventional solid state reaction. • The protonic acidity also gives higher photocatalytic activity to the HNb_3O_8 nanobelts. • A fixed bed quartz tubular reactor (159 mL) is placed horizontally, and the catalysts are put inside on a flat quartz plate.
Lekse et al. (2012)/ [87]	$CuGaO_2$/2.6 eV	Stoichio-metric mixing	CO_2 (saturated), water vapor (–)/300 W Xe arc lamp/–	(–/–/7/–/–), (0.2/ –/60–80 mesh particles/ –/supported)	Carbon monoxide/9 [a]/–	• Alloying the B-site with Fe to form $CuGa_{1-x}Fe_xO_2$ (x=0.05, 0.10, 0.15, 0.20) creates response toward visible and near-infrared region. • A gas-tight cell is built by stainless steel conflat flange components fitted with two inlet/outlet valves, and one UV quartz viewport.
Stock and Dunn (2011)/ [86]	$LiNbO_3$/3.6 eV	Pulverized with a mortar and pestle to produce particles	CO_2 (30%), H_2O (10 mL)/ Natural sunlight or Hg lamp/64.2 mW cm^{-2}	(–/–/–/6/2), (–/–/1 μm particle/ –/supported)	Formic acid/7.7 [b]/–	• The $LiNbO_3$ is kept on a platen ($1.26 \times 10^{-5}\ m^2$) above the water to give a gas–solid catalytic reaction. • MgO doped $LiNbO_3$ gives an energy conversion efficiency of 0.72% is lower than that of 2.2% for $LiNbO_3$. • The ferroelectric material assistances carrier separation and gives an improved catalyst performance.
Zhou et al. (2011)/ [83]	Bi_2WO_6/2.69 eV	Solid state reaction and hydrothermal method	CO_2 (saturated), H_2O (1 mL)/300 W Xe arc lamp (> 420 nm)/–	(298/–/–/5/–), (0.1/ 5.6/nanoplates of 9.5 nm thickness/ –/supported)	Methane/1.1/–	• Bi_2WO_6 nanoplates display excessive potential in the application of visible light energy • Ultrathin geometry of the nanoplates helps charge carriers to move swiftly from the interior to the surface for photoreduction. • Catalysts are evenly dispersed on the glass reactor with an area of 4.2 cm^2.
Dimitrijevic et al. (2011)/ [71]	TiO_2 (Degussa P-25 Aeroxide)/ 3.08 eV	TiO_2 was left in D_2O in order to exchange bound water	CO_2 (saturated), water vapor (2.8 mmol)/100 W Hg lamp (365 nm)/ 11 mW cm^{-2}	(298/1/–/2.6/–), (0.01/55/ nanoparticle/ –/supported)	Methane/4 [c]/–	• It is proposed that two-electron and one-proton reactions are responsible for initial step in the reduction of CO_2 on the surface of TiO_2. • A closed reactor is used having a circular pot sample holder with a diameter of 1.8 cm.
Yui et al. (2011)/ [32]	TiO_2 (Digussa P-25)/3.08 eV	Treated by calcination and washing	CO_2 (–), H_2O (1.5 mL)/ 500 W Hg arc lamp (> 310 nm)/–	(278/–/4.1/5/–), (0.15/ –/nanoparticle/0.1/ suspended)	Carbon monoxide/0.35/ –	• CH_4 was the main product in case of Pd-TiO_2, and CO formation is significantly reduced compared with that on the pretreated TiO_2. • Isotope labeling specifies that CO_2 and CO_3^{2-} are the main carbon sources of the CH_4 production. • Catalysts are kept in a round-shaped quartz vessel of 6 cm diameter.

Table 2 (*continued*)

Researcher (year)/Ref.	Catalyst/band gap energy	Catalyst treatment technique	Reactants (amount)/ radiation source/light intensity	Operating variables (T/P/pH/t/ QE), physical properties (W/SA/ PS/SC/MP)	Major product/ yield ($\mu mol\ h^{-1}\ g^{-1}$ catalyst)/ efficiency (%)	Comments
Liu et al. (2010)/ [84]	Zn_2GeO_4/4.5 eV	Solvothermal method	CO_2 (–), Water vapor (–)/UV light/–	(–/–/–/16/–), (–/28.27/ nanoribbon of 7 nm thickness/ –/supported)	Methane/0.41/–	• Ultralong and ultrathin geometry of the Zn_2GeO_4 nanoribbon shows high performance on photocatalytic activity. • The rate of CH_4 production over the Zn_2GeO_4 nanoribbon could be significantly enhanced by loading of Pt.
Koci et al. (2009)/ [67]	TiO_2 (Anatase)/ 3.0 eV	Sol–gel process	CO_2 (–), NaOH (0.2M, 100 mL solution)/8 W Hg lamp (254 nm)/ 1.41 mW cm^{-2}	(–/1.08/–/24/–), (0.1/106/14 nm nanoparticle/0.001/ suspended)	Methane/0.308/ –	• A stirred batch annular reactor (380 cm^3) with quartz inner tube and stainless steel shell tube is used in this experiment. • The yields is observed in such an order: $H_2 > CH_4 > CH_3OH \geq CO$.
Liu et al. (2009)/ [81]	$BiVO_4$ (monoclinic)/ 2.24 eV	Microwave assisted hydrothermal method	CO_2 (–), H_2O (100 mL)/ 300 W Xe arc lamp (> 400 nm)/–	(273/1/–/1/–), (0.20/ –/nanoparticles/ –/suspended)	Ethanol/110/–	• Photocatalyst $BiVO_4$ exhibits visible-light response. • Intense irradiation creates huge amount of C1 intermediate species anchored on the $BiVO_4$, which dimerizes to form ethanol. • Catalysts are dispersed in water and magnetically stirred inside the reactor.
Yuliati et al. (2008)/ [77]	Ga_2O_3 (Kishida Chemicals)/4.7 eV	Cleaning at 13.3 kPa of oxygen atmosphere at 1073 K for 1 h	CO_2 (200 μmol), CH_4 (200 μmol)/300 W Xe-lamp (220–300 nm)/ 9 mW cm^{-2}	(473/1/–/3/–), (0.2/ 2/–/–/supported)	Hydrogen, carbon monoxide/4.13, 1.8/–	• Supplementary thermal energy enhances the reaction between methane and carbon dioxide by stimulating the thermally activation steps in reaction mechanism. • A closed quartz reactor (30 cm^3) where the catalysts are spread over a flat bottom of reactor (14 cm^2).
Xia et al. (2007)/ [88]	TiO_2 (Digussa P-25)/3.08 eV	Calcined at 723 K for 2 h	CO_2 (1 μmol), water vapor (5 μmol)/15 W UV lamp (365 nm)/–	(298/–/7/5/–), (–/50/nanoparticle/ –/supported)	Methane/15/–	• Appropriate amount of MWCNTs as supports for TiO_2 could extraordinarily progress the efficiency of the photocatalytic reaction. • Catalysts are kept on a piece of transparent glass and then put into a home-made stainless steel reactor.
Lo et al. (2007)/ [80]	ZrO_2 (Prochem)/ 5.0 eV	ZrO_2 is immobilzed by coated glass pellets	CO_2 (99.8%), H_2 (95%)/ 15 W near UV lamps (254 nm)/–	(316/1.1/–/2/–), (0.25/–/100 mesh powder/ –/supported and immobilized)	Carbon monoxide/0.51/ –	• A circulated packed-bed photocatalytic reaction system is made from a quartz tube with 480 mm length and 22.5 mm inner diameter. • One-site Langmuir–Hinshewood kinetic model is successfully fitted to simulate the photoreduction rate.
Tan et al. (2006)/ [69]	TiO_2 (80% anatase and 20% rutile)/ 3.0 and 3.2 eV	Heated-up to 473 K in oven	CO_2 (saturated), Water vapor (saturated)/1.6 W UV light (253.7 nm)/–	(298/1/–/48/–), (100/50/4 mm porous pellet/ –/supported)	Methane/0.014/ –	• A cylindrical quartz tube fixed-bed photocatalytic reactor having dimensions 300 mm (length) and 74 mm inner diameter is operated • 48 h continuously. • A good reduction yield is attained as compared to immobilized catalysts through thin-film technique and anchoring method.
Dey et al. (2004)/ [74]	TiO_2 (Anatase)/ 3.0 eV	Suspension of TiO_2 in presence of 0.5 M 2-propanol	CO_2 (–), H_2O (5 mL)/light (350 nm)/–	(298/1/–/10/–), (0.005/–/325 mesh powder/ –/suspended)	Methane/6/–	• It is observed that surface-adsorbed and in situ generated CO_2 are liable for methane formation through photoreduction by TiO_2. • In presence of saturated O_2, the methane yield is lower as compared to that in aerated system while CO_2 yield is developed. • A quartz cell (16.5 mL) having a gas purging inlet and a gas sampling port is used to run the photoreduction of CO_2.

Table 2 (*continued*)

Researcher (year)/Ref.	Catalyst/band gap energy	Catalyst treatment technique	Reactants (amount)/ radiation source/light intensity	Operating variables (T/P/pH/t/ QE), physical properties (W/SA/ PS/SC/MP)	Major product/ yield ($\mu mol\ h^{-1}\ g^{-1}$ catalyst)/ efficiency (%)	Comments
Teramura et al. (2004)/ [79]	MgO (Merck) and ZrO_2/7.0 eV and 5.0 eV	Hydrated, filtered and calcinated in air at 873 K for 3 h	CO_2 (150 μmol), CH_4 (50 μmol)/500 W Ultra high pressure Hg lamp/–	(293/1/–/5/–), (0.3/110/100 mesh powder/ –/supported)	Carbon monoxide/2.4 and 0.48 respectively/–	• It is found that the substrate-modified insulating material shows reasonable activity in the CO_2 reduction. • Catalysts are kept on a on the flat bottom of a quartz reactor (closed static system) with capacity 18.9 mL.
Yahaya et al. (2004)/ [89]	NiO/–	—	CO_2 (saturated), deionized water (70 mL)/ high photon flux monochromatic light (355 nm)/–	(–/–/7/1.5/–), (0.3/ –/powder/ –/suspended)	Methanol/393/–	• The formation of methanol from CO_2 is a reversible process and degrades photocatalytic process to generate hydrogen and CO_2 again. • A Pyrex cell with optical grade quartz windows is used for photoreduction of CO_2 having 35 mm diameter and 120 mm length.
Kaneco et al. (1999)/ [72]	TiO_2 (Anatase)/ 3.0 eV	Pretreated by boiling in 1 M nitric acid and thoroughly rinsing	CO_2 (saturated), H_2O (5 mL)/990 W Xe lamp (> 340 nm)/ 96 mW cm^{-2}	(308/88.82/3/5/–), (0.05/8.7/230 nm nanoparticle/0.01/ suspended)	Formic acid/1.8/ –	• Adding of acidic solutions rather than pure water is superior for formic acid production. • Stainless steel vessel (557.5 mL) with a glass window is used to carry out the photoreduction of CO_2.
Kaneco et al. (1997)/ [73]	TiO_2 (Anatase)/ 3.0 eV	Purity 99.9% and treated by 1 M nitric acid with distilled-deionized water	CO_2 (saturated), H_2O (57.5 mL)/990 W Xe lamp (340 nm)/96 mW cm^{-2}	(293/64.15/–/30/–), (0.05/8.7/230 nm particle/ –/suspended)	Formic acid/ 0.28/–	• There is no formation of gaseous reduction products, and formic acid is entirely found in the aqueous solution. • The internal surface was totally covered by Teflon to prevent contamination from the stainless steel and its catalytic effect on reduction.
Anpo et al. (1995)/ [90]	Anatase TiO_2 (JRC-TIO) and Rutile TiO_2 (JRC-TIO)/3.47 and 3.32 eV	Degassed and calcined at 452 °C	CO_2 (0.15 mmol), Water vapor (0.25 mmol)/75 W high-pressure Hg lamp (> 280 nm)/–	(275/–/–/8/–), (–/16 and 51/1 μm finely powdered/ –/supported)	Methane/0.03 and 0.02 respectively/–	• The photocatalytic reactions are conducted in a quartz cell with a flat bottom (60 mL), where the catalyst are put on a transparent porous Vycor glass. • TiO_2 (Anatase) with large band gap and many surface –OH groups exhibit high efficiency for the formation of CH_4.
Solymosi and Tombatz (1994)/ [91]	TiO_2/–	Pure TiO_2 from British Drog House	CO_2 (saturated), H_2O (120 mL)/500 W high pressure Xe lamp/–	(333/1/–/–/–), (0.3/ 18/nanoparticle/ 0.0025/suspended)	Formic acid/2/–	• A Pyrex glass cell with Pyrex window is used to conduct the photocatalytic reaction having surrounding water jacket to control the temperature of circulating water by an ultra-thermostat. • An increase in the electron concentration of TiO_2 enhances the photoreduction.
Inoue et al. (1979)/ [61]	TiO_2, ZnO, and WO_3/3.0, 3.2, and 2.8 eV	Purity 99.5 to 99.99%	CO_2 (saturated), H_2O (100 mL)/500 W Xe or Hg lamp/–	(298/1/5/7/–), (1/ –/200–400 mesh powder/ –/suspended)	Formaldehyde/ 16, 17.14, and 0/–	• Methanol formation rate is increased by increasing illumination period in case of TiO_2. • In case of semiconductor electrode, it has been suggested that the charge transfer rate between photogenerated carriers and solution species is related to the energy levels between the semiconductor and redox agents. • A glass cell with quartz window is used to carry out the reaction.

T/P/pH/t/QE: temperature (K)/pressure (atm)/pH/illumination period (h)/quantum efficiency (%).
W/SA/PS/SC/MP: weight of photocatalyst (g)/surface area (m^2/g)/photocatalyst structure (diameter)/semiconductor concentration (g/mL)/mode of photocatalyst.
'–': Not mentioned in the original paper.

[a] ppm $h^{-1}\ g^{-1}$ catalyst.
[b] mmol h^{-1}.
[c] Turn over number.

catalyst in the study by Tan et al. [69]. The schematic view of photocatalytic conversion mechanism of CO_2 on an unmodified metal oxide semiconductor is represented in Fig. 4.

Commercial Degussa P25 is slightly less active than treated TiO_2 (anatase and rutile) [70]. It has been found that metal oxide semiconductors, usually untreated TiO_2 (P25), with a high surface

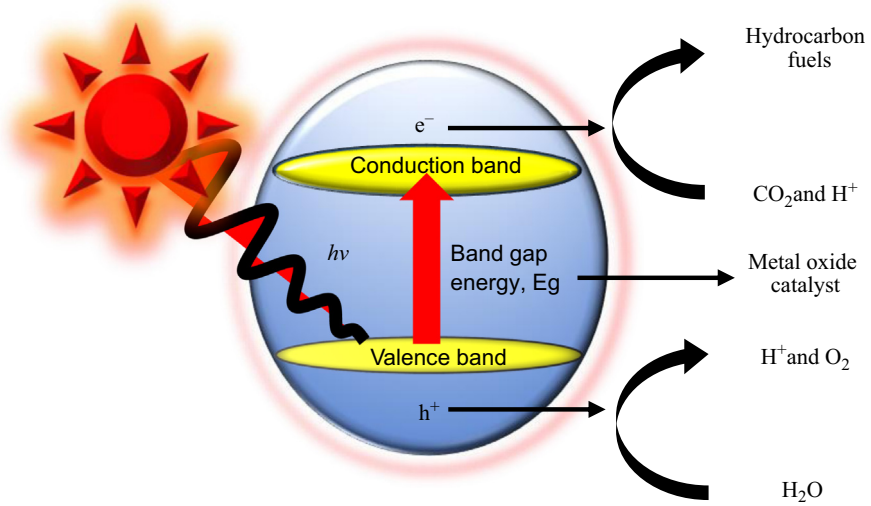

Fig. 4. Scheme of unmodified metal oxide based photocatalytic reaction under light irradiation.

area have the affinity to have organic impurities on their surfaces and these adsorbed organic compounds have the potential to perform as both an electron donor and a carbon source for the products [32]. Moreover, this type of metal oxide catalyst shows better CH_4 yield compared with the treated Degussa P25 by calcination and washing where CO is the major product [32,71]. In many studies, product variation is also observed due to the various treatment procedures on anatase TiO_2 [72–74]. For example, treatment with acidic solutions (1 M nitric acid) is desirable for formic acid development due to the protonation of reaction intermediates on TiO_2 in solution [72]. Treatment with 2-propanol acts as a hole scavenger in CO_2 photoreduction with anatase TiO_2, where the methane formation rate was very high; it was also observed that in absence of 2-propanol, no methane was found [74]. Moreover, the synthesis of TiO_2 by the sol–gel method removes the presence of small brookite nanoparticles that normally arise in low temperature formation reactions and considerably hinder the phase alteration to rutile at elevated temperatures [67,75].

Some prospective metal oxide photocatalysts other than TiO_2 were reported in many investigations. Inoue et al. studied three metal oxides (TiO_2, ZnO and WO_3) to understand their photocatalytic characteristics under UV light radiation [61]. It has been observed that WO_3 does not response to the photocatalytic reduction of CO_2 and shows zero yield because of more negative solution species of redox potential with respect to the conduction band energy level. However, WO_3 possesses low band gap energy (2.8 eV) with respect to visible light irradiation. Xi et al. synthesized $W_{18}O_{49}$ catalyst in the form of nanowires with band gap energy 2.7 eV for the photocatalytic conversion of CO_2 to methane under visible light irradiation [76]. The diameter of $W_{18}O_{49}$ nanowires is approximately 0.9 nm and they hold huge number of oxygen vacancies. These oxygen vacancies indicate an outstanding competency of photochemical carbon dioxide reduction over the visible light region.

Metal oxides like Ga_2O_3, ZrO_2, and MgO with wide band gaps were investigated in different studies and compared with other photocatalytic metal oxides [77–79]. In those studies, methane and hydrogen were used as reductants for the photoreduction of CO_2 and CO was the major product [79,80]. In the case of ZrO_2, the high photoreduction of CO_2 is obtained when H_2 is used rather than that of CH_4. Moreover, it has been found that some intermediates are formed when H_2 is used for the CO_2 photoreduction over ZrO_2 and MgO as a surface formate species, whereas acetate is generated in lieu of formate when CH_4 is used as a reductant over ZrO_2 [78,79]. It was also observed that the surface bidentate formate species showed high photoactivity for the photocatalytic reduction of CO_2 over ZrO_2 and MgO.

Table 3
Textural properties of different types of silica supported samples [65].

Catalysts composition	Specific surface area (m^2/g)	Pore volume (cm^3/g)	Maximum of the pore size distribution (nm)
MCM-41 SiO_2	1051	0.83	2.3
SBA-15 SiO_2	640	0.96	7.5
SBA-15/TMB SiO_2	601	1.62	20.0
Commercial SiO_2	317	1.59	27.5
100% TiO_2 Reference	9	–	–
20% TiO_2 MCM-41	294	0.57	16.0
20% TiO_2 SBA-15	532	0.78	7.0
40% TiO_2 SBA-15	442	0.69	6.5
60% TiO_2 SBA-15	349	0.60	6.5
20% TiO_2 SBA-15/TMB	517	1.40	18.5
40% TiO_2 SBA-15/TMB	414	1.08	18.5
60% TiO_2 SBA-15/TMB	304	0.78	18.5
20% TiO_2 Commercial	299	1.16	22.5
40% TiO_2 Commercial	246	0.94	25.0
60% TiO_2 Commercial	179	0.67	26.0

Recently, visible light response of other fabricated oxide catalysts through various routes like hydrothermal, solvothermal, and solid state reactions have been widely used in the photochemical reduction of CO_2 because of the high yield rate. Microwave-assisted hydrothermally-derived monoclinic $BiVO_4$ catalyst shows high ethanol yield (110 $\mu mol\ h^{-1}\ g^{-1}$ of catalyst) compared to that of tetragonal $BiVO_4$, due to CO_3^{2-} being anchored to the Bi^{3+} sites on the external surface through a weak Bi–O bond to receive the photogenerated electrons effectively from the V 3d-block bands of $BiVO_4$. The asymmetric behavior of monoclinic phase around the Bi^{3+} ion is more effective than in the tetragonal phase. That is why Bi^{3+} ion shows stronger lone pair behavior in the monoclinic phase to increase the tendency of Bi–O bond formation with CO_3^{2-} [81,82]. Zhou et al. and Liu et al. reported visible light responsive 9.5 nm thickness Bi_2WO_6 nanoplates and UV driven single-crystalline Zn_2GeO_4 nanobelts with 7 nm thickness, respectively [83,84]. The ultrathin geometry encourages the charge carriers to transfer swiftly from inside to the external surface for the effective participation in CO_2 photoreduction reaction. It also separates the

Table 4
Recent studies on supported metal oxide catalyst for CO_2 photoreduction; preparation methods and major findings.

Researcher (year)/Ref.	Catalyst composition/ band gap energy	Catalyst preparation technique	Reactants (amount)/ radiation source/light intensity	Operating variables (T/ P/pH/t/QE), physical properties (W/SA/PS/SC/ MP)	Major product/ yield ($\mu mol\ h^{-1}\ g^{-1}$ catalyst)/ selectivity (%)	Comments
Tahir et al. (2013)/[64]	20 wt% Montmorillonite modified TiO_2/ 3.07 eV	Sol–gel method	CO_2 (saturated), water vapor (–)/500 W Hg lamp (365 nm)/–	(393/0.20/–/4/–), (0.05/ 82.62/13.87 nm particle/ 6.33/Supported)	Methane/ 441.5/–	• Loading montmorillonite into TiO_2 structure amplified surface area, reduced particle size and allowed efficient charge separation. • H_2O/CO_2 feed ratio = 0.35 gives the maximum yield for methane (441.5 $\mu mol\ g\ cat^{-1}\ h^{-1}$). • Stainless steel reactor having length of 9.5 cm, width of 3.75 cm and total volume of 106 cm^3 with a quartz window for the passing of light irradiations.
Truong et al. (2012)/[101]	20% $FeTiO_3$–TiO_2/2.7 eV	Facile hydrothermal method	CO_2 (–), $NaHCO_3$ (0.08 M, 30 mL solution)/500 W Xe lamp (> 300 nm)/–	(–/–/–/3/–), (0.05/51.3/ 5 nm particle/ –/suspended)	Methanol/ 0.46/–	• Junction effect of two semiconductors and narrow band gap of $FeTiO_3$ show extraordinary activity under both visible and UV–Vis light irradiation with a supreme yield of CH_3OH that is three times higher than that from bare TiO_2 or Degussa P25. • A Pyrex glass tube reactor where the temperature of the solution is kept constant by a water bath.
Lee et al. (2012)/ [113]	1 wt% NiO–$InNbO_4$/–	Solid-state reaction and wetness impregnation methods	CO_2 (saturated), $KHCO_3$ (0.2 M, 50 mL solution)/500 W halogen lamp (900 nm)/ 143 mW cm^{-2}	(298/–/7/20/–), (0.14/ –/1 μm particle/ –/dispersed and suspended)	Methanol/1.4/–	• Catalyst shows highest activity due to the presence of core–shell type Ni^0 and NiO on the surface and the presence of a small amount of Nb_2O_5 as a promoter under visible light irradiation. • Photocatalytic reduction is carried out in a continuous flow reactor with a Pyrex glass down-window type irradiation cell (75 mL).
Liu et al. (2012)/ [116]	1 wt% Pt and 1 wt% RuO_2 loaded on $Zn_{1.7}GeN_{1.8}O$/ 2.6 eV	Solvothermal route and nitridation	CO_2 (saturated), H_2O (0.4 mL)/ 300 W Xe arc lamp (> 420 nm)/–	(298/1/–/14/0.024), (0.1/ 32.33/0.5–2 μm bundle shape/–/supported)	Methane/11.5/–	• This hybrid photocatalyst allows CO_2 reduction into CH_4 in the presence of H_2O under visible light irradiation. • Photocatalysts are evenly put at the bottom of a pyrex glass reactor with an area of 4.2 cm^2.
Kočí et al. (2011)/[103]	Kaolinite modified TiO_2 composite/–	Thermal hydrolysis	CO_2 (saturated), NaOH (0.2 M, 100 mL solution)/8 W Hg lamps (254 nm)/–	(–/1/7/24/–), (1/40/ 18 nm particle/0.001/ supported)	Hydrogen/ 0.187/–	• Production of methane and methanol were advanced over a kaolinite modified TiO_2 composite than over commercial TiO_2 (Degussa P-25). • Adding of TiO_2 nanoparticles into the kaolinite structure caused a decrease of anatase crystallite size. • Inhibit the recombination of electron–hole pairs and stop the formation of TiO_2 aggregates in suspension. • The photocatalytic reduction is conducted in a homemade apparatus using a stirred batch annular reactor with a suspended catalyst.
Abou Asi et al. (2011)/[104]	23.2 wt% AgBr–TiO_2/2.9 eV	Deposition-precipitation method	CO_2 (saturated), $KHCO_3$ (0.2 M, 100 mL solution)/150-W Xe lamp (420 nm)/–	(298/74/8.5/5/–), (0.5/ 50/5 nm particle/ –/suspended)	Methane, ethanol/25.72, 15.57/–	• AgBr–TiO_2 shows its strong absorption and stability in the repeated uses under visible-light region due to the transmission of photoexcited electrons from the conduction band of well-dispersed AgBr to that of TiO_2. • Photocatalytic reduction is conducted in a stainless steel vessel with valves for evacuation and gas feeding in which an O-ring sealed glass window is kept at the top for focusing light.

Table 4 (*continued*)

Researcher (year)/Ref.	Catalyst composition/ band gap energy	Catalyst preparation technique	Reactants (amount)/ radiation source/light intensity	Operating variables (T/ P/pH/t/QE), physical properties (W/SA/PS/SC/ MP)	Major product/ yield (μmol h^{-1} g^{-1} catalyst)/ selectivity (%)	Comments
Liou et al. (2011)/[111]	1 wt% NiO–$InTaO_4$/2.6 eV	Impregnation method	CO_2 (saturated), Water vapor/ 300 W Xe lamp/ 100 mWc m^{-2}	(303/1/–/6/0.057), (0.12/ 3.58/Composite/ –/supported)	Acetaldehyde/ 0.3/–	• To increase the amount of catalyst loading, a monolith photoreactor is used due to its multiple channels. • Surface carved polymethylmethacrylate optical fibers can transmit and scatter light effectively to illuminate the catalyst inside the channels. • Quantum efficiency was significantly enhanced in the monolith reactor, compared with optical-fiber reactor.
Yan et al. (2011)/[115]	3 wt% RuO_2–Zn_2GeO_4/4.65 eV	Low-temperature (100 °C) solution phase route	CO_2 (saturated), H_2O (–)/ultra-violet irradiation/–	(–/–/–/5/–), (–/14.8/rod-shaped nanostructure/ 0.58/supported)	Carbon monoxide/17.9 [a]/–	•Facile solution phase route synthesized catalysts have low crystal defects, high specific surface area and beneficial microstructure on its surface.
Qin et al. (2011)/ [110]	1 wt% CuO–TiO_2/ 3.2 eV	Laboratory synthesis	CO_2 (saturated), Methanol (30 mL solution)/250 W high pressure Hg lamp (365 nm)/–	(300/1–60/–/6/–), (0.03/ –/13.8 nm particle/ –/suspended)	Methyl-formate/1602/–	• Methanol acts as a sacrificial reagent to react with the photogenerated holes in the valence band. • Hetero-junction photcatalyst reduces the recombination of the electrons and holes. • The photocatalytic reaction is conducted in a slurry reactor having a flat top cover of the vessel is made of Pyrex glass.
Li et al. (2010)/ [95]	SiO_2 supported 0.5 wt% Cu–TiO_2/ 3.1 eV	One-pot sol–gel method	CO_2 (saturated), water vapor (–)/Xe lamp (250–400 nm)/ 2.4 mW cm^{-2}	(273/1/7/4/1.41), (0.1/ 386.2/ < 100 μm powder/–/supported)	Carbon monoxide/45/–	• Experiment is carried out in a continuous-flow reactor having stainless steel wall with a quartz window at the top and the inner cavity is 6.0 cm in diameter and 2.5 cm deep. • High surface area of mesoporous silica substrate significantly improves CO_2 photoreduction because of better TiO_2 dispersion and high CO_2 and H_2O adsorption on the catalyst. • Cu species suppress the electron–hole recombination and enhancing multi-electron reactions.
Xia et al. (2007)/[88]	TiO_2–MWCNT/–	Sol–gel and hydrothermal methods	CO_2 (1 mol), water vapor (5 mol)/15 W UV lamp (365 nm)/–	(298/–/7/5/–), (0.1/50/ nanoparticle/ –/supported)	Ethanol, formic acid/30, 19/–	• Catalyst is placed over a piece of transparent glass and then laid into a home-made stainless steel reactor. • MWCNTs in the composite catalysts can mitigate the accumulation of TiO_2 particles and decrease the recombination of electron–hole pairs. • MWCNTs have enhanced performance in the photocatalytic reactions as supports for TiO_2 compared with activated carbons.
Pan and Chen (2007)/[112]	1.0 wt% NiO–$InTaO_4$/2.6 eV	Solid state reaction and wet impregnation method	CO_2 (saturated), $KHCO_3$ (0.2 M aqueous solution)/500 W halogen lamp (365 nm)/–	(298/–/–/20/–), (0.14/ –/1–2 μm particles and pellets/–/suspended)	Methanol/1.4/–	• Continuous mode down-window type irradiation cell reactor made of Pyrex glass (75 mL) is used to carry out the photoreaction. • The methanol yield increases with the amount of NiO co-catalyst. • Catalysts have ability to reduce CO_2 to methanol under visible light illumination.
Qu et al. (2005)/ [106]	RuO_2-TiO_2 nanotube modified Pt electrode/–	Sol–gel method and laboratory synthesis	CO_2 (saturated), $NaHCO_3$ (0.5 M, 50 mL solution)/ Electrochemical reduction/–	(298/–/–/–/current efficiency 60.5[b]), (0.001/ –/25 nm nanoparticle composite electrode/ –/supported)	Methanol/–/–	• High efficiency and selectivity for electrochemical reduction of CO_2 depends on the surface structure of the nanotubes composite electrode. • Experiments are done in a standard three-electrode electrochemical cell where a saturated calomel electrode is used as the reference electrode.

Table 4 (*continued*)

Researcher (year)/Ref.	Catalyst composition/ band gap energy	Catalyst preparation technique	Reactants (amount)/ radiation source/light intensity	Operating variables (T/ P/pH/t/QE), physical properties (W/SA/PS/SC/ MP)	Major product/ yield (μmol h^{-1} g^{-1} catalyst)/ selectivity (%)	Comments
Slamet et al. (2005)/[109]	3% CuO–TiO_2/ 2.88 eV	Improved impregnating method	CO_2 (saturated), $KHCO_3$ (1M, 300 mL solution)/10 W UV black light lamp (415–700 nm)/2.45 mW cm^{-2}	(333/–/–/6/19.23), (0.3/ 45.8/23 nm particle/ –/suspended)	Methanol/ 442.5/19.23	• Slurry type photocatalytic reactor consists of a horizontal stainless steel vessel with an inner diameter and height of the vessel 140 and 50 mm, respectively having a plate cover at the top of the vessel is made of Pyrex. • The positive values of E_a indicate that desorption of products is the rate limiting step in the photosynthetic formation of methanol.
Gokon et al. (2003)/[97]	5 wt% ZnO on activated carbon/ 3.2 eV	Impregnation method	CO_2 (saturated), –/Xe lamp ($<$400 nm)/34000 mW cm^{-2}	(873/–/–/–/–), (0.10/ –/150–300 mm particle/ –/supported)	Carbon monoxide/ 2×10^5/–	• Sample is kept in quartz tube reactor (8 mm diameter) is supported from the both sides by alumina honey comb covered with quartz wool and irradiated by solar furnace simulator. • This is a high temperature operation for photocatalytic conversion of CO_2.
Xie et al. (2001)/ [107]	Pd–RuO_2 supported on TiO_2/–	Laboratory synthesis	CO_2 (saturated), NaOH with Na_2SO_3 (0.05 M)/450 W Xe short-arc lamp/–	(298/1/–/–/–), (0.02/ –/22 nm particle/ –/suspended)	Formate/72.3 [b]/ –	• Surface noble metal (Pd and Ru) deposition is a costly and economically infeasible for industrial purposes. • Reaction is carried out in a 30 mL Pyrex glass cuvette and stirred continuously by a magnetic stirring bar.
Subrahmanyam et al. (1999)/ [99]	10 wt% TiO_2–Pd supported on Al_2O_3/–	Impregnation method	CO_2 (saturated), $KHCO_3$ (0.5 M solution)/0.25 W Hg arc lamp/ –	(–/–/7.5/6/–), (–/–/particle/ –/suspended)	Acetone/8.5 [c]/–	• The experiment is conducted in a well-mixed heterogeneous batch type reactor. • Catalyst on support accomplishes the condition of a good photocatalyst to produce C1 and C2 compounds.
Liu et al. (1998)/ [96]	TiO_2- SiO_2 matrices/–	Sol–gel method	CO_2 (saturated), Lithium nitrate and propan-2-ol (20 and 1 mmol-dm^{-3},)/500 W Hg arc lamp (280 nm)/ 1000 mW cm^{-2}	(–/–/–/8/0.16), (–/290/ 5.3 nm spherical particle/3.89/Supported)	Formate/0.5 [c]/–	• It is decided that reduction reaction of nitrate ions is the rate-determining step of the formation of urea. • The photoreduction is carried out using a quartz cell (9 cm^3), whose top is sealed with a rubber septum and the transparent TiO_2–SiO_2 film coated on a quartz plate (2 cm^2) was vertically submerged in solutions.
Anpo et al. (1997)/[100]	1.1 wt % TiO_2 –Y zeolite cavities/–	Ion-exchange method	CO_2 (24 μmol), Water vapor (120 μmol)/75 W high-pressure Hg lamp ($>$280 nm)/–	(328/1.31 $\times$ 10^{-9}/–/6/–), (0.15/–/powder/ –/supported)	Methanol/5/–	• Based on Ti^{3+}, H atoms and C radicals, a molecular scale reaction mechanism has been proposed. • Highly dispersed isolated tetrahedral titanium oxide species deliberate the active sites for reaction systems.
Solymosi et al. (1994)/[91]	2% WO_3–TiO_2/–	Wet impregnation method	CO_2 (saturated), H_2O (120 mL)/500 W high pressure Xe lamp/ 0.68 mW cm^{-2}	(333/1/–/5/–), (0.3/18/ nanoparticle/0.0025/ Suspended)	Formic acid/ 1.4/–	•Reaction is carried out in a Pyrex glass cell where the reaction temperature is controlled by a surrounding water jacket in which the temperature of circulating water is regulated by an ultra-thermostat.
Ogura et al. (1992)/[108]	0.5 wt% CeO_2–TiO_2/–	Heating co-precipitation	CO_2 (0.13 atm), H_2O (0.032 atm)/500 W Xe lamp ($<$370 nm)/–	(298/1/–/18/–), (1/111/ nanoparticle/ –/suspended)	Hydrogen/0.26/ –	•Photocatalytic reaction is performed in an apparatus of closed circulating system (1.5 dm^3) and visible light irradiation is applied from the bottom via a rectangular quartz prism.

T/P/pH/t/QE: temperature (K)/pressure (atm)/pH/illumination period (h)/quantum efficiency (%).
W/SA/PS/SC/MP: weight of photocatalyst (g)/surface area (m^2/g)/photocatalyst structure (diameter)/semiconductor concentration (g/mL)/mode of photocatalyst.
'–': Not mentioned in the original paper.

[a] ppm h^{-1}.
[b] ppm.
[c] μmol h^{-1}.

photogenerated electron and hole progressively, and ultimately decreases the recombination rate.

It has been reported that hydrothermally-prepared KNb_3O_8 and HNb_3O_8 nanobelts show a high yield of methane compared with the same catalysts derived from conventional solid state reactions and commercial TiO_2 (Degussa P25) [85]. In the case of hydrothermal synthesis, this nanobelt-like morphology and protonic acidity produce higher photochemical activity for methane production through hydrogen bonding, which is facilitated by the separation and trapping of photogenerated carriers at the interlayer surface of HNb_3O_8 and KNb_3O_8. Ferroelectric materials can be used as remarkable substitutes for the standard semiconductor photocatalysts. Ferroelectric characteristics drive the electrons and holes apart because of the presence of an internal dipole. Therefore, this decreases the probability of the recombination of carriers and also inhibits the reaction of redox products, thus driving equilibrium towards the formation of products. For this ferroelectric behavior, a polar compound, $LiNbO_3$ was used by Stock and Dunn for the photocatalytic CO_2 conversion to formic acid under Hg lamp or direct natural sunlight irradiation [86].

3.1.2. Supported metal oxide photocatalysts

Several types of supportive materials were used in this technology such as zeolite, mesoporous SiO_2, kaolinite, Al_2O_3 and montmorillonite and other pillar materials. Table 3 demonstrates the textural belongings of the silica supports and the TiO_2-loaded samples with specific surface area, pore volume, and maximum pore size distributions [65]. The mesoporous SiO_2-prepared material MCM-41 shows a higher specific surface area and has an average pore size of 2.3 nm. The pore structure of supported materials is a vital factor. The pore structure manages the transportation of reactants and products to and from the surface, and controls the size of the active surface area [92]. In Table 4, detailed features and findings of aspects related to supported metal oxide semiconductors investigated in previous experimental works are highlighted critically. Titania charging on the silica matrix reduces the surface area of the supports and also decreases the pore volume, as the titania content increases. The reduction of pore volume shows that loading of semiconductor particles saturates the maximum space of the ordered channels within the support. This support helps to control the catalysts' size from crystal growth. High catalyst loading can cause pore blockage inside the channels, although the interconnection among the parallel pore channels should have the ability to reduce this effect [93]. The common photocatalytic reaction path for a supported metal oxide semiconductor is illustrated in Fig. 5.

Catalyst on supported materials has been carried out in many photocatalytic aqueous systems due to its immobilization in terms of easier separation of the catalyst after the photocatalytic reactions. It is reported that supported photocatalysts exhibit lower activities than powdered TiO_2 materials. However, treated photocatalysts show high activity because they contain cyanide and represent the dicyanoaurate photoreduction activity in order to $TiO_2/GrSiO_2 >$ Degussa P25 $> TiO_2$/SBA-15. Depending on the treatment processes, TiO_2/SBA-15 materials achieved up to eight times higher activity in comparison with the Degussa P25 TiO_2 [94]. The addition of Cu species on TiO_2–SiO_2 catalysts increased the overall CO_2 conversion efficiency by suppressing the electron–hole recombination and increasing multi-electron reactions [95] compared with only TiO_2–SiO_2 matrices [96]. It is reported that the addition of 0.5% Cu shows a highly specific surface area, but the addition of 1% and 3% Cu successively reduces the specific surface area. A multi-walled carbon nanotube (MWCNT)-supported TiO_2 composite catalyst was introduced by Xia et al. due to its unique electronic properties [88], and the results shows high conversion rates when a proper amount of MWCNTs is used as supports for TiO_2. Moreover, the MWCNT-supported composite catalysts are able to lessen the accumulation of the catalyst particles and reduce the recombination of electron–hole pairs by moving it along the tubes. Carbon is used as a catalyst support in gas-solid reaction phases with suitable temperatures and pressures, under which the carbon support remains stable. In a hydrogenation reaction carbon-supported iron catalysts with high dispersion were used at 1 atm and < 700 K because of carbon stability under these conditions [92]. The stability of activated carbon can be controlled by ZnO catalysts. The high reaction rate of the gasification of the

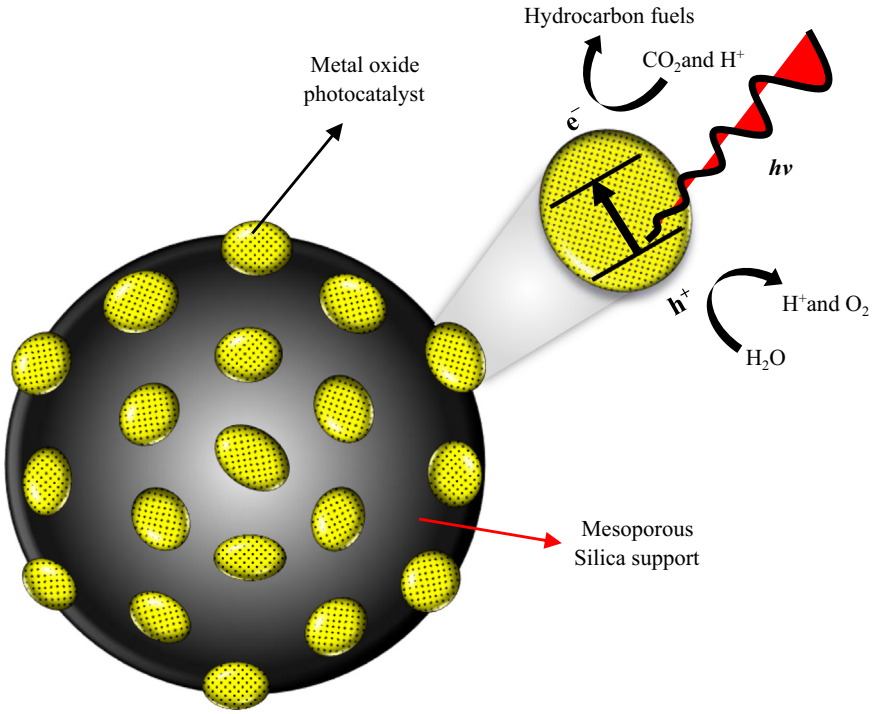

Fig. 5. Scheme of supported metal oxide photocatalysts during the photocatalytic reaction.

activated carbon is carried out with CO_2 by ZnO-loading in low temperatures [97]. The presence of an acidic medium in mixed oxide systems is suitable to achieve more knowledge on the physical nature of photocatalysts [98]. The oxide supported catalysts are treated by acidic medium due to the presence of oxygen species in the reaction systems, which leads to formation of the basic nature of the catalyst, as reported by Subrahmanyam et al. [99]. Zeolites are microporous, aluminosilicate minerals with a porous structure as traps for molecules to be analyzed. Investigation has shown that the TiO_2 particles are highly distributed inside the pore channels of zeolite with tetrahedral coordination which have high selectivity for the formation of CH_3OH [100]. At the same time, it was also found that Pt loading on TiO_2 catalysts in the presence of a zeolite support encourages the charge separation and increases the formation of CH_4 in lieu of CH_3OH by stimulating the reaction between the carbon radicals and H atoms formed on the Pt metals to produce CH_4.

Recently, montmorillonite has been loaded with TiO_2 structures to increase the surface area of TiO_2 particles [64]. Ultimately, in this research, the particle size of the catalyst was reduced from 18.73 to 13.87 nm and efficient charge separation was allowed. The band gap of TiO_2 was also reduced to 3.07 eV and permitted visible light irradiation during the photoreduction of CO_2 in the presence of water vapor. Effectual charge transfer between two semiconductors and response to visible light are found in the $FeTiO_3$–TiO_2 catalyst due to its unique band structure (2.7 eV) [101]. When the loading of $FeTiO_3$ on TiO_2 is increased from 10% to 50%, it shows lower surface area accordingly, from 55.8 to 35.7 $m^2\,g^{-1}$. Due to the small surface area, the high content of $FeTiO_3$ on TiO_2 provides a low production rate. Kaolinite is another promising supporting material in this technology. It is a clay mineral with a layered silicate mineral and one tetrahedral sheet connected through oxygen atoms to one octahedral sheet of octahedral alumina [102]. The Kaolinite/TiO_2 composite decreases the crystallite size of anatase TiO_2. Kaolinite increases the effective surface area for TiO_2 by avoiding TiO_2 aggregates in suspension and prevents the recombination of electron–hole pairs. It also hinders the growth of the crystallite and decreases the particle size from 26 nm to 18 nm [103]. In addition, 23.2% AgBr is highly dispersed on the surface of TiO_2 nanoparticles which exhibit strong absorption ability in the visible-light region and stability during repeated operation because of transferring photoexcited electrons from the conduction band of well-dispersed AgBr to that of TiO_2 [104]. RuO_2 is a favorable material which shows high electrical conductivity and electrochemical stability, intermediate hydrogen over-potential and the capacity to reversibly adsorb hydrogen for CO_2 reduction [105]. RuO_2 supported on TiO_2 nanotubes composite-modified Pt electrodes showed higher activity on the electrochemical reduction of CO_2 to methanol compared with RuO_2-modified Pt electrode according to the investigation of Qu et al. [106]. It was also found that RuO_2–TiO_2 nanotube modified electrodes are promising electrocatalysts compared to RuO_2–TiO_2 nanoparticle-modified electrodes due to the high dispersion of RuO_2 on the TiO_2 nanotubes surface and more surface area creating additional active sites. The photoreduction rate can be improved by the deposition of Pd metal on the surface of RuO_2–TiO_2, where photoelectrons are trapped by Pd and photoholes are confined at the RuO_2/SO_3^{2-} site [107]. WO_3 and CeO_2 were also applied on a TiO_2 support to investigate the photocatalytic activity [91,108], with CeO_2–TiO_2 showing visible light responsiveness. Loading of Rh on TiO_2 containing 2% WO_3 leads to the formation of more formic acid compared with WO_3–TiO_2 [91].

Some other investigations were published based on CuO, which is highly dispersed on TiO_2 [109,110]. By XRD analysis, it was found that the dispersion capability of CuO in the vacant sites of TiO_2 was approximately 4.16 $Cu^{2+}\,nm^{-2}$. A high percentage of CuO loading on TiO_2 slightly reduces the surface area of catalyst particles, and this slight change in surface area has a negligible effect on the reactivity of the catalyst [109]. On the other hand, 1 wt% CuO–TiO_2 exhibits high band gap energy (3.02 eV) with a lower production yield than that of 3 wt% CuO–TiO_2 (2.88 eV) [109]. Calcination temperature is also important in terms of production rate; 1 wt% CuO–TiO_2 calcined at 450 °C represents greater activity than that calcined at 350 °C and 550 °C [110].

Supported materials other than TiO_2 are also found to have reasonable photocatalytic activity. The use of NiO on several metal oxides like $InTaO_4$ and $InNbO_4$ are found in some publications for CO_2 reduction to fuel [111–113]. Also, 1 wt% NiO–$InTaO_4$ catalysts have low band gap energy of 2.6 eV, which is highly responsive to visible light, and can be used in different sorts of reactors like slurry, optical fiber and monolith reactors [40,111,114]. In case of the NiO–$InNbO_4$ catalyst, it also shows better activity due to the presence of core–shell type Ni^0 and NiO on the surface and the presence of a small amount of Nb_2O_5 as a promoter under visible light irradiation [113].

Zn_2GeO_4 is one of the important metal oxide catalysts in photoconversion technology, which is frequently used as a support for other oxide catalyst to enhance the photocatalytic CO_2 conversion. The Zn_2GeO_4 catalyst contains some superior properties like low crystal defects, extraordinary specific surface area and favorable microstructure on the surface of the catalyst, but the band gap energy is high enough (4.65 eV) to show visible light response [115]. Sheaf-like, hyperbranched Zn_2GeO_4 nanoarchitecture was developed by Liu et al., which was further modified by NH_3 flow to yellow $Zn_{1.7}GeN_{1.8}O$ solid solution for CO_2 conversion into carbonaceous fuel in the existence of water at ambient conditions under visible light irradiation [116]. The modified catalyst shows low band gap energy (2.6 eV), which is used as a support for 1 wt% Pt and 1 wt % RuO_2. Moreover, the loading of Pt and RuO_2 on $Zn_{1.7}GeN_{1.8}O$ gives a high conversion rate which is able to arrest the electron–hole pairs by preventing the recombination of electrons and holes.

3.2. *Modified/unmodified non-oxide photocatalysts for CO_2 recycling*

Non-oxide semiconductor photocatalysts are selected for CO_2 recycling because of a low band gap energy to facilitate the photocatalytic response to the visible light region, and high conversion efficiency is achieved due to their unique photobehavior. Elaborately major findings and characteristics of non-oxide semiconductors upon photocatalytic reactions are described in Table 5.

3.2.1. *Metal sulfide semiconductors*

It is investigated that semiconductor catalysts are one of the supreme sources for direct solar energy conversion. Many wide-ranging reviews have already been published on the advancement of oxide or non-oxide semiconductor photoactive materials [117–120]. It was found that beyond the metal oxide semiconductor catalysts, metal sulfide semiconductor materials also have effective photoactivity because of their outstanding ability to absorb solar spectrum with high energy yield [121]. Metal sulfides have comparatively high conduction band states that are more appropriate for enhanced solar responses than metal oxide semiconductors, facilitated by the higher valence band states consisting of S3p orbitals [121]. It was reported that in order to absorb the entire UV and visible light region of solar irradiation, the ZnS–$AgInS_2$–$CuInS_2$ solid solution was capable due to the existence of an absorption edge up to 800 nm [122]. Fujiwara et al. investigated ZnS–DMF(OAc) for the CO_2 photoreduction process [123]. They found that the close interaction of acetate ions to Zn atoms

Table 5
Recent studies on modified/unmodified non-oxide catalysts for CO_2 photoreduction; preparation methods and major findings.

Researcher (year)/Ref.	Catalyst/band gap energy	Catalyst treatment/ preparation technique	Reactants (amount)/ radiation source/light intensity	Operating conditions (T/P/pH/ t/QE), operating variables (W/SA/PS/ SC/MP)	Major product/ yield ($\mu mol\ h^{-1}\ g^{-1}$ catalyst)/ efficiency (%)	Comments
Kočí et al. (2011)/ [125]	ZnS deposited on MMT/ 3.89 ± 0.03 eV	Na_2S, CTA and Zn $(AcO)_2$ Mixing by vigorous stirring	CO_2(saturated), NaOH (0.2 M solution)/8 W Hg lamp (254 nm)/–	(273/1/–/24/–), (0.1/ –/nanocomposite/ 0.001/suspended)	Methanol, methane/1.41, 1.33/–	• It is analyzed that products yields depend on the reactor diameter and on the volume of the liquid phase. • Slurry type two stirred batch annular reactors is used with three quartz glass tubes of different diameters (3.5, 4.0 and 4.5 cm) placed inside the reactors. • Perfect mixing is one of the most important factors in slurry reactors and this mixing is difficult in annular reactors.
Yuan et al. (2011)/ [132]	Pt loaded on CdS–TNT/–	Alkaline hydrothermal method and immersing TNT in $Cd(CH_3COO)_2$ with heat treatment	CO_2 (5000 ppm), Water vapor (–)/UV–vis and visible light irradiation/–	(298/–/–/6/–), (–/–/nanotube/ –/supported)	Methane/ 7800 [b]/–	•Adsorption of intermediate products (CO, O_2) on Pt and the oxidation of Pt might be the reasons for the deterioration of photocatalytic reaction.
Praus et al. (2011)/ [127]	6 wt% CdS–montmorillonite/ 2.63 ± 0.09 eV	Deposition of originated CdS–CTA micelles on montmorillonite	CO_2 (saturated), NaOH (0.2 mM) aquous solution/ 8 W Hg lamp (254 nm)/–	(–/–/6.7/24/–), (0.1/ –/5 nm partical/ 0.001/suspended)	Methane/ 0.93/–	• Montmorillonite (MMT) serves as a carrier of CdS nanoparticles that were attached to its external surface. • A stirred batch annular reactor is used with a suspended catalyst.
Li et al. (2011)/ [133]	15% Bi_2S_3–CdS/ 1.28 eV	Hydrothermal direct reaction	CO_2 (saturated), NaOH–Na_2S aqueous solution (200 mL)/ 500 W Xe lamp (200–700 nm)/–	(–/–/–/5/–), (0.2/24/ 12 nm particles/17/ suspended)	Methanol/ 120/–	• Results show that the photocatalytic activity and visible light response of Bi_2S_3 are higher than those of CdS. • Reaction is carried out in a XPA-II photochemical reactor with a magnetic stirrer, a quartz cool trap, and a condensation tube.
Barton et al. (2008)/ [138]	p-GaP/2.24 eV	–	CO_2 (–), Pyridine (10 mm)/ 200 W Hg–Xe arc light (365 nm)/0.92 mA cm^{-2} [a]	(–/–/5.2/–/44), (–/–/semiconductor electrodes/ –/supported)	Methanol/ –/10.9	•Aqueous photoelectrochemical cell is used where light energy is the only energy used to carry out the reaction.
Zhang et al. (2004)/ [135]	MnS/3.0 eV	Laboratory synthesis	CO_2 (saturated), Deoxygenated water (500 mL)/450 W medium-pressure Hg arc lamp (200–400 nm)/0.6 mW cm^{-2}	(308/–/7.5/0.5/4.5), (0.5/–/particles/ 0.001/suspended)	Formate/ 220 [c]/–	• Results represent some prebiotic syntheses have arose via photoelectrochemical reactions on semiconducting minerals. • Insufficient reductiveness of conduction-band electrons is a limitation in this system. • The reaction is carried out in a commercial photochemical reactor consisting of a 0.5 L glass reaction vessel with a water jacket for temperature control.
Shioya et al. (2003)/ [145]	Ti-mesoporous silica thin film (hexagonal)/–	Solvent evaporation method	CO_2 (36 μmol), water vapor (180 μmol)/100 W high pressure Hg lamp/ 0.265 mWc m^{-2}	(323/9.8×10^{-10}/–/6/ 0.28), (0.05/900/ 1.9 nm pore size/ –/supported)	Methane, methanol/ 7.2, 1.98/–	• Advanced transparent Ti-containing thin film is used as photocatalysts having unique and high photocatalytic activity. • The films have hexagonal pore structure with higher photocatalytic activity than the Ti-MCM-41 powdered catalyst even with the same pore structure. • A quartz cell with a flat bottom (88 cm^3) is used to carry out the reaction.
Ikeue et al. (2002)/ [146]	Ti-containing porous silica thin films/–	Solvent evaporation method	CO_2 (36 μmol), water vapor (180 μmol)/100 W Hg lamp/ 0.265 mWc m^{-2}	(323/9.8×10^{-10}/–/8/ 0.28), (0.05/–/Thin nanofilm/ –/supported)	Methane, methanol/ 8.75, 2.12/–	• Self-standing porous silica thin films with hexagonal pore structures are used as photocatalysts show higher photocatalytic activity than the same pore structured Ti-MCM-41 powder catalyst. • The concentration of the surface OH groups have a role in the high

Table 5 (*continued*)

Researcher (year)/Ref.	Catalyst/band gap energy	Catalyst treatment/ preparation technique	Reactants (amount)/ radiation source/light intensity	Operating conditions (T/P/pH/ t/QE), operating variables (W/SA/PS/ SC/MP)	Major product/ yield (μmol h^{-1} g^{-1} catalyst)/ efficiency (%)	Comments
						selectivity. • Reaction is conducted on a quartz cell with a flat bottom (88 cm^3) linked to a conventional vacuum system.
Ikeue et al. (2001)/ [147]	Ti-β zeolite	Hydrothermal synthesis method	CO_2 (36 μmol), H_2O (180 μmol)/100 W high-pressure Hg lamp (> 250 nm)/0.265 mW cm^{-2}	(323/9.8 × 10^{-10}/–/6/ –), (0.05/630/0.25–0.50 μm particles/ –/suspended)	Methane/5.5/11	• Ti-β zeolite shows the titanium oxide species are highly dispersed in their frameworks in a tetrahedral coordination state. • H_2O attraction to the zeolite surface run to a strong influence on the reactivity and selectivity. • The properties of the zeolite cavities are important factors to regulate the reactivity and selectivity.
Ulagappan and Frei (2000)/ [148]	Ti silicalite (TS-1) molecular sieve/ –	Promoter-induced enhancement method	CO_2(saturated), Methanol (–)/266-nm pulsed Nd:YAG laser at 10 Hz/30 mW cm^{-2}	(298/0.0066/–/4/–), (0.022/–/266 nm sieve nanocomposite/ –/supported)	Formic acid, carbon monoxide/–/–	• TS-1 wafer is held in a small infrared vacuum cell with CaF_2 windows, which is fixed inside an Oxford cryostat model Optistat. • This study first represents the understanding into the initial steps of CO_2 photoreduction in a framework Ti molecular sieve.
Hinogami et al. (1998)/ [143]	Cu, Ag, Au–(p-Si)/1.12 eV	Metal particles are deposited on p-Si electrode	CO_2 (saturated), $KHCO_3$ (0.1 M)/tungston–halogen lamp/100 mW cm^{-2}	(298/1/6.8/–/–), (–/–/Particles on Si electrode/ –/supported)	Carbon monoxide, hydrogen/–/–	• Photoelectrochemical reduction is carried out on p-type silicon electrodes modified with small metal (Cu, Ag, or Au) particles. • Reaction is conducted on H-shaped Pyrex cell with a reference calomel electrode and a Pt plate as the counter electrode.
Eggins et al. (1998)/ [128]	CdS colloids/ 2.4 eV	Laboratory synthesis	CO_2 (saturated), TMACl (solution)/medium pressure Hg lamp/ 2.5 × 10^{-3} einsteins h^{-1}	(–/–/4/42/0.48), (0.3/ –/2–4 nm nanoparticle/ –/suspended)	Glyoxylate/ 53 [d]/–	• Photoreduction using ZnO, SiC, $BaTiO_3$ and Sr TiO_3 in absence of tetramethylammonium ions produced formate and formaldehyde. • In this system, the effectiveness of 'hole acceptor' compounds is shown to be related to their redox potentials.
Liu et al. (1998)/ [129]	CdS surface modified by thiol/–	Laboratory synthesis	CO_2 (–), 2-propanol (1 M)/ 500 W high pressure Hg arc lamp (300 nm)/ 1000 mW cm^{-2}	(298/–/–/7/–), (0.72/ –/50 nm particle/ –/suspended)	Formate, carbon monoxide/1.5, 0.75 [e]/–	• It is found that formate to carbon monoxide production became greater with increase of the surface modification of CdS. • A quartz cell of a 7.0 cm^3 capacity is used to carry out the reaction with sealed top by a rubber septum.
Fujiwara et al. (1998)/ [123]	ZnS–DMF (OAc)/ –	Colloidal ZnS–DMF is prepared from deaerated DMF solution of $Zn(OAc)_2$	CO_2 (saturated), deaerated DMF solvent (2 mL)/UV light (> 290 nm)/–	(298/–/–/5/–), (10 [f]/ –/2 nm nanoparticle/ –/suspended)	$HCOO^-$/–/–	• Excess zinc acetate increases the efficiency of the system and prevents the formation of sulfur vacancies as catalytic sites. • Together HCOO- and CO are produced in presence of excess zinc perchlorate in this system.
Fujiwara et al. (1997)/ [130]	CdS surface modified by DMF/2.4 eV	Laboratory synthesis	CO_2 (–), TEA (1 M)/300-W halogen tungsten lamp (> 400 nm)/–	(298/–/–/–/–), (–/–/nanocrystallites/ –/suspended)	Carbon monoxide/–/–	• Addition of excess Cd^{2+} to the system increases the photocatalytic activity. • Sulfur vacancies supported by in situ Cd changes the coordination numbers of cadmium-sulfur and cadmium–oxygen. • A closed Pyrex tube (8 mm diameter) is used to conduct the photoreduction.

Table 5 (*continued*)

Researcher (year)/Ref.	Catalyst/band gap energy	Catalyst treatment/ preparation technique	Reactants (amount)/ radiation source/light intensity	Operating conditions (T/P/pH/ t/QE), operating variables (W/SA/PS/ SC/MP)	Major product/ yield ($\mu mol\ h^{-1}\ g^{-1}$ catalyst)/ efficiency (%)	Comments
Inoue et al. (1995)/ [134]	0.025 mol% Cd–ZnS/3.66 eV	Photodeposition method	CO_2 (saturated), $NaHCO_3$ (50 μL, 1.5×10^{-3} M solution)/500 W high-pressure Hg arc lamp/–	(–/–/5.5/1/32.5), (–/200/nanoparticle/ –/suspended)	Formate/10.5 [e]/ –	• It is found that solid solutions of ZnS–CdS microcrystals do not show high activities for the photoreduction of CO_2. • The production of CO was observed for a CdS mole fraction of 0.5–0.67.
Cook et al. (1988)/ [144]	Cu–(p-SiC)/–	Suspensions of p-SiC and Cu particles	CO_2 (–), $KHCO_3$ (0.5 M aquous solution)/Hg lamp (> 275 nm)/8 mA cm^{-2}	(313/1/–/–/6), (0.1/ –/particles/ –/suspended)	Methane/0.63/ –	• It is found that formaldehyde can be reduced in aqueous electrolyte to give methane. • Photoelectrochemical (PEC) reduction of CO_2 is done in this system.
Aurian-Blajeni et al. (1983)/ [142]	p-GaAs/–	–	CO_2 (saturated), KCl (0.5 M solution)/150 W Xe lamp/–	(298/8.5/–/–/–), (–/–/semiconductor electrode/ –/supported)	Formic acid/ 170 [e]/–	• A photoelectrochemical autoclave, fitted with a quartz window is used to carry out the reaction. • Adsorption of the CO_2 on the semiconductor surface clearly plays an important role in the process. • The electrodes are not stable, and worsen noticeably within several hours.
Inoue et al. (1979)/ [61]	CdS, GaP and SiC/ 2.4, 2.3 and 3.0 eV	Purity 99.5–99.99%	CO_2 (saturated), H_2O (100 mL)/500 W Xe or high pressure Hg lamp/–	(298/1/5/7/–), (1/ –/200–400 mesh powder/ –/suspended)	Formaldehyde, methanol/(29, 17), (14, 16) and (14, 76)/–	• Magnetic stirred glass cell with quartz window is used for photoreduction of CO_2. • Photoexited electron in the more negative conduction band poses higher ability to reduce CO_2.
Halmann (1978)/ [136]	p-GaP single crystal/2.25 eV	–	CO_2 (saturated), K_2HPO_4 solution (0.05M)/High pressure Hg lamp/ 2.63 mW cm^{-2}	(298/–/6.8/90/–), (–/2.4×10^{-5}/ semiconductor electrode/ –/supported)	Formic acid/50 [f]/0.61	•Closed bubble walled borosilicate glass beaker (30 mL) with thermostat is used as a photoelectrochemical reactor.

T/P/pH/t/QE: temperature (K)/pressure (atm)/pH/illumination period (h)/quantum efficiency (%).
W/SA/PS/SC/MP: weight of photocatalyst (g)/surface area (m^2/g)/Photocatalyst structure (diameter)/semiconductor concentration (g/mL)/mode of photocatalyst.
'–': Not mentioned in the original paper.

[a] current density.
[b] μmol h^{-1}.
[c] μM.
[d] μmol dm^{-3}.
[e] μmol.
[f] mM.

inhibited the creation of sulfur vacancies as catalytic sites of CO production. Moreover, surface dimethylformamide (DMF) solvated Zn atoms give more efficiency to $HCOO^{\bullet -}$ formation. On the other hand, the addition of excess Zn^{2+} increases the size of ZnS–DMF (OAc) through the reaction between excess Zn^{2+} and the surface of ZnS–DMF(OAc) nanocrystallites. ZnS deposited on montmorillonite (MMT) was also fabricated by Koci et al. with particle sizes of 3–5 nm, which provided a significantly high productivity compared with the commercial TiO_2 Degussa P25 [124,125]. They used cetyltrimethylammonium (CTA) with ZnS nanoparticles to inhibit the formation of bigger agglomerates. Different percentages of ZnS loading on a porous SiO_2 matrix was also applied to investigate the improved photocatalytic yields [126].

In 1979, Inoue et al. introduced non-oxide semiconductor catalysts (CdS, GaP and SiC) for the photocatalytic conversion of CO_2 to fuels [61]. Among them, CdS showed comparatively better yields for CO_2 conversion. It can be seen in Table 5 that narrow band gap (2.63 eV) CdS supported on montmorillonite exhibits a lower conversion yield than that of ZnS of 3.89 eV deposited on MMT, while the CdS–MMT system has high stability in presence of CTA [125,127,128]. Not only that, but CTA acts as a binder among CdS and MMT particles. The phtocatalytic conversion of CO_2 on a CdS semiconductor with a surface modified by different types of thiol compounds was performed in the presence of 2-propanol solvent [129]. In this study, the major products were found formate and carbon monoxide. The ratio of formate to carbon monoxide is highly dependent on the solvent, and increases with an increasing dielectric constant of the solvent. Moreover, a surface modifier is used in this system to fix the surface Cd^{2+} sites to decrease the adsorption of $CO_2^{\bullet -}$ on Cd^{2+} sites and, then formate yield will be high, with the increasing surface exposure of the modifier. Another study showed that extra Cd^{2+} addition to the CdS–DMF system forms sulfur vacancies on the surface of nanocrystallites because of the adsorption of excess Cd^{2+} on the surface [130]. Over the surface of sulfur vacancies, CO_2 takes electrons sequentially after developing a $Cd^{2+}OCOCO_2$ complex to react with another CO_2, leading to the formation of CO, as reported in electrical CO_2 reduction to CO [131].

Yuan et al. investigated CdS–TNT loaded with Pt to carry out the photochemical reaction under visible light irradiation, but they

found that a worsening effect of photochemical reaction occurred due to the adsorption of intermediate products (CO, O_2 etc.) on Pt and the oxidation of Pt [132]. Another approach was led by Li et al. for visible light responsive photocatalytic CO_2 reduction on modified CdS with 15% Bi_2S_3 [133]. Investigations show that the Bi_2S_3 catalyst alone has a higher photochemical activity and visible light response than CdS. The addition of Bi_2S_3 increased the photochemical performance of CdS, and maximum yield was obtained 120 $\mu mol\ h^{-1}\ g^{-1}$ catalyst. Cd–ZnS was investigated to compare the photocatalytic behavior with solid solutions of ZnS–CdS microcrystals [134]. Cd–ZnS shows higher activity than ZnS–CdS because Cd is more able to improve the quantum efficiency of the photochemical reduction of formate due to its ability to activate CO_2 more effectively in a photoreaction. Zhang et al. introduced another metal sulfide semiconductor catalyst (MnS) which can be used under solar spectrum more competently due to the lower band gap energy (3.0 eV) [135]. Like CdS, MnS semiconductor materials also have a distinct behavior of containing highly reducing conduction band electrons which are active enough to encourage the reduction of CO_2 [135]. For this reason, MnS semiconductors deliver higher quantum efficiency than other common catalysts such as TiO_2.

3.2.2. Metal phosphide semiconductors

The use of catalysts for photochemical purposes without incorporating co-catalysts such as p-type GaP and p-type InP have also been studied due to the narrow band gap to facilitate a visible light response [136,137]. Basically, in the photoelectrochemical CO_2 conversion process, p-type metal phosphide (GaP) was used mainly in methanol production, but required remarkably high over potentials [138]. However, high faradaic efficiencies for the photoelectrochemical reduction of CO_2 to CO have also been investigated with electrolytes used in the non-aqueous form; nevertheless, high over-potential is necessary to obtain the high faradaic efficiency [139]. Barton et al. found that p-type GaP was able to obtain a faradaic efficiency of 100% while converting CO_2 to methanol at low potentials which was more than 300 mV below the standard potential of −0.5 V versus the saturated calomel electrode (SCE) [138]. Habisreutinger et al. reported that p-type GaP semiconductor exhibits low band gap energy (2.24 eV) and possesses high reducing conduction band electrons to ease the reduction of CO_2 [140]. On the other hand, in CO_2 photocatalytic conversion, it was detected that p-type InP provided high selectivity for formic acid in photoelectrochemical cells [141]. Moreover, according to Kaneco et al., p-InP is an active substantial for the photoelectrochemical reduction of CO_2, which revealed a positive potential of 0.2–0.4 V, which was larger than those of p-Si and p-GaAs photocathodes in the electrolysis of methanol electrolytes [137].

3.2.3. Other non-oxide semiconductors

Blajeni et al. carried out aqueous CO_2 photoelectrochemical reduction by using p-GaP and p-GaAs as photocathodes [142]. Unlike p-GaP, faradaic efficiency increases when the reaction is conducted with a p-GaAs semiconductor with a more negative potential, as this contributes a degree of cathodic protection. Modified p-type silicon (p-Si) electrodes with Cu, Ag, and Au foreign elements have been investigated by Hinogami et al., and extraordinary activation energy was found for CO_2 photoreduction [143]. Metal element deposition on p-Si electrodes not only induce photocatalytic activity, but also produce high photovoltages. Moreover, CO_2 photochemical reduction is activated by an upward shifting of surface band energies of p-Si in terms of achieving an energy level which is identical between the semiconductor and the solution reactants [143]. Another investigation has also been carried out on p-type SiC modified by Cu particles to investigate the photoelectrochemical ability for CO_2 reduction [144].

Ti-containing mesoporous silica thin film materials have been introduced in photochemical reduction of CO_2 due to their unique and high photocatalytic performances [145]. Spectroscopic analysis proved that Ti ions were highly dispersed in silica networks, and the silica thin films acted as effective photocatalysts during the photoreactions. Also, the hexagonal pore construction inside the films revealed superior photosensitivity compared with the same pore structured Ti–MCM-41 powdered catalyst [145,146]. Moreover, FTIR investigations found that Ti-containing silica thin film possessed surface OH groups in various concentrations, which had a significant influence on CH_3OH formation [146]. Ikeue et al. also studied Ti-containing β-zeolite treated with $OH^{\bullet -}$ and $F^{\bullet -}$ ions as structure directing agents (SDA), and showed hydrophilic and hydrophobic properties, respectively [147]. Hydrophilic properties have high photocatalytic efficiency due to the easy interaction of H_2O molecules with the tetrahedral-coordinated titanium oxide species on Ti–β-zeolite (OH) compared to on Ti–β-zeolite (F).

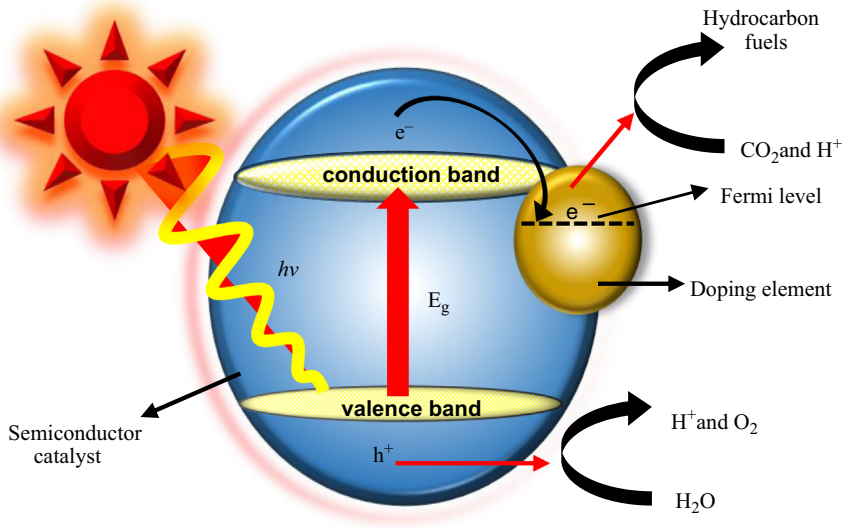

Fig. 6. General photocatalytic view of a doped semiconductor.

Table 6
Recent studies on catalysts which are modified by metal doping for CO_2 photoreduction; preparation methods and major findings.

Researcher (year)/Ref.	Catalyst composition/ band gap energy	Catalyst preparation/ treatment technique	Reactants (amount)/ radiation source/light intensity	Operating variables (T/P/pH/t/ QE), physical properties (W/SA/ PS/SC/MP)	Major Product/ Yield ($\mu mol\ h^{-1}\ g^{-1}$ catalyst)/ selectivity (%)	Comments
Zhai et al. (2013)/ [185]	1.7 wt% Cu–0.9 wt % Pt-TiO_2/–	Photodeposition technique	CO_2 (saturated), H_2O (4.0 mL)/200 W Xe lamp (320–780 nm)/–	(323/2/–/4/–), (0.02/–/7.3 nm particles/ –/suspended)	Methane/33/85	• Cu_2O delivers sites for the activation of CO_2 in presence of H_2O, while Pt extracts the photogenerated electrons from TiO_2. • A stainless-steel reactor with a quartz window on the top is used to carry out the reaction.
Mankidy et al. (2013)/ [187]	Ag–Pt–TiO_2/–	Galvanic replacement reaction and sol–gel method	CO_2 (–), Water vapor (–)/100 W Hg lamp (330 nm)/–	(298/1/–/6/–), (1/ –/nanoparticles/ –/supported)	Methane/–/80	• Combination of both bimetallic co-catalysts and Ag-SiO_2 nanoparticles increase product yields and enhanced activity in comparison to native TiO_2. • A batch reactor is used with three optical windows; one glass window at the top for photoirradiation and two ZnSe windows on two sides.
Li et al. (2012)/ [163]	0.5 wt % Pt–$NaNbO_3$/3.29 eV	Typical furfural alcohol derived polymerization −oxidation process	CO_2 (saturated), H_2O (3 mL)/300 W Xe arc lamp/–	(–/0.78/–/8/–), (0.1/ 28.6/powder/ –/supported)	Methane/4.9/–	• It is found that H_2 development and CO_2 reduction over cubic $NaNbO_3$ are closely twice of those over orthorhombic $NaNbO_3$. • Cubic $NaNbO_3$ can be qualified to its unique electronic structure, which is useful for electron excitation and transfer. • Catalysts are put on a small glass cell inside the Pyrex reaction cell with gas closed circulation system.
Shi and Zou (2012)/ [162]	Pt-$KNbO_3$/3.1 eV	Solid state reaction	CO_2 (saturated), H_2O (3 mL)/300 W Xe lamp/–	(–/–/–/6/–), (0.1/ 3.4/1 μm particle/ –/suspended)	Methane/70 [a]/–	• It is detected that $KNbO_3$ displays a higher photocatalytic activity than $NaNbO_3$ due to the narrower band gap and higher mobile charge carriers. • Catalysts are uniformly put on the bottom of a small glass cell that is placed in a Pyrex glass cell.
Iizuka et al. (2011)/ [172]	1 wt% Ag–$BaLa_4Ti_4O_{15}$, and Ag-$SrLa_4Ti_4O_{15}$/ 3.79 and 3.8 eV	Polymerizable complex method and impregnation method	CO_2 (saturated), H_2O (360 mL)/400 W high pressure Hg lamp/–	(–/–/–/7/–), (0.3/ –/10 nm particles/ –/suspended)	Carbon monoxide, formic acid/ (17.33, –) and (7.7, 4.3)/–	• Ag co-catalyst performs as a CO_2 reduction site to form CO. • Development of O_2 in a stoichiometric ratio (H_2+CO:O_2=2:1 in a molar ratio) shows that water is used up as a reducing reagent • An inner irradiation cell made of quartz is used to carry out the photocatalytic reduction of CO_2.
Yang et al. (2011)/ [180]	0.05 wt% Ti–SBA-15/–	Synthesized by filtration, washing, drying, and calcination at 550C for 6 h	CO_2 (saturated), Water vapor (76 μmol)/120 W high pressure Hg lamp (280 nm)/150 mW cm^{-2}	(313/1/–/7/–), (0.05/81/nano-porous, 3.2 nm pore size/ –/supported)	Ethane, methane/0.02, 0.016/–	• A combination of CO and H_2O leads the highest amounts of CH_4, C_2H_4, and C_2H_6, while a mixture of CO_2 and H_2 leads the lowest production rate of these products. • A multiple batch cylindrical photoreactor (50 mL) is used to conduct the reaction.
Yui et al. (2011)/ [32]	2 wt% Pd–TiO_2/–	Photochemical deposition	CO_2 (saturated), H_2O (1.5 mL)/500 W high-pressure Hg arc lamp (> 310 nm)/–	(278/–/4.1/5/–), (0.15/ –/nanoparticle/0.1/ suspended)	Methane/0.56/–	• Lengthy irradiation shows deactivation of the photocatalysis of Pd–TiO_2 due to the partial oxidation of the deposited Pd to PdO. • Catalysts are put in a round-shaped quartz vessel of inner diameter 6 cm.
Zhang et al. (2011)/ [164]	1 wt% Pt–Zn_2GeO_4/4.5 eV	Ion exchange method	CO_2 (saturated), H_2O (–)/Arc Xe lamp (635 nm)/–	(298/–/14/12/0.2), (–/90.5/200 nm particle/ –/supported)	Methane/28.9 [a]/ –	•Ion exchange synthesized catalyst shows activity activity in photoreduction of CO_2 in comparison with Zn_2GeO_4 synthesized by a solid state reaction.
Wang et al. (2011)/ [188]	[ReI$(CO)_3$(dcbpy) Cl]–$Zr_6O_4(OH)_4$(bpdc)/ –	Mix-and-match synthetic strategy	CO_2 (–), acetonitrile (2 mL) and TEA (0.1 mL)/ 450 W Xe lamp (> 300 nm)/–	(–/–/–/16/–), (0.02/ 277/metal–organic frameworks/ –/suspended)	Carbon monoxide/42/–	•These stable and porous metal complex-derivatives doped metal organic frameworks are very active catalysts for a range of reactions related to solar energy application.

Table 6 (*continued*)

Researcher (year)/Ref.	Catalyst composition/ band gap energy	Catalyst preparation/ treatment technique	Reactants (amount)/ radiation source/light intensity	Operating variables (T/P/pH/t/ QE), physical properties (W/SA/ PS/SC/MP)	Major Product/ Yield (μmol h^{-1} g^{-1} catalyst)/ selectivity (%)	Comments
Ampelli et al. (2010)/ [160]	0.5 wt% Pt–TiO_2/–	Sol–gel dipcoating for TiO_2 film and wet impregnation to add Pt	CO_2 (–), NaOH (1 M aqueous solution)/60 W solar lamp/–	(313/19.3/–/7/–), (–/–/nanoparticle/ –/supported)	Hydrogen/5.3 [b]/ –	• Require development of the current limits, related to the design of the photoanode and electrocathode to increase acitivity. • Photoelectrochemical solar cell is designed by Plexiglas and equipped with a quartz window and 5.7 cm^2 irradiated area.
Nishimura et al. (2010)/ [177]	Cr–TiO_2/–	Sol–gel and dip-coating method	CO_2 (5.76 mmol), H_2O (5.56 mmol)/Xe arc lamp (185–2000 nm)/ 43.67 mW cm^{-2}	(343/9.8/–/72/–), (–/–/film/3.9/ supported)	Carbon monoxide/1285/ –	• The total layer number of Cr–doped TiO_2 film coated is up to 7. • Cr–TiO_2 film is inserted into the stainless pipe, equipped with quartz glass disc fixed to the top of the stainless pipe.
Nguyen and Wu (2008)/ [183]	1 wt% Cu–Fe- TiO_2 films/2.93 eV	Dip coating method or doctor blade technique	CO_2 (saturated), water vapor (–)/150 W UVA lamp (320–500 nm)/ 225 mW cm^{-2}	(348/–/5/4/0.001), (–/47.74/film of 878 nm thickness/ –/supported)	Methane, ethylene/0.06, 0.35/–	• A continuous circular Pyrex glass reactor (216 cm^3) with a quartz window, where catalyst coated optical fibers are gathered inside it. • Fe as a co-dopant is indicated to reduce the photoproduction of methane in this experiment.
Nguyen and Wu (2008)/ [184]	0.5 wt% Cu–Fe-(TiO_2–SiO_2)/ 2.95 eV	Sol–gel method	CO_2 (saturated), H_2O (–)/natural sunlight/ 2.05 mW cm^{-2}	(348/–/–/6/0.0182), (0.5/44.7/53 nm thickness film/ –/supported)	Methane/0.279/ 0.0152	• Introducing of Fe metal into TiO_2–SiO_2 lattice shows the full visible light absorption and superior production of methane as compared to that of bare TiO_2–SiO_2–acac. • A continuous circular Pyrex glass reactor (216 cm^3) with a quartz window, where catalyst coated optical fibers are gathered inside it.
Hwang et al. (2005)/ [181]	0.29 wt% Ti–SBA-15 (Si/Ti=270)/–	Modified hydrothermal method	CO_2 (36 μmol), Water vapor (180 μmol)/100 W High pressure Hg lamp (> 250 nm)/–	(323/9.8 × 10^{-10}/ –/12/–), (0.05/1040/ 6.9 nm pore size/ –/imobilized)	Methane, methanol/0.31, 0.081/–	• Ti–SBA-15 shows reactivity much higher than bulk TiO_2. • Cationic rhenium (I) complex into a mesoporous AlMCM-41 material by ion-exchange method shows visible light response. • A quartz cell (88 cm^3) with a flat bottom is used to carry out the reaction.
Guan et al. (2003)/ [176]	Pt–$K_2Ti_6O_{13}$ with Fe-based catalyst supported on Y-type zeolite/–	Steam dealumination, impregnation and photochemical deposition method	CO_2 (saturated), H_2O (4 mL)/300 W Xe lamp, or concentrated sunlight/–	(298/0.76/–/6/–), (0.3/–/powder/ –/supported)	Hydrogen/15.2/ –	• The reaction temperature expressively influenced by concentrating the solar irradiation, reaching 600 K and increasing the yields. • Catalysts are kept on wet quartz wool (a wet bed for the catalyst layer) in an optical quartz tube cell.
Tseng et al. (2002)/ [168]	2 wt% Cu–TiO_2/–	Modified sol–gel process	CO_2 (–), NaOH (300 mL, 0.2 N aqueous solution)/ Hg lamp (254 nm)/–	(323/–/7/6/–), (0.3/ 26/20 nm particle/ –/suspended)	Methanol/20/–	• Result shows that a higher positive zeta potential at pH 7 can lead higher activity. • A cylindrical quartz reactor with a capacity of 300 mL is used to carry out the reaction.
Anpo et al. (1998)/ [189]	1.0 wt % Pt–Ti-MCM-48 (Si/ Ti=80)/–	Hydrothermal and impregnating methods	CO_2 (24 μmol), water vapor (120 μmol)/high pressure Hg lamp (> 280 nm)/–	(328/1.3 × 10^{-9}/ –/–/–), (–/–/ > 2 nm pore size/ –/supported)	Methane/12/–	• The charge transfer excited state of highly dispersed titanium oxide species plays an important role in the reduction of CO_2 and shows a high selectivity for the formation of CH_3OH. • A quartz cell with a flat bottom is used to reduce CO_2 with H_2O.
Anpo et al. (1997)/ [100]	1 wt % Pt–(TiO_2–Y–zeolite)/–	Impregnation method	CO_2 (24 μmol), water vapor (120 μmol)/75 W high-pressure Hg lamp (> 280 nm)/–	(328/1.3 × 10^{-9}/ –/6/–), (0.15/ –/powder/ –/supported)	Methane/0.08/–	• The titanium oxide species are highly dispersed within the zeolite cavities and exist in a tetrahedral coordination. • Adding Pt to the anchored titanium oxide catalysts encourages the charge separation with increasing CH_4 yields in place of CH_3OH.

Table 6 (*continued*)

Researcher (year)/Ref.	Catalyst composition/ band gap energy	Catalyst preparation/ treatment technique	Reactants (amount)/ radiation source/light intensity	Operating variables (T/P/pH/t/ QE), physical properties (W/SA/ PS/SC/MP)	Major Product/ Yield (μmol h^{-1} g^{-1} catalyst)/ selectivity (%)	Comments
Solymosi and Tombacz (1994)/ [91]	1 wt% Rh–TiO_2/–	Wet impregnation method	CO_2 (saturated), H_2O (120 mL)/500 W high pressure Xe lamp/ 0.68 mW cm^{-2}	(333/1/–/5/–), (0.3/ 18/nanoparticle/ 0.0025/suspended)	Formic acid/1.6/ –	• An increase in the electron concentration of TiO_2 enhances the production of organic compounds. • A Pyrex glass cell is used to carry out the photocatalytic reduction of CO_2 with H_2O.
Adachi et al. (1994)/ [169]	5 wt% Cu–TiO_2/–	Impregnation method	CO_2 (27.09 atm), H_2O (30 mL)/450W Xe lamp/–	(298/1/5.45/48/–), (0.5/8.7/230 nm particle/ –/suspended)	Methane/0.02/–	• Low yield and compulsory separation of the gaseous products may create drawbacks for this system. • Catalysts are placed in a stainless steel vessel (42.5 mL) with a quartz window to run the photocatalytic reduction of CO_2.
Hemminger et al. (1978)/ [190]	$SrTiO_3$–Pt/3.2 eV	–	CO_2 (0.019 atm), water vapor (0.022 atm)/500 W high pressure mercury lamp/–	(315/1/–/0.5/0.01), (–/–/particle/ –/supported)	Methane/–/–	• A batch type isolation chamber is used to carry out the reaction and the samples are kept on a small disk of 1 cm^2 area. • The photo and thermal processes are easily distinguished by the filters used in this experiment.

T/P/pH/t/QE: temperature (K)/pressure (atm)/pH/illumination period (h/quantum efficiency (%).
W/SA/PS/SC/MP: weight of photocatalyst (g)/surface area (m^2/g)/photocatalyst structure (diameter)/semiconductor concentration (g/mL)/mode of photocatalyst.
'–': Not mentioned in the original paper.
[a] ppm h^{-1} g^{-1} catalyst.
[b] mmol h^{-1} g^{-1} catalyst.

3.3. *Photocatalysts modified by doping elements for CO_2 recycling*

To introduce impurities into an extremely pure semiconductor, the doping of foreign elements is deliberately performed for the purpose of controlling its electrical properties. Due to their large band gap, unmodified semiconductor photocatalysts cannot effectively absorb solar radiation with photon energy 1.7–3.1 eV [149]. To decrease its band gap energy, modification of the surface of photocatalysts has been attempted by applying stress along the soft direction of a layered semiconductor [149], introducing oxygen vacancies in a semiconductor [150], or incorporating foreign elements [151–157]. The schematic photocatalytic view of a doped semiconductor is shown in Fig. 6. Also, the recent advancements in different types of doped metal and non-metal elements incorporated with semiconductors found in various research for the photocatalytic conversion of CO_2 are critiqued in Tables 6 and 7, respectively.

3.3.1. *Noble metal doped semiconductors*

Doping metal on a semiconductor acts as an electron trap to provide electrons to CO_2. The photoexcited electrons are shifted from the conduction band of a semiconductor to doped metal to leave holes on the surface of the semiconductor [56]. Noble metals (Ru, Rh, Pd, Ag, Pt, Cu, Ni and Au) have been commonly used with semiconductors as dopants due to the Fermi level or electron accepting area existing at an energy just below the conduction band of semiconductors for the photochemical reduction of CO_2. Among those metals, Pt has been widely used in many investigations. For example, a TiO_2 semiconductor was doped with 0.5 wt% Pt by wet impregnation to avoid very low photocatalytic activity [158,159]. The more homogeneous dispersion of 0.5 wt% Pt on the TiO_2 surface drives the reaction rate swiftly in both the liquid and gas phases [160]. It has been shown that Pt loaded on TiO_2 transforms active sites from Ti^{4+} to Ti^{3+} by shifting electrons from TiO_2 to Pt; this phenomenon facilities visible light responses [161]. Another investigation has shown that Pt doping on anchored titanium oxide catalysts within the Y-zeolite cavities encourages charge separation and increases the formation of CH_4 in lieu of CH_3OH by promoting the reaction between carbon radicals and H atoms formed on the Pt metals [100]. Pt-loaded alkali niobates $ANbO_3$ (A=Na, K) photocatalysts were reported by Li et al. [162]. The results showed that $KNbO_3$ exhibited higher photocatalytic activity than that of $NaNbO_3$ because of the presence of low band gap energy (E_g) and high mobile charge carriers. Here, Pt acts as a co-catalyst to provide the reactive site for hydrogen gas production easily in terms of low H_2 over potential on the Pt surface [163]. It is also noticeable that increasing the Pt proportion from 0.5 wt% to 1.0 wt% promotes the formation of hydrogen gas. The photocatalytic performance of micro- or mesoporous Zn_2GeO_4 loading with various percentages of Pt (from 0.5 to 2.5 wt%) was investigated by Zhang et al., and the results evaluated the highest activity for 1.0 wt% Pt [164].

Ishitani et al. reported that Pd doped on TiO_2 resulted in more effective photocatalytic activity than that of other metals loaded on TiO_2, and also increased the formation of CH_4 instead of CO from CO_2 [165]. On the other hand, Pd on the surface of TiO_2 partly oxidizes to form PdO during the progression of CH_4 formation, which leads to the deactivation of Pd–TiO_2 catalysts [32]. Solymosi and Tombacz assumed that the adsorption and photocatalytic behaviors of Rh were significantly influenced by the existence of an electronic interaction at the Rh–TiO_2 interface [91]. Moreover, the catalytic activity of Rh was affected by doping with altervalent cations (W^{6+}) due to variation of the electron concentration of TiO_2 [166]. Cu is another noble metal which is eminent for its availability and low cost. Not only that, Cu-loading on TiO_2 was a prevalent approach in the photocatalytic conversion of CO_2 because of the high yield provided by lowering of the re-electron–hole recombination probability. According to Tseng et al., optimum Cu-loaded titania (2 wt% Cu) was found to have the

Table 7
Recent studies on non-metal-doped, and modified catalysts for CO_2 photoreduction; preparation methods and major findings.

Researcher (year)/Ref.	Catalyst composition/ band gap energy	Catalyst preparation technique	Reactants (amount)/ radiation source/light intensity	Operating variables (T/P/pH/t/QE), physical properties (W/SA/PS/SC/MP)	Major product/ yield ($\mu mol\ h^{-1}\ g^{-1}$ catalyst)/ selectivity (%)	Comments
Zhang et al. (2011)/ [208]	10 wt% I doped TiO_2 at 375 °C/ 3.0 eV	Hydrothermal method	CO_2 (saturated), Water vapor (0.022 atm)/ 450 W Xe lamp (> 400 nm)/ 233 mW cm^{-2}	(–/–/–/3.5/–), (0.2/ 137.6/ < 45 μm nanoparticle/ –/supported)	Carbon monoxide/2.4/–	• Samples are put on a glass-fiber filter at the bottom of the cylindrical photoreactor (58 cm^3) with stainless steel walls and a quartz window. • High CO_2 reduction activity is detected for I–TiO_2 under visible light than undoped TiO_2 under UV–vis irradiation. • Too high iodine doping level may create recombination centers and thus lower the photocatalytic activity.
Suzuki et al. (2011)/ [200]	N-Ta_2O_5 anchored with Ru-dpbpy/ 2.4 eV	Direct assembly method	CO_2 (saturated), MeCN: TEOA (5:1, 4 mL solution)/500 W Xe lamp (410-750 nm)/–	(–/–/–/60/–), (0.01/ –/20–40 nm nanoparticle/ –/suspended)	Formic acid/60 [a]/ –	•It is found that the photocatalytic activity and stability of the hybrid catalyst depends on the chemical structure of the anchor group.
Tsai et al. (2011)/ [202]	0.42 wt% N doped $InTaO_4$ with 3.2 wt % Ni–NiO core shell/2.28 eV	Impregnating method	CO_2 (saturated), deionized water (50 mL)/Xe lamp/–	(298/–/–/2/–), (0.1/ –/40 nm particles/ –/suspended)	Methanol/165/–	• Nitrogen doping shows visible light responsive photocatalytic activity with additionally high absorbance and gives approximately twice the yield of undoped ones, while the cocatalytic method gives about triple the yield. • Reaction is conducted on a stirred typed continuous flow reactor having a window-type irradiation cell that is made of Pyrex glass (200 mL).
Xue et al. (2011)/ [203]	C doped TiO_2/–	Immersion and calcination methods	CO_2 (saturated), H_2O (10 mL)/175 W high pressure Hg lamp/–	(–/–/2/6/–), (1/ –/nanopowder/ –/suspended)	Formic acid/439/ –	• The doped carbon shows low band gap and expends the absorption of visible light region under the simulated daylight lamp. • A three-concentric cylindrical quartz reactor is used having outermost layer for reaction pool, the middle layer for quartz cold trap and the innermost layer is the light source.
Sato et al. (2010)/ [201]	N–Ta_2O_5 linked with Ru-dcbpy/ 2.4 eV	Thermal treatment method	CO_2 (saturated), MeCN: TEOA (5:1, 4 mL solution)/Xe lamp (405 nm)/–	(298/–/–/20/1.9), (0.005/ –/nanoparticles/ –/suspended)	Formic acid/70/ 75	• Visible light is used to irradiate 8 mL test tubes containing the photocatalysts. • The linkage between the complex and the semiconductor increases greatly the reaction rate.
Varghese et al. (2009)/ [186]	Nitrogen-doped titania nanotube with copper/–	Anodization and annealed at 460 or 600 °C for 3 h	CO_2 (saturated), water vapor (saturated)/ sunlight/100 mW cm^{-2}	(317/ < 0.068/–/3.5/ –), (–/–/nanoparticle/ –/supported)	Methane/4.4/–	• CO_2 to hydrocarbon production rate under outdoor solarlight is at least 20 times higher than using UV illumination. • Samples are loaded into a stainless steel chamber having an O-ring sealed quartz window at the top for admitting solar radiation. • Identical construction of two chambers having volumes 7.5 cm^3 and 8.6 cm^3 are used to allow for two samples simultaneously.

T/P/pH/t/QE: temperature (K)/pressure (atm)/pH/illumination period (h)/quantum efficiency (%).
W/SA/PS/SC/MP: weight of photocatalyst (g)/surface area (m^2/g)/photocatalyst structure (diameter)/semiconductor concentration (g/mL)/mode of photocatalyst.
'–': Not mentioned in the original paper.

[a] Turn over nubmer.

highest photochemical activity which provided lower fluorescence intensity, resulting in higher methanol formation [167,168]. Depending on the amount of Cu loading on TiO_2, the formation of hydrocarbon products can also change [169]. Ag-doped TiO_2 was also investigated in this technology, and reduced the band gap energy of TiO_2 and shifted the band edge from the UV region to the visible region according to the amount of Ag added [170,171]. The Ag co-catalyst loaded on $ALa_4Ti_4O_{15}$ (A=Ca, Sr, and Ba) has been published, and Ag acts as a CO_2 reduction site to generate CO as reported in the electrochemical reduction of CO_2 where Ag was used as an electrocatalyst [172]. Moreover, a plasmon effect has been developed by Au nanoparticles doped with TiO_2, by increasing the visible light response [173–175].

3.3.2. Transition metal doped semiconductors

To improve the photocatalytic activity and efficiency, transition metals are also investigated in many researches due to the high visible light conversion of CO_2 [176]. The interesting thing about transition metals is that their valence electrons exhibit several common oxidation states. Among the transition metals, Co, Mn, Ni, Cr, Mo, Fe, V, and Ti are commonly used as doping elements

in photocatalytic technology to enhance the semiconductor performances under visible light. For visible light responsiveness, Nishimura et al. synthesized Cr-doped TiO_2 film using the sol–gel and dip-coating methods [177]. They stated that a suitable percentage of metal doping on semiconductors improved the catalytic activity, whereas excess percentages of dopant metals beyond the optimum level decreased the photocatalytic performances due to charge recombination. However, the H_2 generation rate was advanced for Fe doped TiO_2 compare to that of Cr doped TiO_2, as recombination enables Fe particles to trap both electrons and holes, whereas Cr can only trap one type of charge carrier [178]. The experiment was done to characterize the different types of transition metal (V, Fe, Ce, Cu, and Cr)-doped TiO_2 prepared by Pan et al. [179]. They reported that V and Fe were placed in the substitution sites of TiO_2, and Ce ions were dispersed in the interstitial sites, although Cr and Cu accumulated on the surface. The following activity order was found: $Fe-TiO_2 > V-TiO_2 > Cr-TiO_2 > Ce-TiO_2 > TiO_2 > Cu-TiO_2$; this indicates that the local structure and type of dopant have vital contributions on photocatalytic technology.

Loading of transition metal species on the nanostructure framework is a commonly used practice to increase the high dispersion of those species. Moreover, for surface immobilization, titanium species are confined onto mesoporous silica. This phenomenon is also effective for photocatalytic reactions of titanium particles as their photocatalytic activities intensely rely on the structures of active sites [180]. It was found that high and exceptional photocatalytic reactivity was obtained for the reduction of CO_2 with H_2O to generate CH_4 and CH_3OH under UV irradiation compared with bulk TiO_2 [181].

3.3.3. CO–metal doped semiconductors

Doping of bimetallic elements together on the semiconductor photocatalysts has been validated as a potential method to progress the visible light response of photocatalysts. Suitable co-dopant combinations are necessary to enhance the photocatalytic activity of semiconductors because not all of the co-dopant configurations are appropriate for this technique [182]. Fe as a co-dopant in Cu–TiO_2 catalysts has been investigated for the photocatalytic reduction of CO_2 with H_2O to ethylene at the quantum yield of 0.024% [183]. An efficient charge transfer mechanism occurs in the combination of TiO_2 and Cu or Fe as co-dopants. However, Cu co-doped with Fe–TiO_2 on SiO_2 supports has also been examined under concentrated natural sunlight with high quantum yield (0.05%) and the full absorption of visible light than that of only Cu co-doped on the Fe–TiO_2 counterpart [184]. The photocatalytic performance of the Cu doped on Pt–TiO_2 catalysts is influenced by the content of Cu loading. High percentage of Cu loading expressively decreases the formation of H_2 and improves the formation of CH_4 and CO [185]. Varghese et al. reported that Pt may have an effect on H_2O activation, whereas Cu plays an important role in the activation of CO_2 to CO [186]. Bimetallic Ag–Pt was used with the TiO_2 semiconductor catalyst as reported by Mankidy et al., who obtained a CH_4 selectivity of almost 80% compared with the selectivity of TiO_2 of 20% [187]. Their investigation found that Ag species had a strong surface plasmon absorption band in the UV–vis region, while Pt species did not show the same behavior. However, the combination of bimetallic Ag–Pt has the ability to tune electronic properties during photochemical reactions. Not only that, but combined Ag–Pt can accumulate electrons by Ag, and transfer the interfacial electron charge from Pt.

3.3.4. Non-metal-doped semiconductors

It has been broadly testified that doping or co-doping of semiconductor photocatalysts with non-metals such as C, N, S, B and F has shown considerably low band gap energy compared to metal doping in different experiments, prominent to efficient photocatalytic activity during visible light irradiation [191–198]. In Table 7, the update of major findings and detailed information regarding non-metal-doped semiconductors are given in detail to evaluate their progress in the photocatalytic conversion of CO_2. Compared with other non-metals, nitrogen-doped semiconductors show the most active results due to their narrow the band gap [199]. High rate solar conversion of carbon dioxide in the presence of water vapor to methane and other hydrocarbons is attained from nitrogen-deposited titania nanotube, arrangements as reported by Varghese et al. [186]. Specifically, the low wall thickness of nanotube arrays promotes the transfer of efficient carriers to the adsorbing species. From the experiment, it was also found that the incorporation of Pt and Cu nanoparticles on the external surface of nanotube arrangement further increases the hydrocarbon yield under the outdoor global AM 1.5 sunlight with 100 mW cm^{-2} intensity. Both Suzuki et al. and Sato et al. studied p-type photoactive nitrogen-doped Ta_2O_5 linkage with metal–complex electrocatalysts and revealed the outstanding photochemical conversion of CO_2 to formic acid under visible light irradiation by increasing the photoexcited electron transfer from the conduction band of the semiconductor to the metal complex [200,201]. The co-catalytic (N-doped $InTaO_4$ modified with Ni–NiO core–shell nanostructure) approach by Tsai et al. not only intensely increases solar light absorbance, but also competently reduces the electron–hole recombination [202]. Investigations with carbon-doped TiO_2 were performed by Xue et al. because doped carbon narrows the band gap, shifts absorption to the visible light region and also facilitates the charge separation efficiency [203]. Hiroshi et al. reported the hydrophilic behavior of C-doped TiO_2 semiconductor, which exhibited a visible light response that was initiated from the localized C (2p) formed above the valence band [204]. S-doped TiO_2 has the ability to reduce band gap energy, and inhibits alterations of the anatase phase into the rutile phase at elevated temperatures [205]. Correspondingly, doping of F on semiconductor catalysts performs better by decreasing the band gap energy [206].

Results showed that iodine doping on semiconductor catalysts exhibited higher photochemical activity due to the close ionic radii of I^{5+} and Ti^{4+} for the substitution of lattice titanium rather that of other non-metal doped elements like nitrogen, carbon, boron, and sulfur [207]. Moreover, the replacement of Ti^{4+} with I^{5+} initiates charge inequality to the formation of Ti^{3+} surface states, which is able to arrest the photoinduced electrons and prevents charge recombination in the photocatalytic conversion of CO_2 [208]. Zhang et al. found that iodine doped TiO_2 semiconductors calcined at 375 °C reduced the particle size significantly and increased photochemical activity [208]. It was also observed that 10% iodine deposition on TiO_2 harvested the maximum yield under visible light irradiation compared with the 5% iodine doping on TiO_2.

3.4. Sensitized photocatalysts for CO_2 recycling

For CO_2 recycling, photosensitization is used, which involves a modification of catalysts which are sensitive to the encouragement of radiant energy, mainly in light irradiation. This practice is usually performed in photochemical applications under light sources which have a deficiency of particular wavelengths for photoexcitation. The mechanism generates photoexcited electrons in the conduction band of photosensitizers under the light source of particular wavelengths, and the electrons are directly shifted to the conduction band of catalysts to make them photoactive under visible light irradiation [209]. According to Tahir and Amin, photosensitization exclusively depends on the band gaps of sensitizers in terms of visible light

Table 8
Recent studies on sensitized catalysts for CO_2 photoreduction; preparation methods and major findings.

Researcher (year)/Ref.	Catalyst composition/ band gap energy	Catalyst preparation technique	Reactants (amount)/ radiation source/light intensity	Operating variables (T/P/pH/t/ QE), physical properties (W/SA/ PS/SC/MP)	Major product/ yield ($\mu mol\ h^{-1}\ g^{-1}$ catalyst)/ efficiency (%)	Comments
Li et al. (2012)/ [211]	Dye sensitized Zn_2SnO_4 with 1 wt % Pt and 1 wt % RuO_2/ 3.87 eV	Nucleation processes and solid-state reaction	CO_2 (saturated), water vapor (0.4 mL)/300 W Xe arc lamp/ 100 mW cm^{-2}	(–/–/–/10/–), (0.1/ 7.71/nanoplates/ –/supported)	Methane/86.7 [a]/ 3.1	• Catalysts are evenly kept at the bottom of a Pyrex glass cell, and the reaction is carried out in a gastight condition. • The unitary geometry of the photoanode improves the solar energy conversion.
Pan et al. (2011)/ [212]	Dye sensitized TiO_2 (anatase) with 1 wt% Pt/ 3.27 eV	Hydrothermal treatment	CO_2 (saturated), water vapor (–)/solar light/–	(–/–/7/10/7.73), (–/25/nano-sized rods/–/supported)	Methane/2.5/–	•Due to distinctive surface atomic or electronic structure, the nanosized rods show a higher activity in converting CO_2 into CH_4 and a comparable energy conversion efficiency.
Wang et al. (2011)/ [230]	Sensitized TiO_2–SiO_2 composite with 0.01 mol% Cu/1.2 eV	FuAR method	CO_2 (saturated), deionized water (3.0 g)/Xe arc lamp (250–400 nm)/2.4 mWc m^{-2}	(–/–/–/8/–), (0.02/ 81.71/265 nm composite particles/ –/supported)	Carbon monoxide/20/–	• Size, composition, and porosity of the composite particles are tailored by controlling the precursor concentration, stoichiometric ratio, and temperature, respectively. • The reactor is cylindrically built with a stainless steel wall and a quartz window having 60 mm in diameter and 25 mm in depth vertically facing the solar lighter.
Hou et al. (2011)/ [229]	Sensitized TiO_2 films with Au/ 2.5 eV	Sol–gel process	CO_2 (saturated), water vapor (–)/UV lamp (254 nm)/ 20 mWc m^{-2}	(348/–/–/15/ 2.3×10^{-2}), (–/–/400 nm thickness film/ –/supported)	Methane/22.4 [b]/ –	• Surface plasmons of the Au nanoparticles create intense electromagnetic fields to enhance sub-band gap absorption in the TiO_2, and improve the photocatalytic activity in the visible range. • Reaction is conducted on a sealed 51.6 mL stainless steel reactor with a quartz window, where the photocatalytic films are kept on the catalyst holder, which is on the bottom of the reactor.
Luo et al. (2011)/ [231]	Sensitized TiO_2 particles with 2 wt% Cu–Ce/–	Wetness impregnation method	CO_2 (saturated), NaOH (0.2 M, 150 mL solution)/ 125 W UV lamp (365 nm)/–	(343/–/–/16/–), (0.15/2.963/powder/ –/suspended)	Methanol/11.3/–	• It is found that Ce atoms affect the reaction more profoundly than Cu atoms do, and Ce atoms activate H_2O and CO_2 molecules. • Reaction is carried out in a hermetic high-pressure reaction still equipped with heating and magnetic stirring system.
Woolerton et al. (2011)/ [228]	Enzyme CODHI-modified TiO_2 with ruthenium bipyridyl/–	Standard system protocol	CO_2 (98%), CH_4 (2%)/250 W (24 V) tungsten–halogen bulb (420 nm)/45 mWc m^{-2}	(293/–/6/4/0.07), (0.005/50/ Nanoparticles (< 100 nm)/ –/suspended)	Carbon monoxide/255/–	• Reaction is carried out in a pressure vessel containing the suspension was sealed tightly with a rubber septum. • Modified enzyme is efficient for CO_2 conversion, and sensitized to visible light.
Li et al. (2010)/ [95]	Sensitized TiO_2 with 0.5 wt% Cu on SiO_2/3.1 eV	One-pot sol–gel method	CO_2 (saturated), Water vapor (–)/Xe lamp (250–400 nm)/ 2.4 mWc m^{-2}	(273/1/7/4/1.41), (0.1/386.2/ < 100 μm powder/ –/supported)	Cabon monoxide/45/–	• High surface area mesoporous silica substrate highly improves photoreduction due to better TiO_2 dispersion and increased adsorption of CO_2 and H_2O on the catalyst, and addition of Cu species increases multi-electron reactions. • A cylindrical continuous-flow reactor is used with a stainless steel wall and a quartz window having 6.0 cm diameter and 2.5 cm depth.
Kočí et al. (2010)/ [170]	Sensitized TiO_2 particles with 7 wt% Ag doping/ 2.74 eV	Sol–gel process	CO_2 (saturated), H_2O (100 mL)/8 W Hg lamp (254 nm)/–	(–/–/–/24/–), (–/79.7/1.65 nm particles/0.001/ suspended)	Methane/0.36/–	• Ag impurity inside the TiO_2 shifts absorption edge to visible light and forms Shottky barrier at the metal–semiconductor interface to reduce electron and holes recombination. • The reaction is conducted on a stirred batch annular reactor with a suspended catalyst.
Woolerton et al. (2010)/ [227]	Enzyme CODHI with RuP modified TiO_2/–	—	CO_2 (98%), CH_4 (2%)/ tungsten–halogen lamp (420 nm)/45 mWc m^{-2}	(293/–/6/4/–), (0.005/ –/nanoparticles/ –/suspended)	Carbon monoxide/250/–	• Photocatalytic reaction is carried out in a Pyrex pressure vessel (9 mL) with gentle stirring. • Reaction is focused on a two-electron

Table 8 (*continued*)

Researcher (year)/Ref.	Catalyst composition/ band gap energy	Catalyst preparation technique	Reactants (amount)/ radiation source/light intensity	Operating variables (T/P/pH/t/ QE), physical properties (W/SA/ PS/SC/MP)	Major product/ yield ($\mu mol\ h^{-1}\ g^{-1}$ catalyst)/ efficiency (%)	Comments
						pathway to avoid the thermodynamically difficult step involved in one-electron CO_2 activations.
Wang et al. (2010)/ [219]	CdSe–Pt–TiO_2/–	Wet impregnation method	CO_2 (0.0004 atm), water vapor (0.004 atm)/300 W Xe arc lamp (> 420 nm)/ 100 mW cm^{-2}	(–/–/–/6/–), (0.3/50/ hetero-structured/ –/supported)	Methane, methanol/ 0.0019, 0.000137/–	• Quantum dot-sensitized TiO_2 heterostructured materials are proficient for photoreduction of CO_2 using visible light. • Results represent that germane can be used on photoreduction reactions for CO_2 capture and reuse.
Zhao et al. (2009)/ [222]	0.7 wt% Co(II)Pc–TiO_2/–	In-situ synthesized by advanced sol–gel method	CO_2 (–), NaOH (100 mL, 0.1 N aqueous solution)/500 W tungsten–halogen lamp/–	(–/–/–/10/–), (0.15/ 75.23/11.35 nm particle/ –/suspended)	Formic acid/150/ –	• The yield of in-situ CoPc–TiO_2 is much higher than those of TiO_2 and physical absorbed CoPc–TiO_2. • Reaction is conducted in a Pyrex glass cell (100 mL) with an optical window.
Zhao et al. (2009)/ [223]	0.5% CoPc–TiO_2/–	Sol–gel method	CO_2 (saturated), NaOH (0.1 N,100 mL aqueous solutions)/500 W tungsten–halogen lamp/–	(673/–/–/6/–), (0.15/ 90.7/11.02 nm particle/0.1/ supported)	Formic acid/57/ –	• CoPc–TiO_2 prepared by sol–gel shows relatively high photocatalytic activity compared with TiO_2 synthesized by sol–gel method. • A Pyrex cell with an optical window (100 mL) is used to conduct the photocatalytic reaction.
Yang et al. (2009)/ [232]	Sensitized 45 wt% Cu–TiO_2 on SBA-15/3.2 eV	Sol–gel synthesis and hydrolysis-condensation process	CO_2 (saturated), NaOH (0.1 N, 550 mL aqueous solution)/ 400 W medium-pressure halide lamp (365 nm)/–	(315/–/7/8/–), (0.05/ 436/5.5 nm particles/ –/suspended)	Methanol/475/–	•Loading amount of TiO_2 on mesoporous SBA-15 composite photocatalysts control the crystallize size of the supported TiO_2 particles and the mesoporous structure of the catalyst.
Wu (2009)/ [213]	Dye-sensitized Cu–Fe loaded on P25/–	Dip-coating method	CO_2 (saturated), water vapor (–)/sunlight (400–800 nm)/ 20 mW cm^{-2}	(–/–/–/–/–), (–/–/film composite/ –/supported)	Methanol/–/–	•Dye-sensitized Cu–Fe loaded on P25 photocatalyst can completely use the light energy of 400–800 nm from sunlight and significantly increase its photoactivity.
Nguyen and Wu (2008)/ [184]	Sensitized TiO_2 with 0.5wt% Cu–Fe loaded on SiO_2/ 2.95 eV	Sol–gel process	CO_2 (saturated), H_2O (–)/natural sunlight/ 2.05 mW cm^{-2}	(348/–/–/6/0.0182), (0.5/44.7/53 nm thickness film/ –/supported)	Methane/0.279/ 0.0152	• An optical-fiber reactor consists of a continuous circular Pyrex glass vessel (216 cm^3) with a quartz window in which catalyst-coated optical fibers are inserted. • Cu–Fe loaded on TiO_2–SiO_2–acac catalyst shows the superior photoactivity as compared to that of bare TiO_2–SiO_2–acac counterpart.
Wu et al. (2008)/ [233]	Sensitized TiO_2 with 1 wt% Ag coated on optical fiber/3.5 eV	Thermal hydrolysis method	CO_2 (1.13 atm), H_2O (0.03 bar)/UV light (365 nm)/ 10,000 mW cm^{-2}	(348/–/–/11/ 0.00013), (–/71.66/ spherical particles of 12 nm/ –/supported)	Methanol/4.1/–	• An optical-fiber photoreactor, built-in 216 × catalyst-coated fibers are supported on circular plates and irradiated through the quartz window having a large external area of optical fiber to disperse catalysts. • Optical-fiber delivers a medium to transmit light uniformly throughout the reactor compared with a traditional packed-bed reactor.
Nguyen et al. (2008)/ [214]	N3 dye-0.5 wt% Cu–0.5 wt% Fe–TiO_2/3.11 eV	Dip-coating method	CO_2 (saturated), water vapor (–)/sunlight/20 mW cm^{-2}	(348/–/–/6/–), (–/48.7/film composite/ –/supported)	Methane/0.617/ –	• A continuous circular Pyrex glass (216 cm^3) optical fiber photoreactor is irradiated by concentrated sunlight through a quartz window. • N3 dye highly increases the photoactivity under concentrated natural sunlight and delivers efficient charge transfer.
Zhao et al. (2007)/ [224]	1 wt% Zn(II)Pc–TiO_2/–	Sol–gel method and in situ chemical synthesis technique	CO_2 (saturated), NaOH (100 mL, 0.1 N aqueous solution)/500 W tungsten–halogen lamp/–	(–/–/–/10/–), (0.15/ –/28 nm particle/ –/suspended)	Formic acid/98/ 0.37	• Results shows that the formic acid production is meaningfully increased by loading ZnPc, and having a higher selectivity than metal catalysts for the reduction of CO_2. • A magnetic stirred Pyrex glass cell (100 mL) with an optical window is used to carry out the reaction.

Table 8 (*continued*)

Researcher (year)/Ref.	Catalyst composition/ band gap energy	Catalyst preparation technique	Reactants (amount)/ radiation source/light intensity	Operating variables (T/P/pH/t/ QE), physical properties (W/SA/ PS/SC/MP)	Major product/ yield ($\mu mol\ h^{-1}\ g^{-1}$ catalyst)/ efficiency (%)	Comments
Ozcan et al. (2007)/ [215]	BrGly–Pt loaded on TiO_2/–	Dip-coat sol–gel technique and wet impregnation method	CO_2 (0.88 atm), water vapor (0.03 atm)/75 W daylight lamp/58 mW cm^{-2}	(–/0.9/–/3/0.0228), (–/–/ > 1 μm thick film composite/ –/supported)	Methane/0.2/–	• Perylene di-imide derivatives are used to show light harvesting capability similar to the tris(2, 2-bipyridyl) ruthenium (II) chloride hexahydrate. • The reaction is conducted on a glass chamber connected to a vacuum line. • It is found that visible light performances of the dyes are in the following order in the presence of Pt: Rubpy > BrAsp > BrGly.
Tseng and Wu (2004)/ [234]	Sensitized TiO_2 with 2 wt% Cu/–	Sol–gel procedures and post-treatments	CO_2 (saturated), NaOH (0.2 N aqueous solution)/Hg lamp (254 nm)/–	(–/–/7/30/–), (0.3/ –/25 nm particle/ –/suspended)	Methanol/17/–	• It is found that photoactivity declines when Cu (I) changes to Cu (0) or aggregates after reduction with H_2. • Reaction is carried out in a cylindrical quartz reactor with a capacity of 300 mL. • It is identified that the photoactivity of Ag-TiO_2 is lower than those of Cu–TiO_2 due to the strong affinity between Ag clusters and photoelectrons.
Hirose et al. (2003)/ [217]	$Co(bpy)_3^{2+}$ sensitized with $Ru(bpy)_3^{2+}$ supported on Nafion film/–	Laboratory preparation	CO_2 (saturated), DMF & TEOA (30 mL solution)/Xe lamp/–	(–/1/ < 1/46/–), (0.1/ –/particles on polymer film/ –/supported)	Carbon monoxide/25 [c]/–	• Long catalytic activity is found more than 400 h under atmospheric pressure. • A gastight photolysis photoreaction vessel (Pyrex) is used to conduct the reaction. • This system permits easy handling and recovery of the Ru complex including repeated cycles using CO_2 refreshing.
Ishitani et al. (1993)/ [165]	Sensitized TiO_2 (Degussa P-25) particles with 2 wt% Pd/8.34 eV	Photochemical deposition method	CO_2 (saturated), H_2O (1.5 mL)/500 W high pressure Hg lamp (310 nm)/–	(278/0.86/–/5/–), (0.15/–/Powder/ –/suspended)	Methane/0.3/–	• It is suggested that product distribution is dependent on the sort of metal on the surface of TiO_2. • Degassed quartz vessel is used to carry out the photoreduction.
Thampi et al. (1987)/ [235]	25% Ru–75% RuO_x sensitized on TiO_2/3 eV	Laboratory preparation	CO_2 (0.05 atm, 1 mL), H_2 (0.6 atm, 12 mL)/150 W high pressure Xe lamp (310–435 nm)/–	(298/1/–/5/0.59), (0.1/55/spherical shape particle/3.8/ suspended)	Methane/0.5 [d]/–	• Photocatalysts are kept on the bottom of a flat Pyrex vessel (20 cm^3) with a side arm and septum. • Elevated temperature and pressure have an important role to advance the reaction rate and yields.
Lehn and Ziessel (1982)/ [216]	Ru-bipyridine–Co (II) chloride/–	Standard laboratory synthesis	CO_2 (700 mL), H_2O (6 mL)/ 1000-W Xe or Hg ozone-free Oriel lamp (400 nm)/–	(303/1/8.5/26/–), (–/–/–/–/suspended)	Carbon monoxide/25 [c]/–	• It has been observed that addition of free bipyridine intensely decreases CO generation but increases H_2 production. • The photocatalytic reaction is carried out in a 50 mL round-bottom flask.

T/P/pH/t/QE: temperature (K)/pressure (atm)/pH/illumination period (h)/quantum efficiency (%).
W/SA/PS/SC/MP: weight of photocatalyst (g)/surface area (m^2/g)/photocatalyst structure (diameter)/semiconductor concentration (m/mL)/mode of photocatalyst.
'–': Not mentioned in the original paper.

[a] ppm $h^{-1}\ g^{-1}$ catalyst.
[b] μmol m^{-2} catalyst.
[c] μmol.
[d] mmol.

response and the high conduction band energy of sensitizers compared with the catalysts' conduction band energy due to facilitating electrons shifting to the catalysts [199]. Some informative characteristics are represented in Table 8 for different types of sensitized photocatalysts which have been applied in many research studies to increase the photocatalytic activity in order to get high photon efficiency and selectivity.

3.4.1. *Dye-sensitized photocatalysts*

Dye-sensitized photocatalysts are widely used in photochemical technology because of their ability to easily create photoactive electrons by visible light hitting the dye compound. This phenomenon helps to transfer those photoactive electrons from the dye to the catalysts' conduction band for their activation during the visible light irradiation [56,210]. The effective response to visible light and efficient electron transfer can enhance the fuel yields. The charge separation can be effectively achieved by adding co-catalysts to trap the electron (Fig. 7).

Li et al. reported that charging of Pt and RuO_2 on dye-sensitized hexagonal nanoplates formed micro-octahedron Zn_2SnO_4, which was able to accumulate photoexcited electrons and holes, respectively [211]. Dye-sensitized Pt loaded nanosized {010} dominant anatase TiO_2 rods were used to obtain exceptional surface atomic

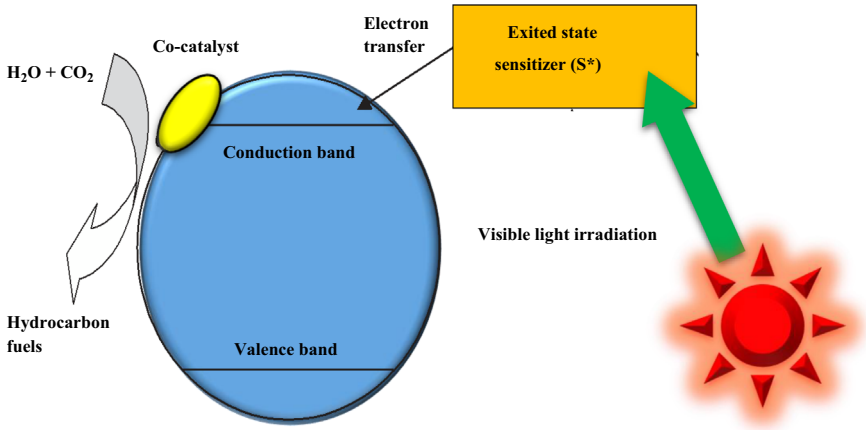

Fig. 7. Scheme of dye-sensitization during visible light irradiation.

structure for the optimum adsorption of dye molecules and to encourage electron transmission from excited dye molecules to anatase TiO_2 [212]. These occurrences also upgraded the current density and solar energy conversion efficiency of that system. Another investigation found that Ru^{II}(2,2′-bipyridyl-4,4′-dicarboxylate)$_2$-(NCS)$_2$ (basically known as N3-dye) sensitized Cu–Fe loaded on P25 photocatalysts was able to absorb the wavelength of 400–800 nm from solar irradiation [213]. Moreover, the results show that N3-dye is not suitable under artificial light (wavelength range is 320–500 nm) irradiation because it is dispersed on the matrix of the photocatalysts before irradiation; as a result, the dye does not show its full response to the light source, but remarkably increases the methane yield to over 100% using concentrated natural sunlight N3-dye. Similar results were found by Nguyen et al., who found that N3-dye caused effectual charge transfer with higher photoreduction under concentrated sunlight [214]. Moreover, it was also found that N3-dye showed its stability up to 6 h under both artificial light and concentrated sunlight. Ozcan et al. used Perylene diimide dyes and revealed a similar visible light response to Ru^{II}(2,2′-bipyridyl)chloride hexahydrate [215]. In this study, Pt was added to the TiO_2 surface where three types of photosensitizing dyes were applied to investigate their activity, such as Rubpy > BrAsp > BrGly.

Much attention has been given to $[Ru(bpy)_3]^{2+}$ cation because of its unique optical characteristics. The combination of $[Ru(bpy)_3]^{2+}$ and cobalt(II) chloride has been investigated over CO_2 photoreduction, where Ru and Co complexes act as a photosensitizer and a catalyst, respectively [216]. By absorbing photon energy, the $[Ru(bpy)_3]^{2+}$ cation transforms to the triplet state, denoted by $[Ru(bpy)_3]^{2+*}$. It was observed that the extra addition of bipyridine intensely reduced CO formation, but increased the H_2 yield. On the other hand, Co(II) chloride acts as an effective mediator for both CO and H_2 productions and highly endorses CO yield. $Co(bpy)_3^{2+}$ sensitized with $Ru(bpy)_3^{2+}$ supported on a cation-exchange nafion film has been synthesized to carry out the photocatalytic reduction of CO_2 for a period of more than 400 h under atmospheric pressure [217]. High stability of the metal complexes was obtained by suppression of the decomposition of the Ru complex fixed on the polymer surface. In this system, $[Ru(bpy)_3]^{2+}$ was immobile on a cation exchange polymer and $[Co(bpy)_3]^{2+}$ was mixed in di-methylformamide (DMF) and triethanol amine (TEOA) as a solvent and reducing agent, respectively. It is assumed that the photoinduced Ru complex transmits an electron to Co(II) complex, which acts as a reaction medium of CO_2, and at that time, tertiary amine (sacrifice reagent) reduced the oxidized Ru(III) complex [217].

3.4.2. Quantum dots (QDs)-sensitized photocatalysts

A quantum dots-sensitized photocatalyst is one of the advanced approaches in the photochemical conversion of CO_2 because of the intrinsic optical and electrical behavior demonstrated. These characteristics are strongly influenced by the size of the quantum dots materials. Usually, chalcogenide metals (CdSe or ZnS) are used with the semiconductors to facilitate the photon transformation of CO_2 into hydrocarbon fuels. In Section 3.2.1, there is brief discussion of the metal sulfide (CdS and ZnS) semiconductors, which also have such unique optical properties as those shown by quantum dots materials. To understand the size reliant on photochemical reduction of CO_2, Wang et al. developed a PbS QDs sensitized Cu–TiO_2 catalyst with three different sizes of PbS QDs samples (3 nm, 4 nm and 5 nm) [218]. Among them, 4 nm PbS QD-sensitized Cu–TiO_2 displayed the maximum CO_2 transformation rate, due to absorption of the visible spectrum ($\lambda > 610$ nm) and charge separation properties. It is found that small-sized dots can facilitate the blue edge of the spectrum, while large-sized dots are closer to the red edge spectrum. Specially, small-size QDs inject electrons swiftly to the conduction band edge of TiO_2 and large-size QDs cover the visible region [219]. Moreover, the electron transfer rate was found to be very fast (less than 1 ns) from the excited PbS QDs state to the TiO_2 conduction band state [220]. Another investigation was conducted on the CdSe QDs-sensitized Pt–TiO_2 composite heterostructure which revealed response to the visible light region ($\lambda > 420$ nm) [219].

3.4.3. Phthalocyanines-sensitized photocatalysts

For visible light irradiation, metal phthalocyanines are also applied in CO_2 photoreduction, as they have outstanding semiconductivity and chemical stability [221]. CoPc–TiO_2 nanocomposites are characterized by Zhao et al. [222,223]. It was observed that excited CoPc molecules emitted electrons to the conduction band of TiO_2 during the visible light irradiation; then, this phenomenon improved the electron–hole separation process in order to increase the photocatalytic efficiency. From Table 8, it can be seen that the incorporation of 0.7% CoPc into TiO_2 exhibited a high yield rate of formic acid (about 150 $\mu mol\ g^{-1}\ h^{-1}$) compared to that seen for the addition of 0.5% CoPc to TiO_2. Their investigation was also conducted on ZnPc–TiO_2, and it was found that ZnPc has a higher selectivity of formic acid than metal catalysts by decreasing the recombination possibility of hole–electron pairs [224]. It is important that the excess loading of ZnPc can reduce the photocatalytic activity, because the active TiO_2 surface sites can be blocked by additional metal phthalocyanines, and the

optimum amount is observed, 1.0 wt% ZnPc. However, according to the observations of Wang et al., the band gap of TiO_2 can be minimized from 2.95 eV (at 0.6 wt% ZnPc) to 2.79 eV by loading 5 wt% ZnPc [225].

3.4.4. Other photosensitizers for CO_2 recycling

Enzymes have effective sensitization ability to red shift of TiO_2 compared with other sensitizers [226]. Woolerton et al. used the carboxydothermus hydrogenoformans (*Ch*)-derived carbon monoxide dehydrogenase (CODH I) enzyme to functionalize the RuP sensitized TiO_2 nanoparticles for CO_2 photoexcitation [227,228]. Anaerobic organisms, *Ch*, contain five forms of CODHs enzymes, each with [Ni4Fe–4S] active sites. The subunit of these enzymes (Ni–CODHs) possesses a buried active site that is supported to the protein exterior by a chain of [4Fe–4S] clusters. Electrons can easily access or leave the enzyme by the distal cluster (D-cluster), which is a joint between the two subunits. In this experiment, visible light excited RuP sensitizer nanoparticles transferred photoinduced electrons to TiO_2 to ease its solar light activation [49,228]. These electrons can easily enter the CODH enzyme through the D-cluster and are also able to move through a second [4Fe–4S] cluster to the active site, where CO_2 reduction takes place.

Recently, co-loaded novel metals have been used with semiconductor catalysts as photosensitizers. For example, sensitized TiO_2 film with Au nanoparticles is modified by Hou et al. for turning CO_2 into fuels [229]. Here, Au nanoparticles are photoexcited by a plasmon effect (generation of robust electric field by the surface plasmon resonance of the Au nanoparticle), and this plasmon excitation shifted the photoinduced electrons from the Au to the TiO_2. Another approach of sensitized TiO_2 with Cu on supportive SiO_2 is applied in terms of solar fuel production from CO_2 [95,230].

3.5. Flexible substrate based photocatalysts for CO_2 recycling

In the photochemical reaction, the involvement of flexible substrates have grown in interest because they deliver a high surface area for catalysts on the film of substrates such as polyethyleneterphthalate (PET), polyethylenenaphtalate (PEN), polyethylene (PE) and polypropylene (PP) [236]. However, the degradation of polymer substrates on solar irradiation depends on the operating period of atmospheric exposure [237]. This photodegradation is carried out via a combination of photolysis and photocatalytic oxidation [236]. The formation of volatile products due to the photodegradation is another limitation of polymeric substrates [238]. Table 9 represents the full information of flexible substrate-based photocatalysts which are gathered from some important investigations related to CO_2 photoconversion.

Table 9
Recent studies on flexible substrate catalyst for CO_2 photoreduction; preparation methods and major findings.

Researcher (year)/Ref.	Catalyst composition/ band gap energy	Catalyst preparation technique	Reactants (amount)/ radiation source/ light intensity	Operating variables (T/P/pH/t/QE), physical properties (W/SA/PS/SC/MP)	Major product/ yield ($\mu mol\ h^{-1}\ g^{-1}$ catalyst)/ selectivity (%)	Comments
Kim et al. (2012)/ [241]	Nafion layer on 1.0 wt% Pd-deposited TiO_2/–	Laboratory synthesis	CO_2 (saturated), H_2O (–)/UV light (> 300 nm)/–	(–/–/3/5/–), (–/–/nanoparticle/ 1.5×10^{-6}/suspended)	Methane/7.6 [a]/–	• Nafion layer enhances proton-coupled multiple electron transfer reactions, stabilizes intermediates and inhibits the re-oxidation of the CO_2 reduction products by increasing the local proton activity within the layer. • Palladium is selected to retard the recombination of H atoms to minimize the production of H_2.
Jensen et al. (2011)/ [236]	TiO_2–PET/–	Spray coating	CO_2 (25 mol), H_2 (75 mol)/Osram light bulb/ 120 mW cm^{-2}	(308/–/–/230/–), (–/–/film with 130 μm μm thickness/ –/supported)	Carbon monoxide/ 0.0013/–	• Polymer substrates are applied in this studies with high active area of 100 cm^2 enable to achieve catalyst-covered film within a short time and at a reasonable production cost. • UV degradation of polymer substrates (photocatalytic oxidation) can be suppressed, but not avoided, by using oxygen free conditions.
Arai et al. (2011)/ [242]	Cu_2ZnSnS_4 modified by ruthenium complex polymer/ 1.5 eV	Chemical polymerization method	CO_2 (saturated), H_2O (–)/visible light irradiation (200–400 nm)/–	(–/–/–/3/–), (–/–/photocathode/ –/supported)	Formic acid/0.49 [b]/ > 80	• Sulfide semiconductor that shows a narrow band gap with high selectivity in photoelectrochemical CO_2 reduction. • The insertion of Se into the catalyst enhances the hole mobility and increase the photocurrent.
Hirose et al. (2003)/ [217]	$Co(bpy)_3^{2+}$ with $Ru(bpy)_3^{2+}$ supported on Nafion film/–	Laboratory preparation	CO_2 (saturated), DMF with TEOA (30 mL solution)/Xe lamp/–	(–/1/ < 1/46/–), (1/ –/perticles on polymer film/–/supported)	Carbon monoxide/ 25 [a]/–	• Catalytic activity shows more than 400 h under atmospheric pressure. • Photoreaction is carried out in a gastight photolysis photoreaction vessel (Pyrex). • This system allows easy handling and recovery of the Ru complex with repeated cycles using CO_2 refreshing.

T/P/pH/t/QE: temperature (K)/pressure (atm)/pH/illumination period (h)/quantum efficiency (%).
W/SA/PS/SC/MP: weight of photocatalyst (g)/surface area (m^2/g)/photocatalyst structure (diameter)/semiconductor concentration (g/mL)/mode of photocatalyst.
'–': Not mentioned in the original paper.

[a] μmol.
[b] mM.

Some aromatic polyesters such as PET, PEN and similar flexible substrates act in a different way under light irradiation compared with olefins (PE and PP). Aromatic polyesters are able to absorb light with a long wavelength (<330 nm) due to the presence of aromatic rings of carbonyl groups [238]. Another important factor is the oxygen diffusion constant of flexible substrates. Higher oxygen diffusion constants may lead to oxidation in all parts of the surface [239]. Comparatively, polymer degradation is lower on the surface of PET because of its restriction to diffuse oxygen, whereas the diffusion is higher in PE [236,239,240].

Nafion (perfluorinated polymer with sulfonate groups) thin film on Pd-loaded TiO_2 nanoparticles was introduced by Kim et al. due to its stability against photocatalytic oxidation, and its ability to increase the photochemical conversion of CO_2 under visible light irradiation [241]. To provide multiple electrons, the nafion layer can increase the local proton activity inside the layer. It also helps to stabilize the intermediates and prevent the re-oxidation of CO_2 reduction yields because it inhibits the direct interactions between products and the surfaces of catalysts. Another investigation shows that nafion film acts as a good supportive material for catalysts due to the cation exchange ability [217]. This nafion-supported $Co(bpy)_3^{2+}$ and $Ru(bpy)_3^{2+}$ system can increase the catalytic activity maximum by about 400 h in atmospheric conditions as the breakdown of $[Ru(bpy)_3]^{2+}$ complexes that are trapped on the cation exchange polymer surface is obstructed, and hence the separation of ligands is minimized. Low band gap (1.5 eV) Cu_2ZnSnS_4 modified by a ruthenium complex polymer is a new addition to determine the photochemical performance of CO_2 reduction under visible light regions, which shows the high selectivity of formate ($>80\%$) [242].

4. Advances in photoreactors for photocatalytic conversion of CO_2

CO_2 recycling by artificial photosynthesis is a surface reaction process involving two vital stages: (i) the greenhouse gas CO_2 has to transfer to the catalysts' surface; and (ii) the CO_2 is decomposed by the photocatalysts under light irradiation in the presence of reductants. Therefore, the convective mass transfer rate of CO_2, the reaction rate and the catalysts' reaction surface area are the most significant factors for efficient photocatalytic performance [243]. Physical geometry of photoreactor and utilization of the supreme solar spectrum on the catalytic surface are also necessary to enhance CO_2 conversion. Therefore, the mode of catalysts during the photochemical reaction is an important concern to increase yields. Based on the catalysts' mode several types of reactors have been introduced in this technology to utilize the maximum light irradiation by the catalysts' active surface area. Fig. 8 illustrates the different categories of photoreactors based upon the modes of catalysts during the reactions. The recent developments in photocatalytic reactors in many investigations to upgrade the efficiency of reactors are given in Table 10 according to the year of investigation.

Ideally, the solar light driven photoreactors must have: (i) a high coverage area for catalyst holding and spectral distribution; (ii) a support with small-through channels allowing high CO_2 velocity and high mass transfer; (iii) no flow routes through the reactor where the catalysts remain without light irradiation; and (iv) an efficient reflector to harvest maximum illumination and intensity. Thus, it is essential to ensure contact between photo-generated photons and photocatalysts to initiate photoreduction. Usually, solar driven reactors are less reliant on temperature and pressures. Several features are crucial to select an effective photo-reactor compared with the other conventional reactors, such as resourceful radiation source, optimum design of radiation enhancement devices like mirrors or reflectors, types of window materials and their shape [199]. Various photochemical reactors have been categorized according to the position of the light sources with regard to the photoreaction area.

4.1. Slurry reactors

In a slurry reactor, the catalysts are suspended in the liquid phase with the help of mechanical or gas-promoted agitation (Fig. 9). Slurry reactors are the most common and conventional reactors in photocatalytic technology. The slurry process is usually operated in three-phase contacting. It is also useful for temperature adjustment and to minimize the scope of intraparticle diffusion [244]. Since these reactors operate at moderate conditions, higher selectivity can also be envisaged. For the photochemical transformation of CO_2, in 1979, Inoue et al. introduced a slurry reactor where the catalysts were suspended in water [61]. Until 2000, slurry reactors were widely used with different photocatalysts for CO_2 photoreduction under UV or visible light irradiation [245,246]. Recently, Wang et al. reported on a batch mode Pyrex glass cell as a slurry reactor to convert CO_2 into fuels under 500 W simulated solar light [225]. The reactor was firmly closed during the reaction and stirred continuously with a magnetic stirring bar to avoid catalyst sedimentation. On the other hand, Tahir and Amin suggested that this type of reactor is not efficient for enhancing the photocatalytic activity due to the low surface area and complicated separation process required to isolate the miniature catalyst grains [199].

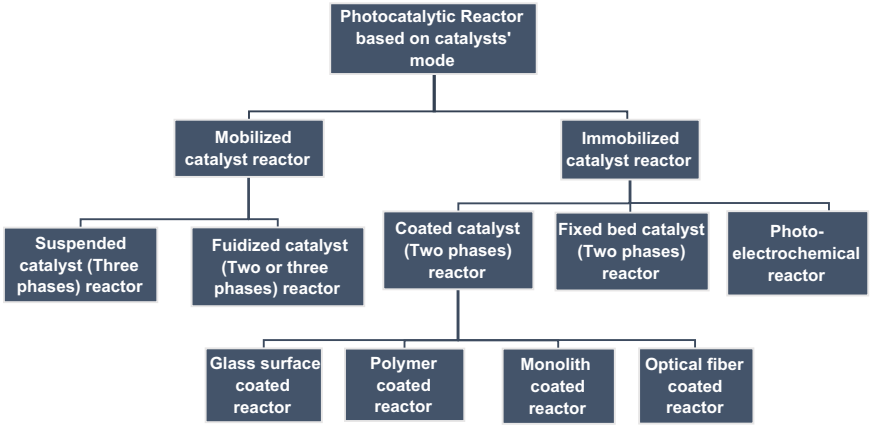

Fig. 8. Photocatalytic reactors based on the catalysts' mode during the operation.

Table 10
Recent developments in photocatalytic reactors to turn CO_2 into fuel.

Authors (year)/ Ref.	Light source (wavelelngth)/ light intensity	Photocatalyst (amounts)	Reactor type (reactor volume, illuminationn area)/no. of phases	Operating variables (T/P/pH/t/ QE)	Reactants (amounts)	Major product/ yield ($\mu mol\ h^{-1}\ g^{-1}$ catalyst)/ selectivity (%)	Comments
Slurry reactors							
Slamet et al. (2005)/ [156]	10 W UV black light lamp (415–700 nm)/ 2.45 mW cm^{-2}	3% CuO–TiO_2 (0.3 g)	Slurry type photocatalytic reactor (770 cm^3, –)/three phases	333/–/–/6/ 19.23	CO_2 (saturated), $KHCO_3$ (1M, 300 mL solution)	Methanol/ 442.5/19.23	• Slurry type photocatalytic reactor consists of a horizontal stainless steel vessel with an inner diameter and height of the vessel 140 and 50 mm, respectively having a plate cover at the top of the vessel is made of Pyrex. • The positive values of E_a indicate that desorption of products is the rate limiting step in the photosynthetic formation of methanol.
Lee et al. (2013)/ [260]	Simulated sunlight AM 1.5 G (–)/90 mW cm^{-2}	0.8 wt% Pt–$SrTiO_3$:Rh (0.15 g) and WO_3 (0.03 g)	Continuous mode twin reactor separated by a membrane (225 cm^3, –)/three phases	–/–/2.6/4/ 0.0051	CO_2 (saturated), $FeCl_2$ and $FeCl_3$ solution (2 mM)	Methanol/6/–	• CO_2 reduction is carried out in a novel twin reactor to mimic photosynthesis process in nature. • Hydrogen and oxygen produced separately in the twin reactor through water splitting prevents the regressive reaction to form water again. • Oxygen from water splitting can be effectively inaccessible to avoid the oxidation of hydrocarbon products.
Wang et al. (2012)/ [225]	500 W simulated solar light (–)/–	0.6 wt% ZnPc–TiO_2 (1.5 g)	Batch mode Pyrex glass cell (–)/three phases	–/–/–/8/–	CO_2 (saturated), NaOH solution (150 cm^3, 0.1 M)	Methanol/ 248.06/–	• ZnPc modified TiO_2 is successfully prepared by microwave assisted method and microwave treatment improves the catalytic activity. • 500 W Xe arc lamp is selected as it delivers bright white light that can closely mimic natural sunlight. • The reactor is firmly closed during the reaction and stirred continuously by a magnetic stirring bar to avoid catalyst sedimentation.
Fixed bed reactors							
Liu et al. (2013)/ [261]	150 W simulated solar irradiation (200–1000 nm)/ 90 mW cm^{-2}	1 wt% Cu–TiO_2 with H_2 treated (0.05 g)	Continuous flow mode cylindrical photoreactor with stainless steel wall and a quartz window (–)/two phases	298/–/–/2/ –	CO_2 (saturated), Water vapor (–)	Methane/1.5/–	• Nanoparticle catalysts are synthesized by a simple precipitation and calcination methods, and the sample is dominated by Cu^{2+} species. • Thermal pretreatment is also induced the formation of defect sites such as oxygen vacancies and Ti^{3+}, promoting CO_2 adsorption and subsequent charge transfer to the adsorbed CO_2. • The existence of Cu^+/Cu^0 couples assist to trap electron and hole at different sites. • CH_4 selectivity is promoted significantly on H_2-reduced Cu–TiO_2 samples is possibly related to interstitial H atoms.
Wang et al. (2013)/ [262]	300 W modified sunlight (–)/–	CeO_2–TiO_2 −1.0 with template SBA-15 (0.10 g)	Batch mode stainless steel reactor with quartz window (1500 cm^3, –)/two phases	303/1.08/ –/5.5/–	CO_2 (95.5%), water vapor (4.5%)	Methanol, carbon monoxide/215, 12727/–	• Catalyst composition is prepared through a nanocasting route using ordered mesoporous SBA-15 as a template. • CeO_2–TiO_2 composite shows ordered 2D hexagonal mesostructures with high specific surface area and hierarchical porosity.

Table 10 (*continued*)

Authors (year)/ Ref.	Light source (wavelelngth)/ light intensity	Photocatalyst (amounts)	Reactor type (reactor volume, illuminationn area)/no. of phases	Operating variables (T/P/pH/t/ QE)	Reactants (amounts)	Major product/ yield ($\mu mol\ h^{-1}\ g^{-1}$ catalyst)/ selectivity (%)	Comments
							• Excellent photocatalytic activity is achieved in the reduction of CO_2 with H_2O under simulated solar irradiation. • Radiation spectrum is placed at the top of quartz window with the distance of 8 cm, which can irradiate the whole catalyst powder. • Xe lamp is put in a cold trap and the whole reactor system is in the air circulation to control the reaction temperature.
Wang et al. (2014)/ [263]	300 W Simulated solar irradiation (–)/–	Mesoporous 20% Fe doped CeO_2 with siliceous SBA-15 (0.1 g)	Batch mode stainless steel reactor with quartz window (1500 cm^3, –)/two phases	303/1.08/ –/6/–	CO_2 (95.5%), water vapor (4.5%)	Carbon monoxide, methane/12.38, 3/–	• Catalyst is prepared through a nanocasting route using ordered mesoporous SBA-15 as the template. • Catalysts have ordered 2D hexagonal mesostructures with high specific surface area and porosity. • Introduction of Fe species increases the Ce^{3+} concentrations and surface chemisorbed oxygen species also accelerate the photocatalytic activity. • Catalyst powder was dispersed on the stainless steel omentum which is fixed in the center of reactor.
Zhao et al. (2012)/ [264]	150 W solar Simulator (200–1000 nm)/ 69.6 mW cm^{-2}	2 wt% Ag–TiO_2–SP (0.1 g)	Continuous flow mode cylindrical photoreactor with stainless steel walls and a quartz window (–)/three phases	293/–/7/4/ –	CO_2 (saturated), Water vapor and methanol mixture (2.2 and 0.6%)	Hydrogen/ 1130/98.3	• It is investigated that water using methanol acts as a hole scavenger in Ag-modified TiO_2 nanocomposite catalysts. • Mesoporous Ag–TiO_2 composite particles are synthesized by ultrasonic spray pyrolysis method, and shows larger specific surface area and a high dispersion of Ag nanoparticles on TiO_2 than conventional wet-impregnation method. • Powder catalysts are dispersed on a glass fiber filter and put at the bottom of the reactor. • The selectivity is changeable by varying the reaction gas composition and the H_2/CO ratio in the range from 2 to 10 has been attained.
Shi et al. (2004)/ [249]	125 W ultra-high pressure Hg lamp/ 20 mW cm^{-2}	0.5 wt% Cu–CdS loaded on TiO_2–SiO_2 (10 g)	Continuous mode quartz fixed bed reactor (–, 10 cm^2)/Two phases	373–473/ 1/–/–/–	CO_2, methane (1:1 M ratio)	Acetone, ethane/–/92.3, 3.1	• Coupled semiconductor (CS) photocatalyst is synthesized by using a mutli-step impregnation method, and fine CdS particles are dispersed on the surface of anatase TiO_2–SiO_2 substrate. • Chemisorption and IR analysis represents that methane absorbs in the molecular state interacts weakly with the surface of catalyst and product formation is varied based on interaction. • The temperature of the catalyst bed is measured by a chromel–alumel thermocouple.

Table 10 (*continued*)

Authors (year)/ Ref.	Light source (wavelelngth)/ light intensity	Photocatalyst (amounts)	Reactor type (reactor volume, illuminationn area)/no. of phases	Operating variables (T/P/pH/t/ QE)	Reactants (amounts)	Major product/ yield (μmol h^{-1} g^{-1} catalyst)/ selectivity (%)	Comments
Annular reactors							
Varghese et al. (2009)/ [186]	Global AM 1.5 sunlight (–)/100 mW cm^{-2}	N-doped titania nanotube loaded with copper (–)	Continuous mode two stainless steel chambers with an O-ring sealed quartz window at the top (7.5 cm^3 and 8.6 cm^3, 3.5 cm^2)/ two phases	317/ <0.068/ –/3.5/–	CO_2 (saturated), water vapor (saturated)	Methane/4.4/–	• This rate of CO_2 to hydrocarbon production obtains under outdoor sunlight is at least 20 times higher than which are conducted UV illumination. • Surface area of N-titania with copper nanotube arrays is high enough.
Kocí et al. (2011)/ [103]	8 W Hg lamps (254 nm)/–	Kaolinite modified TiO_2 composite (1 g)	Stirred batch annular reactor (–)/two phases	–/1/7/24/–	CO_2 (saturated), NaOH (0.2 M, 100 mL solution)	Hydrogen/ 0.187/–	• Production of methane and methanol were advanced over a kaolinite modified TiO_2 composite than over commercial TiO_2 (Degussa P-25). • Adding of TiO_2 nanoparticles into the kaolinite structure caused a decrease of anatase crystallite size. • Inhibit the recombination of electron–hole pairs and stop the formation of TiO_2 aggregates in suspension. • The photocatalytic reduction is conducted in a homemade apparatus using a stirred batch annular reactor with a suspended catalyst.
Koci et al. (2011)/ [125]	8 W Hg lamp (254 nm)/–	ZnS deposited on MMT (0.1 g)	Stirred batch annular reactor (–)/two phases	273/1/ –/24/–	CO_2 (saturated), NaOH (0.2 M solution)	Methanol, methane/ 1.41, 1.33/–	• It is analyzed that products yields depend on the reactor diameter and on the volume of the liquid phase. • Slurry type two stirred batch annular reactors is used with three quartz glass tubes of different diameters (3.5, 4.0 and 4.5 cm) placed inside the reactors. • Perfect mixing is one of the most important factors in slurry reactors and this mixing is difficult in annular reactors.
Fiber optics based reactors							
Nguyen et al. (2008)/ [214]	Concentrated natural sunlight (–)/20 mW cm^{-2}	N3 dye–0.5 wt % Cu–0.5 wt% Fe–TiO_2 (–)	Continuous mode circular optical-fiber, Pyrex glass reactor with a quartz window (216 cm^3, –)/two phases	348/–/–/6/ –	CO_2 (saturated), water vapor (–)	Methane/ 0.617/–	• Efficient charge transfer in N3 dye–TiO_2 system gives superior photoreduction of the resulting dye adsorbed catalyst. • Concentrated natural sunlight is collected by using a solar concentrator and the reflection dish of the solar concentrator is able to track the sun trajectory during a day can obtain the maximum sunlight intensity. • The reactor is shielded with a heating tape connected with a thermocouple to control temperature placed at the top of the catalyst bed.
Wu and Lin (2005)/ [252]	Hg lamp (365 nm)/ 16000 mW cm^{-2}	1.2 wt%–Cu–TiO_2 (–)	Continuous mode optical-fiber photo reactor with quartz window (8 cm^2, 16 cm long)/two phases	–/1.3/–/–/–	CO_2 (1.29 atm), water vapor (0.026 atm)	Methanol/ 0.45/–	• Titania and Cu-loaded solution is synthesized by a thermal hydrolysis method with a bang gap energy 3.3 eV. • Photocatalytic CO_2 conversion is conducted by a steady-state optical-fiber photoreactor, comprised of near 120Cu–TiO_2-coated fibers which is designed and assembled to transmit and spread

Table 10 (*continued*)

Authors (year)/ Ref.	Light source (wavelelngth)/ light intensity	Photocatalyst (amounts)	Reactor type (reactor volume, illuminationn area)/no. of phases	Operating variables (T/P/pH/t/ QE)	Reactants (amounts)	Major product/ yield (μmol h^{-1} g^{-1} catalyst)/ selectivity (%)	Comments
							light evenly inside reactor than a traditional packed-bed reactor. • The methanol yield is increased with UV irradiative intensity and photoactivity increased with increasing Cu loadings. • Optical fiber photoreactor is a promising photoreactor that can be applied to any aqueous or gas-phase photo reaction.
Wu et al. (2008)/ [233]	UV light (365 nm)/ 10,000 mW cm^{-2}	Sensitized TiO_2 with 1 wt % Ag (–)	Optical-fiber photoreactor (–)/two phases	348/ –/–/11/ 0.00013	CO_2 (1.13 atm), H_2O (0.03 bar)	Methanol/4.1/–	• An optical-fiber photoreactor, built-in 216 × catalyst-coated fibers are supported on circular plates and irradiated through the quartz window having a large external area of optical fiber to disperse catalysts. • Optical-fiber delivers a medium to transmit light uniformly throughout the reactor compared with a traditional packed-bed reactor.
Guan et al. (2003)/ [253]	Concentrated sunlight/ 5.57 kW m^{-2}	Pt-$K_2Ti_6O_{13}$ combined with Cu–ZnO (0.3 g)	Batch mode wet bed optical quartz tube cell (24.7 cm^3, –)/three phases	556/2/–/6/ –	CO_2 (saturated), water (4 cm^3)	Hydrogen, methanol/ 15.55, 5.33/–	• Reaction temperature exceeds 580 K due to concentrating the sunlight is sufficient for the Cu–ZnO catalyst to reduce CO_2 with H_2 into CH_3OH. • Product yields for the photocatalysts are much enhanced under concentrated sunlight. • It is observed that a simultaneous supply of photons and thermal energy can progress the activity of photocatalysts. • For focusing the sunlight on the catalyst layer, a concave mirror is also fixed on the support bar so that the catalyst layer is positioned at the focal point of the mirror. • This experiment found that merging photocatalysts with CO_2 hydrogenation catalysts is effective for synthesizing CH_3OH from CO_2 and water without addition of H_2 under concentrated sunlight.
Honeycomb monolith reactors							
Liou et al. (2011)/ [111]	300 W AM 1.5 G artificial sunlight/ 100 mWc m^{-2}	2.6 wt% NiO–$InTaO_4$ (–)	Continuous mode monolith reactor placed optical fibers into a circular Pyrex glass with quartz window (216 cm^3, –)/two phases	343/1/–/6/ 0.057	CO_2 (saturated), water vapor(–)	Acetaldehyde/ 0.3/–	• Monolith photoreactor increases the amount of catalyst loading due to its multiple channels. • Carved surface of polymethylmethacrylate optical fibers transmits and scatters light to illuminate the catalyst effectively inside the channels. • The quantum efficiency is significantly enhanced in the monolith reactor compared with optical-fiber reactor.
Ola et al. (2012)/ [258]	High pressure Hg lamp (320–500 nm)/ 41.62 mW cm^{-2}	1 wt% Pd–0.01 wt% Rh–TiO_2 (0.1099 g)	Continuous mode monolith placed into a cylindrical Pyrex glass reactor with quartz window (216 cm^3, 24 cm^2)/three phases	298/1/–/4/ 0.015, 0.047	CO_2 (saturated), water (–)	Methane, acetaldehyde/ 0.2, 0.31/–	• This modified photocatalyst is prepared by the improved sol–gel method. • The quantum efficiency of the internally illuminated monolith reactor was near one order of magnitude higher than the slurry batch annular reactor.

Table 10 (*continued*)

Authors (year)/ Ref.	Light source (wavelelngth)/ light intensity	Photocatalyst (amounts)	Reactor type (reactor volume, illuminationn area)/no. of phases	Operating variables (T/P/pH/t/ QE)	Reactants (amounts)	Major product/ yield (μmol h^{-1} g^{-1} catalyst)/ selectivity (%)	Comments
							• It is observed that metal loaded TiO_2 ceramic honeycomb monolithic structures threaded with optical fibers show high activity than the metal loaded TiO_2 nanoparticles suspended in aqueous media. • Flexible configuration of the monolith reactor provides maximum misuse of the high surface area and eliminates uneven light distribution through the optical fibers.
Photoelectrochemical (PEC) reactors							
Ampelli et al. (2010)/ [160]	60 W Solar lamp (–)/–	0.5 wt% Pt–TiO_2 (–)	Continuous mode PEC reactor made of Plexiglas and equipped with a quartz window (–, 5.7 cm^2)/three phases	313/19.35/ –/7/–	CO_2 (saturated), NaOH (1 M aqueous solution)	Hydrogen, Iso-propanol/5300, –/–	• Photoanodes TiO_2 thin films on an ordered array of titania-nanotubes are used to produce H_2 by water splitting or photoreforming of ethanol. • Carbon-nanotube based electrodes for the gas-phase reduction of CO_2 to liquid fuels is also investigated. • H_2O oxidation and CO_2 reduction in a photoanode and electrocathode, respectively, is necessary to increase the efficiency and limit charge recombination.
Ampelli et al. (2011)/ [259]	Solar light (–)/–	Pt–TiO_2 thin film on porous Ti foil (–)	Batch mode photoelectrochemical (PEC) reactor built in Plexiglas with quartz window (–)/three phases	343/1/ –/–/–	CO_2 (saturated), ethanol–water vapor (10%)	Hydrogen, iso-propanol/288 [a], –/–	• Reactor has two compartments with two electrodes, and it can be used either H_2 production from water splitting or CO_2 to liquid fuels. • Reactor is working like a reverse fuel cell in terms of minimizing light scattering phenomenon and increasing the photoefficiency. • Photoanode is used to produce H_2 by solar light and electrocathode is used to reduce CO_2 by current application, and it also limits charge recombination. • Two electrodes are joint together by a protonic membrane named Nafion.
Barton et al. (2008)/ [138]	200 W Hg–Xe arc light (365 nm)/–	p-GaP (–)	Photoelectrochemical cell (–)/three phases	–/–/5.2/ –/44	CO_2 (–), Pyridine (10 mM)	Methanol/ –/10.9	•Aqueous photoelectrochemical cell is used where light energy is the only energy used to carry out the reaction.

T/P/**pH**/**t**/**QE**: temperature (K)/pressure (atm)/pH/illumination period (h)/quantum efficiency (%); **'–':** Not mentioned in the original paper.

[a] μmol h^{-1}.

4.2. Fixed bed reactors

In this photochemical reactor, the fluid stream to be treated by flowing through the fixed bed, comes into contact with the light-exposed catalyst particles (Fig. 10). Several drawbacks exist in this reactor geometry, such as a low surface area to reactor volume ratio and poor utilization of photon energy, which hinders both light absorption and scattering [247]. Various sorts of fixed bed reactors have been employed for placing catalysts in different photocatalytic operation processes: (i) flat or curved surface, (ii) corrugated surface, (iii) monoliths, (iv) packed bed, and (v) reticular geometry. A fixed parallel flat glass fiber mesh was also used in a photocatalytic reaction by Esterkin et al. to get a high illuminated surface area with respect to the volume of the reacting mixture [248]. The fixed bed facilitates the radiation field having the catalysts immobilized on an inactive support. Shi et al. carried out the photocatalytic conversion of CO_2 into fuel by using a continuous mode quartz fixed bed (10 cm^2) reactor [249]. In the investigation by Wang et al., they placed photo-catalysts on a glass surface inside a quartz vessel, and the light irradiation was carried out from the top of the vessel [219]. A fixed bed reactor provides low pressure drops during operation, and gives a high yield per unit of catalyst mass through the plug flow system [199].

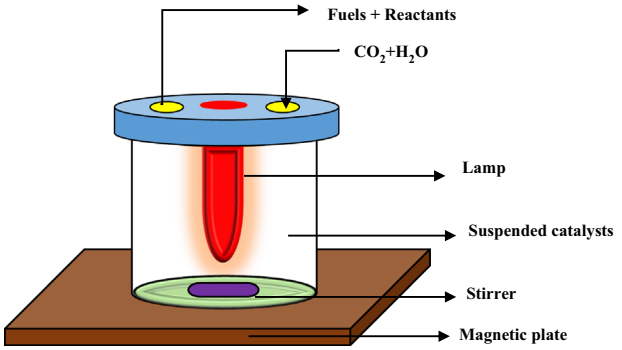

Fig. 9. Schematic view of a slurry reactor.

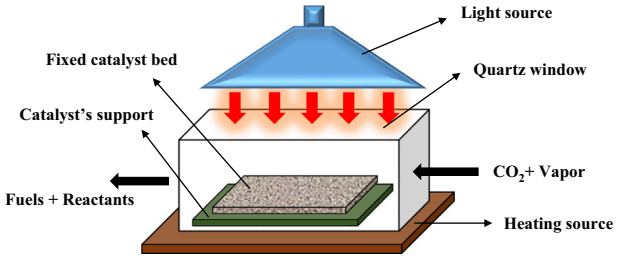

Fig. 10. Schematic of a fixed bed photocatalytic reactor.

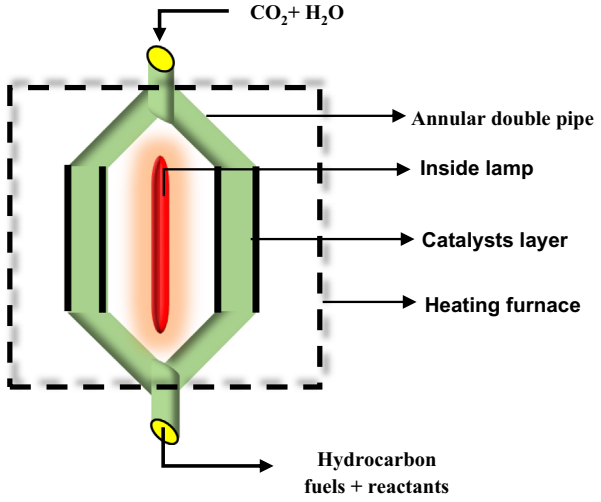

Fig. 11. Schematic diagram of the annular reactor with an inside lamp.

4.3. Annular reactors

Annular reactors usually consist of two concentric cylinders that form an annular space with a certain distance, as shown in Fig. 11. The catalyst layer is placed on the inner wall of the outer cylinder. The light source is located in the center, and the width of the catalyst layer on the surface of the reactor is low enough to allow all of the catalysts to be exposed to the light irradiation. Conversely, when light is passed from outside the reactor, the catalyst is covered on the surface of two centric cylinders. Due to there being a smaller cross-section, the gas velocity through the reactor is high enough to prevent the product adsorption on the catalysts' surface [250]. Koci et al. fabricated a different type of annular reactor, because it is difficult to obtain perfect mixing in conventional annular geometry of the reactor [125]. They designed a stirred batch annular photoreactor where the lamp was adjacent

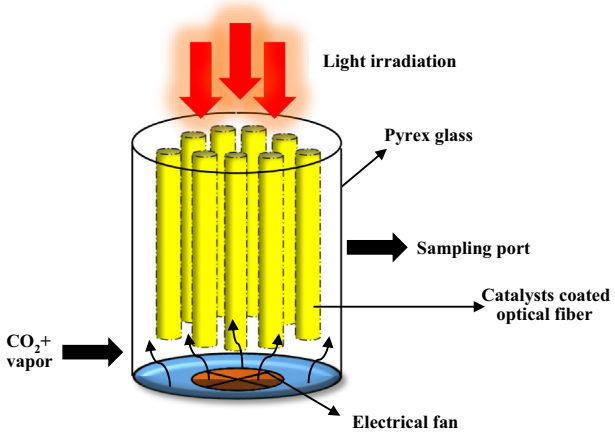

Fig. 12. Schematic diagram of the optical fiber photocatalytic reactor.

to the surface of the liquid in the reactor. Another photocatalytic reactor-like shell and tube heat exchanger, which consists of a bundle of external catalyst-coated hollow glass tubes, can be used in the photocatalytic reduction of CO_2.

4.4. Fiber optics based reactors

In a fiber optic photochemical reactor, rather than using a single irradiation lamp, a package of optical fibers can be used as media to provide light irradiation inside the photocatalytic reactor (Fig. 12). This optical fiber reactor is a favorable photoreactor for carrying out the reaction in any aqueous or gas-phase [251]. Wu and Lin are the pioneers of the use of fiber-optics in the production of fuels through CO_2 photoconversion due to the high transmission and uniform light distribution inside the reactor [252]. They designed a continuous mode optical-fiber photo reactor (including approximately 120Cu–TiO_2-coated fibers) with a quartz window (8 cm^2, 16 cm long) for a two-phase reaction using Hg lamp (365 nm wavelength) of 16,000 mW cm^{-2}.

Nguyen et al. performed the photochemical conversion of CO_2 using a continuous mode circular optical fiber reactor (216 cm^3) under concentrated natural sunlight with an intensity of 20 mW cm^{-2} [214]. Another investigation was carried out by Guan et al. to understand the performance of a batch mode wet-bed optical quartz tube cell (24.7 cm^3) upon the photochemical reduction of CO_2 under concentrated sunlight [253]. For focusing sunlight on the catalyst layer, a concave mirror was also fixed on the support bar, so that the catalyst layer was positioned at the focal point of the mirror. It was revealed that instantaneous supply of photons and thermal energy enhanced the catalytic activity. Besides these advantages of fiber-optic-based photoreactors, some drawbacks were also shown, like poor adhesion strength to the catalysts over the surface of optical fibers, comparatively low surface area, low reactor volume and a small area for photon energy absorption [254].

4.5. Honeycomb monolith reactors

A honeycomb monolith reactor consists of a definite number of channels, as illustrated in Fig. 13; each single channel characteristically has an internal dimension of 1 mm. The cross-sectional figures of channels are square or circular and the catalyst is layered onto the walls of channels in a very thin wash coat [255,256]. Some researchers applied coated optical fibers employed in the channels of the monolith substrate to develop the reactor configuration [257]. The advantages of monolith structure are its low pressure decrease and its high surface area to volume ratio. Light-illuminating fibers are

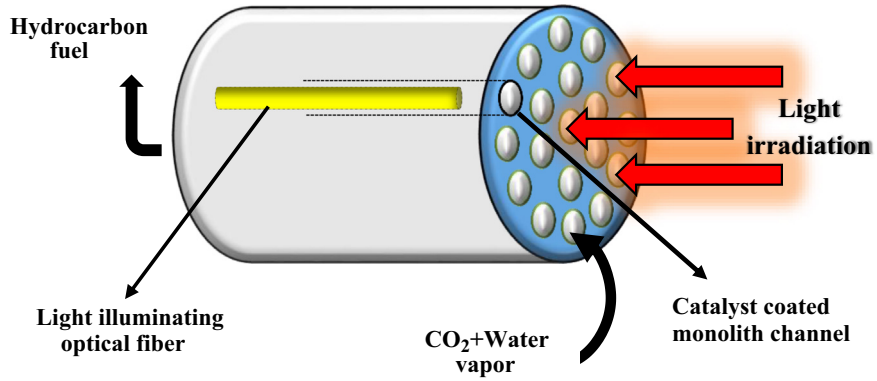

Fig. 13. Illustration of the monolith reactor with light illuminating optical fiber.

positioned inside the passages of a ceramic monolith, arranged with a photocatalyst layer on the wall of each distinct passageway [254].

Liou et al. reported an internally-illuminated continuous mode monolith reactor (216 cm^3) where optical fibers were placed inside the reactor's channels [111]. This system was run in a circular Pyrex glass vessel with a quartz window, which was a two-phase reaction system to convert CO_2 into fuel under 300 W AM 1.5 G artificial sunlight (100 mW cm^{-2}). They chose both NiO–$InTaO_4$ catalysts and the monolith reactor because of a high solar response ability and multiple passageways to load a huge amount of catalysts, respectively. Graven surface of optical fibers also facilitated the light transmission and distribution efficiently on the catalyst surface coated inside the passageways of the monolith reactor. It was also observed that the utilization of photon energy was more than that of conventional optical fiber reactors. In another research, Ola et al. conducted their photocatalytic reduction of CO_2 in a continuous mode cylindrical Pyrex glass vessel with a quartz window (216 cm^3, 24 cm^2), where the monolith was kept inside the vessel [258]. It is a three-phase reaction process in which a high pressure Hg lamp (320–500 nm wavelength) of 41.62 mW cm^{-2} intensity was used as a light source. The quantum productivity of an internally-irradiated continuous mode monolith reactor was found to be 23.5 times higher compared with the slurry batch annular reactor due to the formation of active sites by the decent contact between the monoliths and reactants; and the exclusion of uneven light scattering through the optical fibers.

4.6. Photoelectrochemical (PEC) reactors

Beside photocatalytic reactors, the photoelectrochemical reactors are widely used for the photocatalytic conversion of CO_2 into hydrocarbon fuels. In this reactor, semiconductors are coated on the electrode surface which are truly stable under solar lighting; this leads to a significant over-potential for CO_2 reduction on semiconductor surfaces. A simple photoelectrochemical reactor is depicted in Fig. 14 for the photocatalytic transformation of CO_2 into fuels. Direct conversion of solar energy to chemical energy is also possible in this process. Ampelli et al. worked on a batch mode PEC reactor built in plexiglas with a quartz window for CO_2 conversion under solar light irradiation [160,259]. Here, the reactor has two compartments with two electrodes joined together by a nafion membrane, and either H_2 production from water splitting or CO_2 to liquid fuels can be used. The reactor also works like a reverse fuel cell in terms of minimizing the light scattering phenomenon and increasing photoefficiency. A photoanode is used to produce H_2 by solar light and electrocathodes are used to reduce CO_2 by current application; it also limits charge recombination.

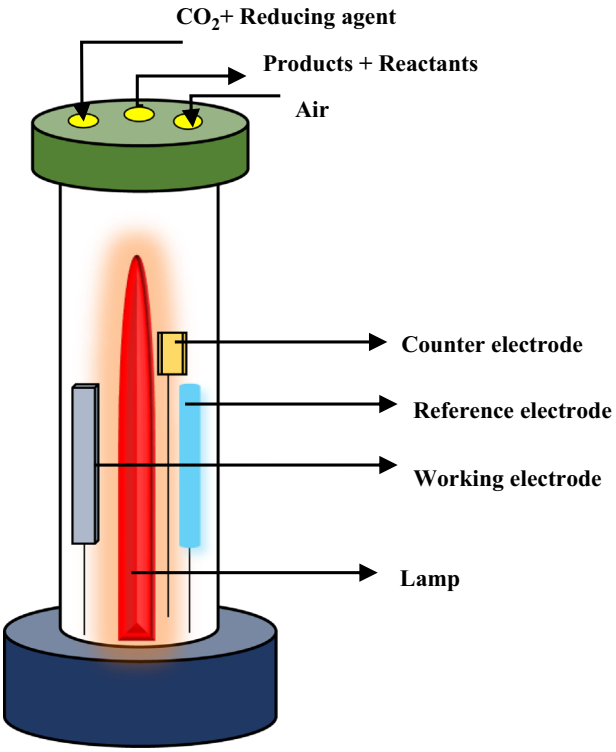

Fig. 14. Simple photoelectrochemical (PEC) reactor.

However, there are some limitation in this technology such as fouling and precipitation on the electrode surface which can hamper efficient electron transfer, the fact that the catalytic reduction process needs an external electrical potential bias to proceed and reactor design are still obligatory to permit the development of commercial processes.

5. Conclusion

The conversion of CO_2 into solar fuels is an alternative remediation to control both the fuel crisis and global warming. Since 1978, numerous investigations have been performed to evaluate the photocatalytic performance over CO_2 conversion into fuels. The photocatalytic transformation of CO_2 was found to be more favorable compared with the other transformation approaches such as thermochemical, electrochemical, and biological processes. In this paper, a general overview is highlighted on the behavior of different sorts of photocatalysts and photoreactors

with respect to the photochemical conversion of CO_2. From this review, it was found that most of the photochemical experiments were performed in the presence of an artificial light source, but some researchers have recently emphasized their knowledge of solar-derived fuels from CO_2 mainly by developing catalysts and reactors. In the case of catalyst selection, catalysts must have a desired band gap energy for visible light responses. Previously, unmodified oxide and non-oxide semiconductors have been widely used in this technology. However, some of them have high band gap energy and low conversion yields. To facilitate this, some techniques have been followed to minimize the band gap energy such as doping of foreign elements like novel metals, transition metals, co-metals, and non-metals with semiconductors. It also influences the charge transfer rate and reduces the electron–hole recombination. Furthermore, different substrate materials were used to achieve high surface areas and catalyst immobilization during the photocatalytic irradiation. Recently, different types of sensitization techniques have been incorporated to improve the photocatalytic performance under visible light irradiation, like dye sensitization, enzyme-based sensitization, QDs, and phthalocyanines sensitization. Both doped and sensitized semiconductors were employed for higher conversion. The selectivity of products not only depends on the catalyst's composition, but also on the choice of reductant. Water is the most common reductant used as a liquid or gaseous medium in the photochemical CO_2 conversion process. Although it is available and affordable, there are some limitations like low CO_2 solubility and encouraging water splitting reactions rather than CO_2 reduction. Instead, CH_4 and H_2 were used as influential reductants in many investigations reported in this review. Initially, the photocatalytic reduction of CO_2 was carried out in slurry-type reactors with a UV light source. Later, fixed bed reactors were also used to give support and immobilize the catalyst during the operation. After that, optical fiber reactors and monolith reactors are introduced in this technology to obtain the sufficient loading of catalysts with enough surface area exposed, efficient light distribution over the surface of catalysts and other benefits like multi-channels, facility to visible light or direct solar irradiation. For effective solar irradiation, parabolic trough reactors, falling film reactors, tubular reactors and flat plate reactors have been recommended in many investigations. Other factors are definitely considerable for evaluating photocatalytic performance on CO_2 reduction such as catalysts dosage, reactants' ratio, reaction temperature, time, system pressure, pH, light intensity and wavelength. Deep knowledge is essential for understanding reaction mechanisms together with charge carrier dynamics within the catalysts and at their interfaces with the metal co-catalysts.

From the above discussion, it is clear that the existing techniques are not sufficient to make them applicable for industrial production of fuels. The necessary efficient photocatalysts and suitable design of photocatalysts must be focused on the future studies. For solar light harnessing, the photocatalysts must be concentrated on the appropriate band gap energy and proper structure. Among different types of photocatalysts, sensitized and metal sulfide photocatalysts could be effective for efficient CO_2 conversion by direct solar irradiation. The operating parameters could also be optimized to maximize conversion and yield rates. The strategy of photocatalytic reactors for CO_2 conversion is unlike that of conventional chemical reactors used for water and air treatment; each research group has an individual design without any set standards. The reactor design needs more advancement to increase the efficiency of CO_2 reduction, which is capable of efficiently harnessing solar radiation. Among the different types of photoreactors, for future prospects, optical fiber and monolith photoreactors have high illuminated surface area and solar light harnessing capability for CO_2 reduction applications. Therefore, the selection of direct sunlight reactive high yield photocatalysts, and the unique architecture of solar light operating reactors are the crucial challenges for establishing economically approachable and industrially feasible technologies to turn CO_2 into valuable fuels.

Acknowledgments

The authors acknowledge financial support from projects RP015/2012D and D000011-16001, Center of Research Grant Management, University of Malaya, 50603 Kuala Lumpur, Malaysia.

References

[1] BP: Statistical Review of World Energy. London; 2013. Retrieved from: ⟨http://www.bp.com/content/dam/bp/pdf/statistical-review/statistical_review_of_world_energy_2013.pdf⟩.
[2] Shafiullah G, Amanullah M, Shawkat Ali A, Jarvis D, Wolfs P. Prospects of renewable energy—a feasibility study in the australian context. Renew Energy 2012;39:183–97.
[3] Panwar N, Kaushik S, Kothari S. Role of renewable energy sources in environmental protection: a review. Renew Sustain Energy Rev 2011;15:1513–24.
[4] Mekhilef S, Siga S, Saidur R. A review on palm oil biodiesel as a source of renewable fuel. Renew Sustain Energy Rev 2011;15:1937–49.
[5] Centi G, van Santen RA. Catalysis for renewables. Weinheim: Wiley; 2008.
[6] Li H, Dai Y, Köhler M, Wang R. Simulation and parameter analysis of a two-stage desiccant cooing/heating system driven by solar air collectors. Energy Convers Manage 2013;67:309–17.
[7] Shukla R, Sumathy K, Erickson P, Gong J. Recent advances in the solar water heating systems: a review. Renew Sustain Energy Rev 2013;19:173–90.
[8] Mansouri NY, Crookes RJ, Korakianitis T. A projection of energy consumption and carbon dioxide emissions in the electricity sector for Saudi Arabia: the case for carbon capture and storage and solar photovoltaics. Energy Policy 2013;63:681–95.
[9] Branker K, Pathak M, Pearce JM. A review of solar photovoltaic levelized cost of electricity. Renew Sustain Energy Rev 2011;15:4470–82.
[10] Angew Chem Int EdJamel M, Abd Rahman A, Shamsuddin A. Advances in the integration of solar thermal energy with conventional and non-conventional power plants. Renew Sustain Energy Rev 2013;20:71–81.
[11] Behar O, Khellaf A, Mohammedi K. A review of studies on central receiver solar thermal power plants. Renew Sustain Energy Rev 2013;23:12–39.
[12] Lee J, Back H, Kong J, Kang H, Suhee S, Hongsuk S, et al. Seamless polymer solar cell module architecture built upon self-aligned alternating interfacial layers. Energy Environ Sci 2013;6:1152–7.
[13] Ralegaonkar RV, Gupta R. Review of intelligent building construction: a passive solar architecture approach. Renew Sustain Energy Rev 2010;14:2238–42.
[14] Liu C, Dasgupta NP, Yang P. Semiconductor nanowires for artificial photosynthesis. Chem Mater 2014;26:415–22.
[15] Ganesh I. Conversion of carbon dioxide into methanol—a potential liquid fuel: fundamental challenges and opportunities (a review). Renew Sustain Energy Rev 2014;31:221–57.
[16] Sivula K. Metal oxide photoelectrodes for solar fuel production, surface traps, and catalysis. J Phys Chem Lett 2013;4:1624–33.
[17] Lacis AA, Schmidt GA, Rind D, Ruedy RA. Atmospheric CO_2: principal control knob governing Earth's temperature. Science 2010;330:356–9.
[18] Florides GA, Christodoulides P, Messaritis V. Reviewing the effect of CO_2 and the sun on global climate. Renew Sustain Energy Rev 2013;26:639–51.
[19] Ibrahim MH, Law SH. Social capital and CO_2 emission—output relations: a panel analysis. Renew Sustain Energy Rev 2014;29:528–34.
[20] Köne AÇ, Büke T. Forecasting of CO_2 emissions from fuel combustion using trend analysis. Renew Sustain Energy Rev 2010;14:2906–15.
[21] International energy agency annual report. 2012. Retrieved from: ⟨http://www.iea.org/publications/freepublications/publication/English.pdf⟩.
[22] Li X, Lin B. Global convergence in per capita CO_2 emissions. Renew Sustain Energy Rev 2013;24:357–63.
[23] Omae I. Recent developments in carbon dioxide utilization for the production of organic chemicals. Coord Chem Rev 2012;256:1384–405.
[24] U.S. Department of Energy (DOE); 2013. Retrieved from: www.doe.gov/.
[25] Lee ZH, Sethupathi S, Lee KT, Bhatia S, Mohamed AR. An overview on global warming in Southeast Asia: CO_2 emission status, efforts done, and barriers. Renew Sustain Energy Rev 2013;28:71–81.
[26] Hosseini SE, Wahid MA, Aghili N. The scenario of greenhouse gases reduction in Malaysia. Renew Sustain Energy Rev 2013;28:400–9.
[27] Ming T, de_Richter R, Liu W, Caillol S. Fighting global warming by climate engineering: is the Earth radiation management and the solar radiation management any option for fighting climate change? Renew Sustain Energy Rev 2014;31:792–834.
[28] Mikkelsen M, Jørgensen M, Krebs FC. The teraton challenge. A review of fixation and transformation of carbon dioxide. Energy Environ Sci 2010;3:43–81.

[29] Sakakura T, Choi J-C, Yasuda H. Transformation of carbon dioxide. Chem Rev 2007;107:2365–87.
[30] Obert R, Dave BC. Enzymatic conversion of carbon dioxide to methanol: enhanced methanol production in silica sol–gel matrices. J Am Chem Soc 1999;121:12192–3.
[31] Abe T, Tanizawa M, Watanabe K, Taguchi A. CO_2 methanation property of Ru nanoparticle-loaded TiO_2 prepared by a polygonal barrel-sputtering method. Energy Environ Sci 2009;2:315–21.
[32] Yui T, Kan A, Saitoh C, Koike K, Ibusuki T, Ishitani O. Photochemical reduction of CO_2 Using TiO_2: effects of organic adsorbates on TiO_2 and deposition of Pd onto TiO_2. ACS Appl Mater Interfaces 2011;3:2594–600.
[33] Angamuthu R, Byers P, Lutz M, Spek AL, Bouwman E. Electrocatalytic CO_2 conversion to oxalate by a copper complex. Science 2010;327:313–5.
[34] Ichikawa S, Doi R. Hydrogen production from water and conversion of carbon dioxide to useful chemicals by room temperature photoelectrocatalysis. Catal Today 1996;27:271–7.
[35] Chueh WC, Falter C, Abbott M, Scipio D, Furler P, Haile SM, et al. High-flux solar-driven thermochemical dissociation of CO_2 and H_2O using nonstoichiometric ceria. Science 2010;330:1797–801.
[36] Olah GA, Goeppert A, Prakash GS. Chemical recycling of carbon dioxide to methanol and dimethyl ether: from greenhouse gas to renewable, environmentally carbon neutral fuels and synthetic hydrocarbons. J Org Chem 2008;74:487–98.
[37] Wee J-H. Carbon dioxide emission reduction using molten carbonate fuel cell systems. Renew Sustain Energy Rev 2014;32:178–91.
[38] Jitaru M. Electrochemical carbon dioxide reduction—fundamental and applied topics. J Univ Chem Technol Metall 2007;42:333–44.
[39] Benson EE, Kubiak CP, Sathrum AJ, Smieja JM. Electrocatalytic and homogeneous approaches to conversion of CO_2 to liquid fuels. Chem Soc Rev 2009;38:89–99.
[40] Usubharatana P, McMartin D, Veawab A, Tontiwachwuthikul P. Photocatalytic process for CO_2 emission reduction from industrial flue gas streams. Ind Eng Chem Res 2006;45:2558–68.
[41] Razzak SA, Hossain MM, Lucky RA, Bassi AS, de Lasa H. Integrated CO_2 capture, wastewater treatment and biofuel production by microalgae culturing—a review. Renew Sustain Energy Rev 2013;27:622–53.
[42] Stewart C, Hessami M-A. A study of methods of carbon dioxide capture and sequestration—the sustainability of a photosynthetic bioreactor approach. Energy Convers Manage 2005;46:403–20.
[43] Usui N, Ikenouchi M. The biological CO_2 fixation and utilization project by RITE (1)—highly-effective photobioreactor system. Energy Convers Manage 1997;38:S487–92.
[44] Zeng X, Danquah MK, Chen XD, Lu Y. Microalgae bioengineering: from CO_2 fixation to biofuel production. Renew Sustain Energy Rev 2011;15:3252–60.
[45] Yang H, Xu Z, Fan M, Gupta R, Slimane RB, Bland AE, et al. Progress in carbon dioxide separation and capture: a review. J Environ Sci 2008;20:14–27.
[46] Razali NAM, Lee KT, Bhatia S, Mohamed AR. Heterogeneous catalysts for production of chemicals using carbon dioxide as raw material: a review. Renew Sustain Energy Rev 2012;16:4951–64.
[47] Tahir M, Amin NS. Recycling of carbon dioxide to renewable fuels by photocatalysis: prospects and challenges. Renew Sustain Energy Rev 2013;25:560–79.
[48] Bradford MC, Vannice MA. Catalytic reforming of methane with carbon dioxide over nickel catalysts I. Catalyst characterization and activity. Appl Catal A: Gen 1996;142:73–96.
[49] Arakawa H, Aresta M, Armor JN, Barteau MA, Beckman EJ, Bell AT, et al. Catalysis research of relevance to carbon management: progress, challenges, and opportunities. Chem Rev 2001;101:953–96.
[50] Abe R, Sayama K, Sugihara H. Development of new photocatalytic water splitting into H_2 and O_2 using two different semiconductor photocatalysts and a shuttle redox mediator IO^{3-}/I. J Phys Chem B 2005;109:16052–61.
[51] Graves C, Ebbesen SD, Mogensen M, Lackner KS. Sustainable hydrocarbon fuels by recycling CO_2 and H_2O with renewable or nuclear energy. Renew Sustain Energy Rev 2011;15:1–23.
[52] Wang Z-Y, Chou H-C, Wu J, Tsai DP, Mul G. CO_2 photoreduction using NiO/$InTaO_4$ in optical-fiber reactor for renewable energy. Appl Catal A: Gen 2010;380:172–7.
[53] Hori H, Ishitani O, Koike K, Johnson F, Ibusuki T. Efficient carbon dioxide photoreduction by novel metal complexes and its reaction mechanisms. Energy Convers Manage 1995;36:621–4.
[54] Das S, Daud WMAW. A review on advances in photocatalysts towards CO_2 conversion. RSC Adv 2014;4:20856–93.
[55] Zou Z, Ye J, Sayama K, Arakawa H. Direct splitting of water under visible light irradiation with an oxide semiconductor photocatalyst. Nature 2001;414:625–7.
[56] Ni M, Leung MK, Leung DY, Sumathy K. A review and recent developments in photocatalytic water-splitting using TiO_2 for hydrogen production. Renew Sustain Energy Rev 2007;11:401–25.
[57] Han F, Kambala VSR, Srinivasan M, Rajarathnam D, Naidu R. Tailored titanium dioxide photocatalysts for the degradation of organic dyes in wastewater treatment: a review. Appl Catal A: Gen 2009;359:25–40.
[58] Bahnemann D. Photocatalytic water treatment: solar energy applications. Sol Energy 2004;77:445–59.
[59] Benedix R, Dehn F, Quaas J, Orgass M. Application of titanium dioxide photocatalysis to create self-cleaning building materials. Lacer 2000;5:157–68.
[60] Fujishima A, Rao TN, Tryk DA. Titanium dioxide photocatalysis. J Photochem Photobiol C: Photochem Rev 2000;1:1–21.
[61] Inoue T, Fujishima A, Konishi S, Honda K. Photoelectrocatalytic reduction of carbon dioxide in aqueous suspensions of semiconductor powders. Nature 1979;277:637–8.
[62] Sakthivel S, Kisch H. Daylight photocatalysis by carbon-modified titanium dioxide. Angew Chem Int Ed 2003;42:4908–11.
[63] Tada H, Jin Q, Nishijima H, Yamamoto H, Fujishima M, Si Okuoka, et al. Titanium (IV) dioxide surface-modified with iron oxide as a visible light photocatalyst. Angew Chem 2011;123:3563–7.
[64] Tahir M, Amin NS. Photocatalytic reduction of carbon dioxide with water vapours over montmorillonite modified TiO_2 nanocomposites. Appl Catal B: Environ 2013;142–143:512–22.
[65] Van Grieken R, Aguado J, López-Muñoz M, Marugán J. Synthesis of size-controlled silica-supported TiO_2 photocatalysts. J Photochem Photobiol A: Chem 2002;148:315–22.
[66] Bouras P, Stathatos E, Lianos P. Pure versus metal-ion-doped nanocrystalline titania for photocatalysis. Appl Catal B: Environ 2007;73:51–9.
[67] Kočí K, Obalová L, Matějová L, Plachá D, Lacný Z, Jirkovský J, et al. Effect of TiO_2 particle size on the photocatalytic reduction of CO_2. Appl Catal B: Environ 2009;89:494–502.
[68] Kočí K, Obalová L, Lacný Z. Photocatalytic reduction of CO_2 over TiO_2 based catalysts. Chem Pap 2008;62:1–9.
[69] Tan SS, Zou L, Hu E. Photocatalytic reduction of carbon dioxide into gaseous hydrocarbon using TiO_2 pellets. Catal Today 2006;115:269–73.
[70] Fotou GP, Pratsinis SE. Photocatalytic destruction of phenol and salicylic acid with aerosol-made and commercial titania powders. Chem Eng Commun 1996;151:251–69.
[71] Dimitrijevic NM, Vijayan BK, Poluektov OG, Rajh T, Gray KA, He H, et al. Role of water and carbonates in photocatalytic transformation of CO_2 to CH_4 on titania. J Am Chem Soc 2011;133:3964–71.
[72] Kaneco S, Kurimoto H, Shimizu Y, Ohta K, Mizuno T. Photocatalytic reduction of CO_2 using TiO_2 powders in supercritical fluid CO_2. Energy 1999;24:21–30.
[73] Kaneco S, Kurimoto H, Ohta K, Mizuno T, Saji A. Photocatalytic reduction of CO_2 using TiO_2 powders in liquid CO_2 medium. J Photochem Photobiol A: Chem 1997;109:59–63.
[74] Dey G, Belapurkar A, Kishore K. Photo-catalytic reduction of carbon dioxide to methane using TiO_2 as suspension in water. J Photochem Photobiol A: Chem 2004;163:503–8.
[75] Li G, Li L, Boerio-Goates J, Woodfield BF. High purity anatase TiO_2 nanocrystals: near room-temperature synthesis, grain growth kinetics, and surface hydration chemistry. J Am Chem Soc 2005;127:8659–66.
[76] Xi G, Ouyang S, Li P, Ye J, Ma Q, Su N, et al. Ultrathin $W_{18}O_{49}$ nanowires with diameters below 1 nm: synthesis, near-infrared absorption, photoluminescence, and photochemical reduction of carbon dioxide. Angew Chem Int Ed 2012;51:2395–9.
[77] Yuliati L, Itoh H, Yoshida H. Photocatalytic conversion of methane and carbon dioxide over gallium oxide. Chem Phys Lett 2008;452:178–82.
[78] Kohno Y, Tanaka T, Funabiki T, Yoshida S. Reaction mechanism in the photoreduction of CO_2 with CH_4 over ZrO_2. Phys Chem Chem Phys 2000;2:5302–7.
[79] Teramura K, Tanaka T, Ishikawa H, Kohno Y, Funabiki T. Photocatalytic Reduction of CO_2 to CO in the presence of H_2 or CH_4 as a reductant over MgO. J Phys Chem B 2004;108:346–54.
[80] Lo C-C, Hung C-H, Yuan C-S, Wu J-F. Photoreduction of carbon dioxide with H_2 and H_2O over TiO_2 and ZrO_2 in a circulated photocatalytic reactor. Sol Energy Mater Sol Cells 2007;91:1765–74.
[81] Liu Y, Huang B, Dai Y, Zhang X, Qin X, Jiang M, et al. Selective ethanol formation from photocatalytic reduction of carbon dioxide in water with $BiVO_4$ photocatalyst. Catal Commun 2009;11:210–3.
[82] Yu J, Kudo A. Effects of structural variation on the photocatalytic performance of hydrothermally synthesized $BiVO_4$. Adv Funct Mater 2006;16:2163–9.
[83] Zhou Y, Tian Z, Zhao Z, Liu Q, Kou J, Chen X, et al. High-yield synthesis of ultrathin and uniform Bi_2WO_6 square nanoplates benefitting from photocatalytic reduction of CO_2 into renewable hydrocarbon fuel under visible light. ACS Appl Mater Interfaces 2011;3:3594–601.
[84] Liu Q, Zhou Y, Kou J, Chen X, Tian Z, Gao J, et al. High-yield synthesis of ultralong and ultrathin Zn_2GeO_4 nanoribbons toward improved photocatalytic reduction of CO_2 into renewable hydrocarbon fuel. J Am Chem Soc 2010;132:14385–7.
[85] Li X, Pan H, Li W, Zhuang Z. Photocatalytic reduction of CO_2 to methane over HNb_3O_8 nanobelts. Appl Catal A: Gen 2012;413:103–8.
[86] Stock M, Dunn S. $LiNbO_3$—a polar material for solid–gas artificial photosynthesis. Ferroelectrics 2011;419:9–13.
[87] Lekse JW, Underwood MK, Lewis JP, Matranga C. Synthesis, characterization, electronic structure, and photocatalytic behavior of $CuGaO_2$ and $CuGa_{1-x}Fe_xO_2$ (x=0.05, 0.10, 0.15, 0.20) delafossites. J Phys Chem C 2012;116:1865–72.
[88] Xia X-H, Jia Z-J, Yu Y, Liang Y, Wang Z, Ma L-L. Preparation of multi-walled carbon nanotube supported TiO_2 and its photocatalytic activity in the reduction of CO_2 with H_2O. Carbon 2007;45:717–21.
[89] Yahaya A, Gondal M, Hameed A. Selective laser enhanced photocatalytic conversion of CO_2 into methanol. Chem Phys Lett 2004;400:206–12.
[90] Anpo M, Yamashita H, Ichihashi Y, Ehara S. Photocatalytic reduction of CO_2 with H_2O on various titanium oxide catalysts. J Electroanal Chem 1995;396:21–6.

[91] Solymosi F, Tombacz I. Photocatalytic reaction of H_2O+CO_2 over pure and doped Rh/TiO_2. Catal Lett 1994;27:61–5.
[92] Jüntgen H. Activated carbon as catalyst support: a review of new research results. Fuel 1986;65:1436–46.
[93] Kruk M, Jaroniec M, Ko CH, Ryoo R. Characterization of the porous structure of SBA-15. Chem Mater 2000;12:1961–8.
[94] López-Muñoz M-J, Rv Grieken, Aguado J, Marugán J. Role of the support on the activity of silica-supported TiO_2 photocatalysts: structure of the TiO_2/SBA-15 photocatalysts. Catal Today 2005;101:307–14.
[95] Li Y, Wang W-N, Zhan Z, Woo M-H, Wu C-Y, Biswas P. Photocatalytic reduction of CO_2 with H_2O on mesoporous silica supported Cu/TiO_2 catalysts. Appl Catal B: Environ 2010;100:386–92.
[96] Liu B-J, Torimoto T, Yoneyama H. Photocatalytic reduction of carbon dioxide in the presence of nitrate using TiO_2 nanocrystal photocatalyst embedded in SiO_2 matrices. J Photochem Photobiol A: Chem 1998;115:227–30.
[97] Gokon N, Hasegawa N, Kaneko H, Aoki H, Tamaura Y, Kitamura M. Photocatalytic effect of ZnO on carbon gasification with CO_2 for high temperature solar thermochemistry. Sol Energy Mater Sol Cells 2003;80:335–41.
[98] Papp J, Soled S, Dwight K, Wold A. Surface acidity and photocatalytic activity of TiO_2, WO_3/TiO_2, and MoO_3/TiO_2 photocatalysts. Chem Mater 1994;6:496–500.
[99] Subrahmanyam M, Kaneco S, Alonso-Vante N. A screening for the photo reduction of carbon dioxide supported on metal oxide catalysts for C_1–C_3 selectivity. Appl Catal B: Environ 1999;23:169–74.
[100] Anpo M, Yamashita H, Ichihashi Y, Fujii Y, Honda M. Photocatalytic reduction of CO_2 with H_2O on titanium oxides anchored within micropores of zeolites: effects of the structure of the active sites and the addition of Pt. J Phys Chem B 1997;101:2632–6.
[101] Truong QD, Liu J-Y, Chung C-C, Ling Y-C. Photocatalytic reduction of CO_2 on $FeTiO_3/TiO_2$ photocatalyst. Catal Commun 2012;19:85–9.
[102] Deer RAH WA, Zussman J. An introduction to the rock-forming minerals. 2nd ed.. Harlow: Longman; 1992.
[103] Kočí K, Matějka V, Kovář P, Lacný Z, Obalová L. Comparison of the pure TiO_2 and kaolinite/TiO_2 composite as catalyst for CO_2 photocatalytic reduction. Catal Today 2011;161:105–9.
[104] Abou Asi M, He C, Su M, Xia D, Lin L, Deng H, et al. Photocatalytic reduction of CO_2 to hydrocarbons using $AgBr/TiO_2$ nanocomposites under visible light. Catal Today 2011;175:256–63.
[105] Popić J, Avramov-Ivić M, Vuković N. Reduction of carbon dioxide on ruthenium oxide and modified ruthenium oxide electrodes in 0.5 M $NaHCO_3$. J Electroanal Chem 1997;421:105–10.
[106] Qu J, Zhang X, Wang Y, Xie C. Electrochemical reduction of CO_2 on RuO_2/TiO_2 nanotubes composite modified Pt electrode. Electrochim Acta 2005;50:3576–80.
[107] Xie T-f, Wang D-j, Zhu L-j, Li T-j, Xu Y-j. Application of surface photovoltage technique in photocatalysis studies on modified TiO_2 photo-catalysts for photo-reduction of CO_2. Materials Chem Phys 2001;70:103–6.
[108] Ogura K, Kawano M, Yano J, Sakata Y. Visible-light-assisted decomposition of H_2O and photomethanation of CO_2 over CeO_2–TiO_2 catalyst. J Photochem Photobiol A: Chem 1992;66:91–7.
[109] Nasution HW, Purnama E, Kosela S, Gunlazuardi J. Photocatalytic reduction of CO_2 on copper-doped Titania catalysts prepared by improved-impregnation method. Catal Commun 2005;6:313–9.
[110] Qin S, Xin F, Liu Y, Yin X, Ma W. Photocatalytic reduction of CO_2 in methanol to methyl formate over CuO–TiO_2 composite catalysts. J Colloid Interface Sci 2011;356:257–61.
[111] Liou P-Y, Chen S-C, Wu JC, Liu D, Mackintosh S, Maroto-Valer M, et al. Photocatalytic CO_2 reduction using an internally illuminated monolith photoreactor. Energy Environ Sci 2011;4:1487–94.
[112] Pan P-W, Chen Y-W. Photocatalytic reduction of carbon dioxide on NiO/$InTaO_4$ under visible light irradiation. Catal Commun 2007;8:1546–9.
[113] Lee D-S, Chen H-J, Chen Y-W. Photocatalytic reduction of carbon dioxide with water using $InNbO_4$ catalyst with NiO and Co_3O_4 cocatalysts. J Phys Chem Solids 2012;73:661–9.
[114] Wang W, Ku Y. Photocatalytic degradation of gaseous benzene in air streams by using an optical fiber photoreactor. J Photochem Photobiol A: Chem 2003;159:47–59.
[115] Yan S, Wan L, Li Z, Zou Z. Facile temperature-controlled synthesis of hexagonal Zn_2GeO_4 nanorods with different aspect ratios toward improved photocatalytic activity for overall water splitting and photoreduction of CO_2. Chem Commun 2011;47:5632–4.
[116] Liu Q, Zhou Y, Tian Z, Chen X, Gao J, Zou Z. Zn_2GeO_4 crystal splitting toward sheaf-like, hyperbranched nanostructures and photocatalytic reduction of CO_2 into CH_4 under visible light after nitridation. J Mater Chem 2012;22:2033–8.
[117] Kudo A, Miseki Y. Heterogeneous photocatalyst materials for water splitting. Chem Soc Rev 2009;38:253–78.
[118] Maeda K, Domen K. New non-oxide photocatalysts designed for overall water splitting under visible light. J Phys Chem C 2007;111:7851–61.
[119] Chen X, Shen S, Guo L, Mao SS. Semiconductor-based photocatalytic hydrogen generation. Chem Rev 2010;110:6503–70.
[120] Tong H, Ouyang S, Bi Y, Umezawa N, Oshikiri M, Ye J. Nano-photocatalytic materials: possibilities and challenges. Adv Mater 2012;24:229–51.
[121] Zhang K, Guo L. Metal sulfide semiconductors for photocatalytic hydrogen production. Catal Sci Technol 2013;3:1672–90.
[122] Tsuji I, Kato H, Kudo A. Photocatalytic hydrogen evolution on ZnS–$CuInS_2$–$AgInS_2$ solid solution photocatalysts with wide visible light absorption bands. Chem Mater 2006;18:1969–75.
[123] Fujiwara H, Hosokawa H, Murakoshi K, Wada Y, Yanagida S. Surface characteristics of ZnS nanocrystallites relating to their photocatalysis for CO_2 reduction 1. Langmuir 1998;14:5154–9.
[124] Kozák O, Praus P, Kočí K, Klementová M. Preparation and characterization of ZnS nanoparticles deposited on montmorillonite. J Colloid Interface Sci 2010;352:244–51.
[125] Kočí K, Reli M, Kozák O, Lacný Z, Plachá D, Praus P, et al. Influence of reactor geometry on the yield of CO_2 photocatalytic reduction. Catal Today 2011;176:212–4.
[126] Johne P, Kisch H. Photoreduction of carbon dioxide catalysed by free and supported zinc and cadmium sulfide powders. J Photochem Photobiol A: Chem 1997;111:223–8.
[127] Praus P, Kozák O, Kočí K, Panáček A, Dvorský R. CdS nanoparticles deposited on montmorillonite: preparation, characterization and application for photoreduction of carbon dioxide. J Colloid Interface Sci 2011;360:574–9.
[128] Eggins BR, Robertson PK, Murphy EP, Woods E, Irvine JT. Factors affecting the photoelectrochemical fixation of carbon dioxide with semiconductor colloids. J Photochem Photobiol A: Chem 1998;118:31–40.
[129] Liu B-J, Torimoto T, Yoneyama H. Photocatalytic reduction of CO_2 using surface-modified CdS photocatalysts in organic solvents. J Photochem Photobiol A: Chem 1998;113:93–7.
[130] Fujiwara H, Hosokawa H, Murakoshi K, Wada Y, Yanagida S, Okada T, et al. Effect of surface structures on photocatalytic CO_2 reduction using quantized CdS nanocrystallites 1. J Phys Chem B 1997;101:8270–8.
[131] Amatore C, Saveant JM. Mechanism and kinetic characteristics of the electrochemical reduction of carbon dioxide in media of low proton availability. J Am Chem Soc 1981;103:5021–3.
[132] Yuan J, Zhang C, Li C, Chen M, Shangguan W. Pt–CdS/TiO_2 nanotube catalyst for photocatalytic reduction of CO_2 with water under visible light irradiation. In: MRS Proceedings. Cambridge University Press; 2011.
[133] Li X, Chen J, Li H, Li J, Xu Y, Liu Y, et al. Photoreduction of CO_2 to methanol over Bi_2S_3/CdS photocatalyst under visible light irradiation. J Nat Gas Chem 2011;20:413–7.
[134] Inoue H, Moriwaki H, Maeda K, Yoneyama H. Photoreduction of carbon dioxide using chalcogenide semiconductor microcrystals. J Photochem Photobiol A: Chem 1995;86:191–6.
[135] Zhang XV, Martin ST, Friend CM, Schoonen MA, Holland HD. Mineral-assisted pathways in prebiotic synthesis: photoelectrochemical reduction of carbon (+IV) by manganese sulfide. J Am Chem Soc 2004;126:11247–53.
[136] Halmann M. Photoelectrochemical reduction of aqueous carbon dioxide on p-type gallium phosphide in liquid junction solar cells. Nature 1978;275:115–6.
[137] Kaneco S, Katsumata H, Suzuki T, Ohta K. Photoelectrochemical reduction of carbon dioxide at p-type gallium arsenide and p-type indium phosphide electrodes in methanol. Chem Eng J 2006;116:227–31.
[138] Barton EE, Rampulla DM, Bocarsly AB. Selective solar-driven reduction of CO_2 to methanol using a catalyzed p-GaP based photoelectrochemical cell. J Am Chem Soc 2008;130:6342–4.
[139] Hirota K, Tryk DA, Yamamoto T, Hashimoto K, Okawa M, Fujishima A. Photoelectrochemical reduction of CO_2 in a high-pressure CO_2^+ methanol medium at p-type semiconductor electrodes. J Phys Chem B 1998;102:9834–43.
[140] Habisreutinger SN, Schmidt-Mende L, Stolarczyk JK. Photocatalytic reduction of CO_2 on TiO_2 and other semiconductors. Angew Chem Int Ed 2013;52:7372–408.
[141] Parkinson BA, Weaver PF. Photoelectrochemical pumping of enzymatic CO_2 reduction. Nature 1984;309:148–9.
[142] Aurian-Blajeni B, Halmann M, Manassen J. Electrochemical measurement on the photoelectrochemical reduction of aqueous carbon dioxide on p-Gallium phosphide and p-Gallium arsenide semiconductor electrodes. Sol Energy Mater 1983;8:425–40.
[143] Hinogami R, Nakamura Y, Yae S, Nakato Y. An approach to ideal semiconductor electrodes for efficient photoelectrochemical reduction of carbon dioxide by modification with small metal particles. J Phys Chem B 1998;102:974–80.
[144] Cook RL, MacDuff RC, Sammells AF. Photoelectrochemical carbon dioxide reduction to hydrocarbons at ambient temperature and pressure. J Electrochem Soc (United States) 1988;135:3069–70.
[145] Shioya Y, Ikeue K, Ogawa M, Anpo M. Synthesis of transparent Ti-containing mesoporous silica thin film materials and their unique photocatalytic activity for the reduction of CO_2 with H_2O. Appl Catal A: Gen 2003;254:251–9.
[146] Ikeue K, Nozaki S, Ogawa M, Anpo M. Characterization of self-standing Ti-containing porous silica thin films and their reactivity for the photocatalytic reduction of CO_2 with H_2O. Catal Today 2002;74:241–8.
[147] Ikeue K, Yamashita H, Anpo M, Takewaki T. Photocatalytic reduction of CO_2 with H_2O on Ti-β zeolite photocatalysts: effect of the hydrophobic and hydrophilic properties. J Phys Chem B 2001;105:8350–5.
[148] Ulagappan N, Frei H. Mechanistic study of CO_2 photoreduction in Ti silicalite molecular sieve by FT-IR spectroscopy. J Phys Chem A 2000;104:7834–9.
[149] Yin W-J, Chen S, Yang J-H, Gong X-G, Yan Y, Wei S-H. Effective band gap narrowing of anatase TiO_2 by strain along a soft crystal direction. Appl Phys Lett 2010221901–3.

[150] Nakamura I, Negishi N, Kutsuna S, Ihara T, Sugihara S, Takeuchi K. Role of oxygen vacancy in the plasma-treated TiO_2 photocatalyst with visible light activity for NO removal. J Mol Catal A: Chem 2000;161:205–12.
[151] Irie H, Watanabe Y, Hashimoto K. Carbon-doped anatase TiO_2 powders as a visible-light sensitive photocatalyst. Chem Lett 2003;32:772–3.
[152] Weng H, Yang X, Dong J, Mizuseki H, Kawasaki M, Kawazoe Y. Electronic structure and optical properties of the Co-doped anatase TiO_2 studied from first principles. Phys Rev B 2004;69:125219.
[153] Gai Y, Li J, Li S-S, Xia J-B, Wei S-H. Design of narrow-gap TiO_2: a passivated codoping approach for enhanced photoelectrochemical activity. Phys Rev Lett 2009;102:036402.
[154] Long R, English NJ. First-principles calculation of nitrogen-tungsten codoping effects on the band structure of anatase–titania. Appl Phys Lett 2009132102–3.
[155] Fazio E, Calandra P, Liveri VT, Santo N, Trusso S. Synthesis and physico-chemical characterization of Au/TiO_2 nanostructures formed by novel cold and hot nanosoldering of Au and TiO_2 nanoparticles dispersed in water. Colloids Surf A: Physicochem Eng Asp 2011;392:171–7.
[156] Slamet HWN, Purnama E, Riyani K, Gunlazuardi J. Effect of copper species in a photocatalytic synthesis of methanol from carbon dioxide over copper-doped titania catalysts. World Appl Sci J 2009;6:112–22.
[157] Sayama K, Arakawa H. Photocatalytic decomposition of water and photo-catalytic reduction of carbon dioxide over zirconia catalyst. J Phys Chem 1993;97:531–3.
[158] Antoniadou M, Kondarides DI, Lianos P. Photooxidation products of ethanol during photoelectrochemical operation using a nanocrystalline titania anode and a two compartment chemically biased cell. Catal Lett 2009;129:344–9.
[159] Daskalaki VM, Kondarides DI. Efficient production of hydrogen by photo-induced reforming of glycerol at ambient conditions. Catal Today 2009;144: 75–80.
[160] Ampelli C, Centi G, Passalacqua R, Perathoner S. Synthesis of solar fuels by a novel photoelectrocatalytic approach. Energy Environ Sci 2010;3:292–301.
[161] Qamar M. Improved photocatalytic activity of surface modified TiO_2 with platinum. Int J Nanosci 2010;9:579–83.
[162] Shi H, Zou Z. Photophysical and photocatalytic properties of $ANbO_3$(A=Na, K) photocatalysts. J Phys Chem Solids 2012;73:788–92.
[163] Li P, Ouyang S, Xi G, Kako T, Ye J. The effects of crystal structure and electronic structure on photocatalytic H_2 evolution and CO_2 reduction over two phases of perovskite-structured $NaNbO_3$. J Phys Chem C 2012;116: 7621–8.
[164] Zhang N, Ouyang S, Li P, Zhang Y, Xi G, Kako T, et al. Ion-exchange synthesis of a micro/mesoporous Zn_2GeO_4 photocatalyst at room temperature for photoreduction of CO_2. Chem Commun 2011;47:2041–3.
[165] Ishitani O, Inoue C, Suzuki Y, Ibusuki T. Photocatalytic reduction of carbon dioxide to methane and acetic acid by an aqueous suspension of metal-deposited TiO_2. J Photochem Photobiol A: Chem 1993;72:269–71.
[166] Solymosi F, Tombácz I, Koszta J. Effects of variation of electric properties of TiO_2 support on hydrogenation of CO and CO_2 over Rh catalysts. J Catal 1985;95:578–86.
[167] Tseng I, Wu J, Chou H-Y. Effects of sol–gel procedures on the photocatalysis of Cu/TiO_2 in CO_2 photoreduction. J Catal 2004;221:432–40.
[168] Tseng I, Chang W-C, Wu J. Photoreduction of CO_2 using sol–gel derived titania and titania-supported copper catalysts. Appl Catal B: Environ 2002;37:37–48.
[169] Adachi K, Ohta K, Mizuno T. Photocatalytic reduction of carbon dioxide to hydrocarbon using copper-loaded titanium dioxide. Sol Energy 1994;53: 187–90.
[170] Kočí K, Matějů K, Obalová L, Krejčíková S, Lacný Z, Plachá D, et al. Effect of silver doping on the TiO_2 for photocatalytic reduction of CO_2. Appl Catal B: Environ 2010;96:239–44.
[171] Krejčíková S, Matějová L, Kočí K, Obalová L, Matěj Z, Čapek L, et al. Preparation and characterization of Ag-doped crystalline titania for photo-catalysis applications. Appl Catal B: Environ 2012;111:119–25.
[172] Iizuka K, Wato T, Miseki Y, Saito K, Kudo A. Photocatalytic reduction of carbon dioxide over Ag cocatalyst-loaded $ALa_4Ti_4O_{15}$ (A=Ca, Sr, and Ba) using water as a reducing reagent. J Am Chem Soc 2011;133:20863–8.
[173] Ji P, Takeuchi M, Cuong T-M, Zhang J, Matsuoka M, Anpo M. Recent advances in visible light-responsive titanium oxide-based photocatalysts. Res Chem Intermed 2010;36:327–47.
[174] Alvaro M, Aprile C, Ferrer B, Sastre F, García H. Photochemistry of gold nanoparticles functionalized with an iron (II) terpyridine complex. An integrated visible light photocatalyst for hydrogen generation. Dalton Trans 2009:7437–44.
[175] Aprile C, Herranz MÁ, Carbonell E, Garcia H, Martín N. Microsecond charge separation upon photoexcitation of gold nanoparticles in imidazolium ionic liquids. Dalton Trans 2009:134–9.
[176] Guan G, Kida T, Yoshida A. Reduction of carbon dioxide with water under concentrated sunlight using photocatalyst combined with Fe-based catalyst. Appl Catal B: Environ 2003;41:387–96.
[177] Nishimura A, Mitsui G, Hirota M, Hu E. CO_2 Reforming performance and visible light responsibility of Cr-doped TiO_2 prepared by sol–gel and dip-coating method. Int J Chem Eng 2010;2010:1–9.
[178] Dholam R, Patel N, Adami M, Miotello A. Hydrogen production by photo-catalytic water-splitting using Cr-or Fe-doped TiO_2 composite thin films photocatalyst. Int J Hydrog Energy 2009;34:5337–46.
[179] Pan L, Zou J-J, Zhang X, Wang L. Photoisomerization of norbornadiene to quadricyclane using transition metal doped TiO_2. Ind Eng Chem Res 2010;49:8526–31.
[180] Yang C-C, Vernimmen J, Meynen V, Cool P, Mul G. Mechanistic study of hydrocarbon formation in photocatalytic CO_2 reduction over Ti–SBA-15. J Catal 2011;284:1–8.
[181] Hwang J-S, Chang J-S, Park S-E, Ikeue K, Anpo M. Photoreduction of carbondioxide on surface functionalized nanoporous catalysts. Top Catal 2005;35:311–9.
[182] Srinivasan SS, Wade J, Stefanakos EK, Goswami Y. Synergistic effects of sulfation and co-doping on the visible light photocatalysis of TiO_2. J Alloys Compd 2006;424:322–6.
[183] Wu J. Photoreduction of CO_2 in an optical-fiber photoreactor: effects of metals addition and catalyst carrier. Appl Catal A: Gen 2008;335:112–20.
[184] Wu J. Photoreduction of CO_2 to fuels under sunlight using optical-fiber reactor. Sol Energy Mater Sol Cells 2008;92:864–72.
[185] Zhai Q, Xie S, Fan W, Zhang Q, Wang Y, Deng W, et al. Photocatalytic conversion of carbon dioxide with water into methane: platinum and copper (I) oxide co-catalysts with a core–shell structure. Angew Chem 2013;125: 5888–91.
[186] Varghese OK, Paulose M, LaTempa TJ, Grimes CA. High-rate solar photo-catalytic conversion of CO_2 and water vapor to hydrocarbon fuels. Nano Lett 2009;9:731–7.
[187] Mankidy BD, Joseph B, Gupta VK. Photo-conversion of CO_2 using titanium dioxide: enhancements by plasmonic and co-catalytic nanoparticles. Nano-technology 2013;24:405402.
[188] Wang C, Xie Z, deKrafft KE, Lin W. Doping metal–organic frameworks for water oxidation, carbon dioxide reduction, and organic photocatalysis. J Am Chem Soc 2011;133:13445–54.
[189] Anpo M, Yamashita H, Ikeue K, Fujii Y, Zhang SG, Ichihashi Y, et al. Photocatalytic reduction of CO_2 with H_2O on Ti–MCM-41 and Ti–MCM-48 mesoporous zeolite catalysts. Catal Today 1998;44:327–32.
[190] Hemminger J, Carr R, Somorjai G. The photoassisted reaction of gaseous water and carbon dioxide adsorbed on the $SrTiO_3$(111) crystal face to form methane. Chem Phys Lett 1978;57:100–4.
[191] Hamadanian M, Reisi-Vanani A, Majedi A. Preparation and characterization of S-doped TiO_2 nanoparticles, effect of calcination temperature and evaluation of photocatalytic activity. Mater Chem Phys 2009;116:376–82.
[192] Wen C, Zhu Y-J, Kanbara T, Zhu H-Z, Xiao C-F. Effects of I and F codoped TiO_2 on the photocatalytic degradation of methylene blue. Desalination 2009;249: 621–5.
[193] Zhou L, Deng J, Zhao Y, Liu W, An L, Chen F. Preparation and characterization of N–I co-doped nanocrystal anatase TiO_2 with enhanced photocatalytic activity under visible-light irradiation. Mater Chem Phys 2009;117:522–7.
[194] In S, Orlov A, Berg R, García F, Pedrosa-Jimenez S, Tikhov MS, et al. Effective visible light-activated B-doped and B, N-codoped TiO_2 photocatalysts. J Am Chem Soc 2007;129:13790–1.
[195] Khan SU, Al-Shahry M, Ingler WB. Efficient photochemical water splitting by a chemically modified n-TiO_2. Science 2002;297:2243–5.
[196] Yu JC, Yu J, Ho W, Jiang Z, Zhang L. Effects of F-doping on the photocatalytic activity and microstructures of nanocrystalline TiO_2 powders. Chem Mater 2002;14:3808–16.
[197] Wu G, Wen J, Wang J, Thomas DF, Chen A. A facile approach to synthesize N and B co-doped TiO_2 nanomaterials with superior visible-light response. Mater Lett 2010;64:1728–31.
[198] Pelaez M, de la Cruz AA, Stathatos E, Falaras P, Dionysiou DD. Visible light-activated NF-codoped TiO_2 nanoparticles for the photocatalytic degradation of microcystin-LR in water. Catal Today 2009;144:19–25.
[199] Tahir M, Amin NS. Advances in visible light responsive titanium oxide-based photocatalysts for CO_2 conversion to hydrocarbon fuels. Energy Convers Manage 2013;76:194–214.
[200] Suzuki TM, Tanaka H, Morikawa T, Iwaki M, Sato S, Saeki S, et al. Direct assembly synthesis of metal complex–semiconductor hybrid photocatalysts anchored by phosphonate for highly efficient CO_2 reduction. Chem Commun 2011;47:8673–5.
[201] Sato S, Morikawa T, Saeki S, Kajino T, Motohiro T. Visible-light-induced selective CO_2 reduction utilizing a ruthenium complex electrocatalyst linked to ap-type nitrogen-doped Ta_2O_5 semiconductor. Angew Chem Int Ed 2010;49:5101–5.
[202] Tsai C-W, Chen HM, Liu R-S, Asakura K, Chan T-S. Ni@NiO core–shell structure-modified nitrogen-doped $InTaO_4$ for solar-driven highly efficient CO_2 reduction to methanol. J Phys Chem C 2011;115:10180–6.
[203] Xue LM, Zhang FH, Fan HJ, Bai XF. Preparation of C doped TiO_2 photocatalysts and their photocatalytic reduction of carbon dioxide. Adv Mater Res 2011;183:1842–6.
[204] Irie H, Washizuka S, Hashimoto K. Hydrophilicity on carbon-doped TiO_2 thin films under visible light. Thin Solid Films 2006;510:21–5.
[205] Ohno T, Akiyoshi M, Umebayashi T, Asai K, Mitsui T, Matsumura M. Preparation of S-doped TiO_2 photocatalysts and their photocatalytic activities under visible light. Appl Catal A: Gen 2004;265:115–21.
[206] Li D, Haneda H, Hishita S, Ohashi N, Labhsetwar NK. Fluorine-doped TiO_2 powders prepared by spray pyrolysis and their improved photo-catalytic activity for decomposition of gas-phase acetaldehyde. J Fluor Chem 2005;126:69–77.
[207] He Z, Xie L, Song S, Wang C, Tu J, Hong F, et al. The impact of silver modification on the catalytic activity of iodine-doped titania for p-chloro-

phenol degradation under visible-light irradiation. J Mol Catal A: Chem 2010;319:78–84.
[208] Zhang Q, Li Y, Ackerman EA, Gajdardziska-Josifovska M, Li H. Visible light responsive iodine-doped TiO_2 for photocatalytic reduction of CO_2 to fuels. Appl Catal A: Gen 2011;400:195–202.
[209] Heleg-Shabtai V, Zahavy E, Willner I. Photochemical CO_2-fixation by functionalized reconstituted protein assemblies. Energy Convers Manage 1995;36:609–12.
[210] Yanagida S, Ogata T, Yamamoto Y, Wada Y, Murakoshi K, Kusaba M, et al. A novel CO_2 photoreduction system consisting of phenazine as a photosensitizer and cobalt cyclam as a CO_2 scavenger. Energy Convers Manage 1995;36:601–4.
[211] Li Z, Zhou Y, Zhang J, Tu W, Liu Q, Yu T, et al. Hexagonal nanoplate-textured micro-octahedron Zn_2SnO_4: combined effects toward enhanced efficiencies of dye-sensitized solar cell and photoreduction of CO_2 into hydrocarbon fuels. Cryst Growth Des 2012;12:1476–81.
[212] Pan J, Wu X, Wang L, Liu G, Lu GQM, Cheng H-M. Synthesis of anatase TiO_2 rods with dominant reactive {010} facets for the photoreduction of CO_2 to CH_4 and use in dye-sensitized solar cells. Chem Commun 2011;47:8361–3.
[213] Wu JC. Photocatalytic reduction of greenhouse gas CO_2 to fuel. Catal Surv Asia 2009;13:30–40.
[214] Wu J, Chiou C-H. Photoreduction of CO_2 over Ruthenium dye-sensitized TiO_2-based catalysts under concentrated natural sunlight. Catal Commun 2008;9:2073–6.
[215] Ozcan O, Yukruk F, Akkaya E, Uner D. Dye sensitized CO_2 reduction over pure and platinized TiO_2. Top Catal 2007;44:523–8.
[216] Lehn J-M, Ziessel R. Photochemical generation of carbon monoxide and hydrogen by reduction of carbon dioxide and water under visible light irradiation. Proc Natl Acad Sci 1982;79:701–4.
[217] Hirose T, Maeno Y, Himeda Y. Photocatalytic carbon dioxide photoreduction by Co $(bpy)_3^{2+}$ sensitized by Ru $(bpy)_3^{2+}$ fixed to cation exchange polymer. J Mol Catal A: Chem 2003;193:27–32.
[218] Wang C, Thompson RL, Ohodnicki P, Baltrus J, Matranga C. Size-dependent photocatalytic reduction of CO_2 with PbS quantum dot sensitized TiO_2 heterostructured photocatalysts. J Mater Chem 2011;21:13452–7.
[219] Wang C, Thompson RL, Baltrus J, Matranga C. Visible light photoreduction of CO_2 using CdSe/Pt/TiO_2 heterostructured catalysts. J Phys Chem Lett 2009;1:48–53.
[220] Tisdale WA, Williams KJ, Timp BA, Norris DJ, Aydil ES, Zhu X-Y. Hot-electron transfer from semiconductor nanocrystals. Science 2010;328:1543–7.
[221] Seoudi R, El-Bahy G, El Sayed Z. Ultraviolet and visible spectroscopic studies of phthalocyanine and its complexes thin films. Opt Mater 2006;29:304–12.
[222] Zhao Z, Fan J, Xie M, Wang Z. Photo-catalytic reduction of carbon dioxide with in-situ synthesized CoPc/TiO_2 under visible light irradiation. J Clean Prod 2009;17:1025–9.
[223] Zhao Z, Fan J, Liu S, Wang Z. Optimal design and preparation of titania-supported CoPc using sol–gel for the photo-reduction of CO_2. Chem Eng J 2009;151:134–40.
[224] Zhao Z-H, Fan J-M, Wang Z-Z. Photo-catalytic CO_2 reduction using sol–gel derived titania-supported zinc-phthalocyanine. J Clean Prod 2007;15:1894–7.
[225] Wang Q, Wu W, Chen J, Chu G, Ma K, Zou H. Novel synthesis of ZnPc/TiO_2 composite particles and carbon dioxide photo-catalytic reduction efficiency study under simulated solar radiation conditions. Colloids Surf A: Physicochem Eng Asp 2012;409:118–25.
[226] Ettedgui J, Diskin-Posner Y, Weiner L, Neumann R. Photoreduction of carbon dioxide to carbon monoxide with hydrogen catalyzed by a Rhenium (I) phenanthroline–polyoxometalate hybrid complex. J Am Chem Soc 2010;133:188–90.
[227] Woolerton TW, Sheard S, Reisner E, Pierce E, Ragsdale SW, Armstrong FA. Efficient and clean photoreduction of CO_2 to CO by enzyme-modified TiO_2 nanoparticles using visible light. J Am Chem Soc 2010;132:2132–3.
[228] Woolerton TW, Sheard S, Pierce E, Ragsdale SW, Armstrong FA. CO_2 photoreduction at enzyme-modified metal oxide nanoparticles. Energy Environ Sci 2011;4:2393–9.
[229] Hou W, Hung WH, Pavaskar P, Goeppert A, Aykol M, Cronin SB. Photocatalytic conversion of CO_2 to hydrocarbon fuels via plasmon-enhanced absorption and metallic interband transitions. ACS Catal 2011;1:929–36.
[230] Wang W-N, Park J, Biswas P. Rapid synthesis of nanostructured Cu–TiO_2–SiO_2 composites for CO_2 photoreduction by evaporation driven self-assembly. Catal Sci Technol 2011;1:593–600.
[231] Luo D, Bi Y, Kan W, Zhang N, Hong S. Copper and cerium co-doped titanium dioxide on catalytic photo reduction of carbon dioxide with water: experimental and theoretical studies. J Mol Struct 2011;994:325–31.
[232] Yang H-C, Lin H-Y, Chien Y-S, Wu JC-S Wu H-H. Mesoporous TiO_2/SBA-15, and Cu/TiO_2/SBA-15 composite photocatalysts for photoreduction of CO_2 to methanol. Catal Lett 2009;131:381–7.
[233] Wu JC, Wu T-H, Chu T, Huang H, Tsai D. Application of optical-fiber photoreactor for CO_2 photocatalytic reduction. Top Catal 2008;47:131–6.
[234] Tseng I, Wu JC-S. Chemical states of metal-loaded titania in the photoreduction of CO_2. Catal Today 2004;97:113–9.
[235] Thampi KR, Kiwi J, Graetzel M. Methanation and photo-methanation of carbon dioxide at room temperature and atmospheric pressure. Nature 1987;327:506–8.
[236] Jensen J, Mikkelsen M, Krebs FC. Flexible substrates as basis for photocatalytic reduction of carbon dioxide. Sol Energy Mater Sol Cells 2011;95:2949–58.
[237] Gijsman P, Meijers G, Vitarelli G. Comparison of the UV-degradation chemistry of polypropylene, polyethylene, polyamide 6 and polybutylene terephthalate. Polym Degrad Stabil 1999;65:433–41.
[238] Jin C, Christensen P, Egerton T, Lawson E, White J. Rapid measurement of polymer photo-degradation by FTIR spectrometry of evolved carbon dioxide. Polym Degrad Stabil 2006;91:1086–96.
[239] Kesting RE. Synthetic polymeric membranes: a structural perspective. NY: Wiley; 1985.
[240] Fernando S, Christensen P, Egerton T, Eveson R, Martins-Franchetti S, Voisin D, et al. Carbon dioxide formation during initial stages of photodegradation of poly (ethyleneterephthalate)(PET) films. Mater Sci Technol 2009;25:549–55.
[241] Kim W, Seok T, Choi W. Nafion layer-enhanced photosynthetic conversion of CO_2 into hydrocarbons on TiO_2 nanoparticles. Energy Environ Sci 2012;5:6066–70.
[242] Arai T, Tajima S, Sato S, Uemura K, Morikawa T, Kajino T. Selective CO_2 conversion to formate in water using a CZTS photocathode modified with a ruthenium complex polymer. Chem Commun 2011;47:12664–6.
[243] Henderson MA. A surface science perspective on photocatalysis. Surf Sci Rep 2011;66:185–297.
[244] Chaudhari R, Ramachandran P. Three phase slurry reactors. AIChE J 1980;26:177–201.
[245] Halmann M, Ulman M, Aurian-Blajeni B. Photochemical solar collector for the photoassisted reduction of aqueous carbon dioxide. Sol Energy 1983;31:429–31.
[246] Halmann M, Katzir V, Borgarello E, Kiwi J. Photoassisted carbon dioxide reduction on aqueous suspensions of titanium dioxide. Sol Energy Mater 1984;10:85–91.
[247] Roupp GB, Nico JA, Annangi S, Changrani R, Annapragada R. Two-flux radiation-field model for an annular packed-bed photocatalytic oxidation reactor. AIChE J 1997;43:792–801.
[248] Esterkin C, Negro A, Alfano O, Cassano A. Air pollution remediation in a fixed bed photocatalytic reactor coated with TiO_2. AIChE J 2005;51:2298–310.
[249] Shi D, Feng Y, Zhong S. Photocatalytic conversion of CH_4 and CO_2 to oxygenated compounds over Cu/CdS–TiO_2/SiO_2 catalyst. Catal Today 2004;98:505–9.
[250] Larson SA, Widegren JA, Falconer JL. Transient studies of 2-propanol photocatalytic oxidation on titania. J Catal 1995;157:611–25.
[251] Wang T, Yang L, Du X, Yang Y. Numerical investigation on CO_2 photocatalytic reduction in optical fiber monolith reactor. Energy Convers Manage 2013;65:299–307.
[252] Wu J, Lin H-M. Photo reduction of CO_2 to methanol via TiO_2 photocatalyst. Int J Photoenergy 2005;7:115–9.
[253] Guan G, Kida T, Harada T, Isayama M, Yoshida A. Photoreduction of carbon dioxide with water over $K_2Ti_6O_{13}$ photocatalyst combined with Cu/ZnO catalyst under concentrated sunlight. Appl Catal A: Gen 2003;249:11–8.
[254] Du P, Carneiro JT, Moulijn JA, Mul G. A novel photocatalytic monolith reactor for multiphase heterogeneous photocatalysis. Appl Catal A: Gen 2008;334:119–28.
[255] Hayes R, Kolaczkowski S, Thomas W. Finite-element model for a catalytic monolith reactor. Comput Chem Eng 1992;16:645–57.
[256] Hayes R, Kolaczkowski S. Mass and heat transfer effects in catalytic monolith reactors. Chem Eng Sci 1994;49:3587–99.
[257] Lin H, Valsaraj KT. Development of an optical fiber monolith reactor for photocatalytic wastewater treatment. J Appl Electrochem 2005;35:699–708.
[258] Ola O, Maroto-Valer M, Liu D, Mackintosh S, Lee C-W, Wu J. Performance comparison of CO_2 conversion in slurry and monolith photoreactors using Pd and Rh–TiO_2 catalyst under ultraviolet irradiation. Appl Catal B: Environ 2012;126:172–9.
[259] Ampelli C, Passalacqua R, Genovese C, Perathoner S, Centi G. A novel photoelectrochemical approach for the chemical recycling of carbon dioxide to fuels. Chem Eng Trans 2011;25:683–8.
[260] Lee W-H, Liao C-H, Tsai M-F, Huang C-W, Wu J. A novel twin reactor for CO_2 photoreduction to mimic artificial photosynthesis. Appl Catal B: Environ 2012;132–133:445–51.
[261] Liu L, Gao F, Zhao H, Li Y. Tailoring Cu valence and oxygen vacancy in Cu/TiO_2 catalysts for enhanced CO_2 photoreduction efficiency. Appl Catal B: Environ 2013;134–135:349–58.
[262] Wang Y, Li B, Zhang C, Cui L, Kang S, Li X, et al. Ordered mesoporous CeO_2–TiO_2 composites: Highly efficient photocatalysts for the reduction of CO_2 with H_2O under simulated solar irradiation. Appl Catal B: Environ 2012;130-131:277–84.
[263] Wang Y, Wang F, Chen Y, Zhang D, Li B, Kang S, et al. Enhanced photocatalytic performance of ordered mesoporous Fe-doped CeO_2 catalysts for the reduction of CO_2 with H_2O under simulated solar irradiation. Appl Catal B: Environ 2014;147:602–9.
[264] Zhao C, Krall A, Zhao H, Zhang Q, Li Y. Ultrasonic spray pyrolysis synthesis of Ag/TiO_2 nanocomposite photocatalysts for simultaneous H_2 production and CO_2 reduction. Int J Hydrog Energy 2012;37:9967–76.